TNFα-mediated subtype switch and tumor progression in pancreatic cancer

DISSERTATION

For the award of the degree

"Doctoral of Philosophy (Ph.D.)"

Division of Mathematics and Natural Science

of the Georg-August-Universität Göttingen

within the doctoral program "Molecular Medicine"

of the Georg-August University School of Science (GAUSS)

Submitted by

Mengyu Tu

Born in

Korla, China

Göttingen, July 2021

Members of the Thesis Committee

Dr. Shiv K. Singh (**1st Referee**)

Department of Gastroenterology GI Oncology & Endocrinology

University Medical Center, Göttingen

Prof. Dr. Holger Reichardt (**2nd Referee**)

Department of Cellular and Molecular Immunology

University Medical Center, Göttingen

Prof. Dr. Dieter Kube

Department of Haematology and Oncology

University Medical Center, Göttingen

Extended Examination Board Members:

Prof. Dr. Argyris Papantonis

Department of Pathology

University Medical Center, Göttingen

Dr. Ufuk Günesdogan

Department of Developmental Biology

University of Göttingen

Dr. Nico Posnien

Department of Developmental Biology

University of Göttingen

Date of submission of thesis: 15.07.2021

Date of the oral examination: 08.09.2021

AFFIDAVIT

I hereby declare that the thesis entitled "TNFα mediated subtype switch and tumor progression in pancreatic cancer" has been written independently and with no other sources and aids than quoted.

_____

Mengyu Tu

Göttingen. 15.07.2021

Table of Contents

List of figures

List of abbreviation

5-FU	5-fluorouracil
ADEX	Aberrantly differentiated endocrine exocrine
AGR2	Anterior Gradient 2
AP1	Activator protein 1
ATAC-seq	Assay for transposase-accessible chromatin with sequencing
BSA	Bovine serum albumin
BL	Basal-like
BRD4	Bromodomain-containing protein 4
CAF	Cancer-associated fibroblast
CCL2	CC-chemokine ligand 2
CDH1	Cadherin1
CDKN2A	Cyclin dependent kinase inhibitor 2A
cDNA	Complementary DNA
CEACAM5	Carcinoembryonic Antigen-Related Cell Adhesion Molecule 5
CEACAM6	Carcinoembryonic Antigen-Related Cell Adhesion Molecule 6
ChIP	Chromatin immunoprecipitation
ChIP-seq	ChIP followed by sequencing
CLA	Classical
CO2	Carbondioxide
CSF1	Colony stimulating factor 1

CSF1R	Colony stimulating factor 1 receptor
DAPI	4',6-diamidino-2-phenylindole
DMEM	Dulbecco's modified eagle medium
DMSO	Dimethyl sulfoxide
DNA	Deoxyribo nucleic acid
ECAD	E-cadherin
ECM	Extracellular matrix
EDTA	Ethylenediaminetetraacetic acid
EGF	Epidermal growth factor
EFGR	Epidermal growth factor receptor
EGTA	Ethylene glycol-bis (β-aminoethyl ether)-N,N,N',N'-tetraacetic acid
ELF3	E74-like ETS transcription factor 3
EMT	Epithelial to mesenchymal transition
FCS	Fetal calf serum
FDA	Food and drug administration
FOLFIRINOX	Folinic acid, fluorouracil, irinotecan, oxaliplatin
Foxn1$^{nu/nu}$	Homozygous nude mutant Forkhead box protein N1
FOXQ1	Forkhead Box Q1
GATA6	GATA-binding factor 6
GCDX	Cell line derived from PDX established in Göttingen
GEMM	Genetically engineered mouse models
GO	Gene ontology

GSEA	Gene set enrichment analysis
GTP	Guanidine triphosphate
H3K4me3	Histone 3 lysine 4 trimethylation
H3K27ac	Histone 3 lysine 27 acetylation
H3K27me3	Histone 3 lysine 27 trimethylation
HE	Hematoxylin & eosin
HNF4A	Hepatocyte Nuclear Factor 4 Alpha
HRP	Horse raddish peroxidase
IC$_{50}$	Inhibitory concentration 50 %
IF	Immunofluorescence
IgG	Immunoglobulin G
IGV	Integrative genomics viewer
IL-1	Interleukin-1
IL-6	Interleukin-6
IL-10	Interleukin-10
KDM6	Lysine demethylase 6A
KLF5	Krueppel-like factor 5
KPC	*Kras^{G12D};Trp53^{R172H};PdxCre*
KRAS	Kirsten rat sarcoma viral oncogene homolog
KRT5	Keratin 5
KRT14	Keratin 14
LiCl	Lithium chloride

log2FC	Log2 fold change
mRNA	Messenger RNA
NaCl	Sodium chloride
NaF	Sodium fluride
NaO	Sodium oxide
NEAA	Nonessential amino acids
NES	Normalized enrichment score
NGS	Normal goat serum
PAGE	Polyacrylamide gel electrophoresis
PanIN	Pancreatic intraepithelial neoplasia
PARP	Poly-ADP ribose polymerase
PB	Phosphate buffer
PBT	Phosphate buffer with Triton X-100
PBS	Phosphate-buffered saline
PCA	Principal component analysis
PCR	Polymerase chain reaction
PDAC	Pancreatic ductal adenocarcinoma
PDX	Patient-derive xenograft
PFA	Paraformaldehyde
PMSF	Phenylmethylsulfonyl fluoride
QM	Quasi-mesenchymal
qRT-PCR	Quantitative real-time polymerase chain reaction

RNA	Ribonucleic acid
RNA-seq	RNA sequencing
RPMI	Roswell Park Memorial Institute
SD	Standard deviation
SDS	Sodium dodecyl sulfate
SDS-PAGE	Sodium dodecyl sulfate polyacrylamide gel electrophoresis
siRNA	Small interfering RNA
SMAD	Mothers against decapentaplegic homolog
TAM	Tumor associated macrophage
TBS	Tris-buffered saline
TBST	Tris-buffered saline with Tween-20
TCGA	The cancer genome atlas
TEMED	Tetramethylethylenediamine
TFs	Transcription factors
TGFβ	Transforming growth factor β
TMA	Tissue microarray
TME	Tumor microenvironment
TNFα	Tumor necrosis factor α
TP53	Tumor protein 53
TRIS	Tris(hydroxymethyl)aminomethane
VIM	Vimentin
V	Volt(s)

v/v   Volume percent

vs.   Versus

ZEB1   Zinc finger E-box-binding homeobox 1

α   Alpha

β   Beta

μ   Micro

Abstract

Pancreatic cancer (PDAC) represents an extremely poor clinical outcome with a 5-year survival rate of <9%. It is anticipated to become the second leading cause of cancer-related deaths in the industrialized countries by 2030. A vast majority of PDAC patients exhibit locally advanced or distant metastases at the time of diagnosis, which makes surgical resection challenging. The complex molecular heterogeneity within neoplastic-epithelium and stromal cells profoundly attributes to this poor prognosis, and makes therapy challenging. Extensive whole genome sequencing and transcriptional profiling of PDAC biopsies identified the two most clinically relevant and molecularly distinct subtypes: the basal-like (BL) subtype displays highly aggressive phenotype, metastatic disease and chemoresistance profile in PDAC patients, whereas classical (CLA) subtype often responds to therapy and exhibits better prognosis. However, the coexisting stromal components (e.g. inflammatory macrophages and cancer-associated fibroblasts) within CLA or BL subtypes underlie distinct prognosis. Whether and how CLA or BL neoplastic cells shape the stromal microenvironment, and hence, determine PDAC aggressiveness and therapeutic vulnerabilities remain largely unresolved. Herein, we show that BL neoplastic cells recruit inflammatory macrophages, which foster highly inflamed and aggressive tumor phenotype in PDAC. We identified a mutually exclusive AP1-driven transcriptional program, which determines PDAC subtype identity and prognosis. CLA-restricted JUNB/AP1 is associated with less aggressive and chemoresponsive CLA tumors; conversely, BL-restricted cJUN/AP1 largely controls tumor invasiveness, chemoresistance and proinflammatory program. Mechanistically, cJUN controls CCL2 expression via enhancer-promoter regulation, which, in turn, facilitate recruitment of TNFα-producing macrophages in the PDAC microenvironment. Subsequently, TNFα switches PDAC subtype identity through converting CLA tumors into a highly aggressive BL phenotypic state by activating cJUN-CCL2 signaling axis, thus, forming a positive feed forward loop. Finally, we show that BRD4 regulates cJUN-transcription via enhancer-promoter interactions; hence, pharmacological inhibition of the BRD4-cJUN axis induces a favorable subtype switch and improves overall survival in preclinical models. This study

provides compelling evidence that subtype-specific transcriptional program shapes the subtype identity, tumor aggressiveness and prognosis in PDAC. Thus, cJUN^{high}/TNFα^{high} subtype-specific precision therapy has the potential to overcome the highly aggressive and chemoresistant PDAC.

1. Introduction

1.1 Pancreatic cancer

Pancreatic cancer (PDAC) is a deadly disease, which has the highest mortality rate among solid tumors with a 5-year survival rate of less than 9 % (Siegel et al., 2020). According to the record of incidence and mortality associated with PDAC, it is set to become the second leading cause of cancer-related death by 2030 (Rahib et al., 2014). In comparison to breast and lung cancer, where treatment and early detection approaches have led to a significant improvement in prognosis (Andre and Pusztai, 2006; Rudin et al., 2019; Tsao et al., 2015), PDAC has an invariably poor prognosis since there is no biomarkers available for the early diagnosis. Besides, PDAC is highly aggressive and metastatic, showing strong resistance to chemotherapies. One of the major biomedical challenge in the poor prognosis and treatment of PDAC is the complex tumor stroma heterogeneity. However, factors involved in promoting cross-talk between tumor and stromal cells in the microenvironment remain unresolved.

1.1.1 Pathophysiology

The pancreas is a soft and glandular organ that mainly consists of endocrine and exocrine functional units (Zhou and Melton, 2018). The endocrine pancreas is responsible for regulating metabolism in the body, for example by regulating the blood glucose level. The exocrine compartment consists of acinar and ductal cells, where the acinar cells secrete the digestive enzymes (e.g. amylase, lipases, and proteinases) and ductal cells transport the secretion of enzymes to the small intestine (Zhou and Melton, 2018). In general, there are rare tumors arising from the endocrine pancreas; however, mainly neuroendocrine tumors (Kleeff et al., 2016). Over 90% of pancreatic tumors originate from the exocrine pancreas, with pancreatic ductal adenocarcinoma (PDAC) being the predominant type of tumors (Hezel et al., 2006; Prinz, 2012). Most PDAC arise from the head of the pancreas (60 %), some arise from the body (15 %) and tail (5-10%) (Ghaneh et al., 2008).

1.1.2 Tumor initiation and progression

The well-accepted PDAC progression model states that PDAC gradually develops from transformation of normal ductal epithelial cells to aggressive adenocarcinoma with the activation of certain oncogenes sequentially through the formation of well-defined precursor lesions called pancreatic intraepithelial neoplasia (PanIN-1 to 3) (**Figure 1**) (Hruban et al., 2001). PanIN-1 are lesions of flat or papillary architecture without any abnormalities. PanIN-2 lesions show enlarged and crowed nuclei, mild dysplasia with increased abnormalities and papillary architecture. PanIN-3 displays severe nuclear atypia, a high grade of dysplasia on the verge of carcinoma (Hruban et al., 2001).

In PDAC, *KRAS* mutations are the prevalent alterations in more than 90% cases (Olive and Tuveson, 2006). Further, mutations in *KRAS* are one of the earliest genetic events, which is essential for the initiation and development of PDAC (Kanda et al., 2012; Hingorani et al., 2003). KRAS protein is a Guanosine triphisphatase (GTPase), which is part of RAS/MAPK pathway (Iguchi et al., 2016). *KRAS* mutation leads to continuously binding of GTP in regardless of external stimulus and therefore promote tumor cell growth (Vigil et al., 2010; Waters and Der, 2018). Besides *KRAS* mutations, *TP53*, *CDKN2A* and *SMAD4* are also considered as the most important driver mutations, which occur, in pancreatic carcinogenesis (Kleeff et al., 2016). For instance, *CDKN2*A encodes p16INK4A protein that binds and inactivates CDK4, leading to cell cycle G1 arrest (McWilliams et al., 2011; Zhao et al., 2016). On the other hand, *CDKN2A* encodes p16ARF for stabilizing p53 (Bartsch et al., 2002). Alterations in *CDKN2A* are observed in PanIN-2 lesions and more than 90 % of PDAC tumors (Wilentz et al., 1998). *TP53* is inactivated in more than 70 % of PDAC (Puleo et al., 2018; Chan-Seng-Yue et al., 2020). Loss of *TP53* favours tumor cell proliferation and survival as well as promoting additional unfavourable genetic alterations (Koorstra et al., 2009). Similarly, tumor suppressor *SMAD4* is altered in more than 55 % late stage PDAC (Iacobuzio-Donahue, 2012). Mechanistically, SMAD4 is involved in transforming growth factor (TGF-β) mediated signaling pathway (Iacobuzio-Donahue, 2012; Xia et al., 2015). During the progression of PDAC, pancreatic tissue is highly inflamed with cytokines e.g. TGF-β (Shen et al., 2017).
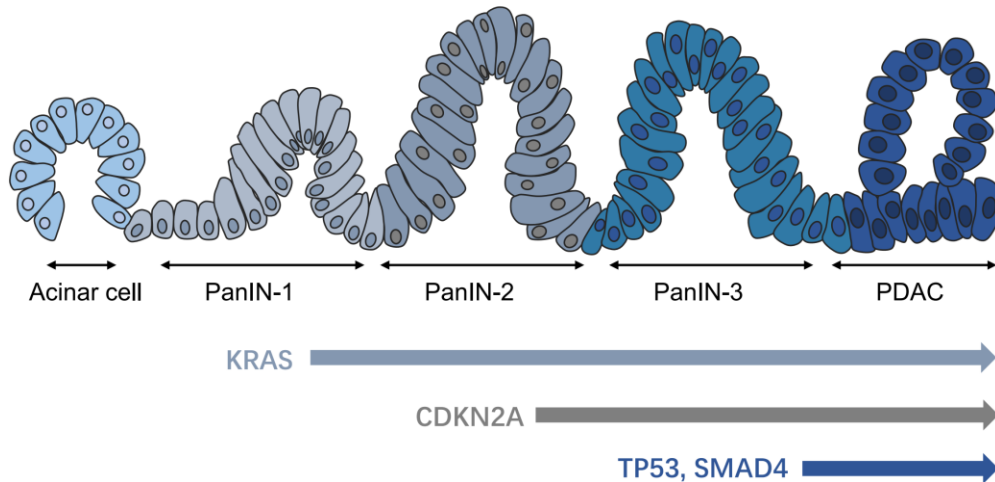
Figure 1. PDAC progression model. Illustration diagram of PDAC development from normal pancreatic tissue to PDAC through PanIN lesions (PanIN-1 to PanIN-3) and sequential activation of driver mutations *KRAS*, *CDKN2A*, *TP53* and *SMAD4*.

1.1.3 Therapeutic strategies of PDAC

Due to the highly aggressive nature of PDAC, surgery is the only potentially curative therapeutic option (Hartwig et al., 2013). However, majority of patients are not amenable to surgery due to locally advanced or metastatic PDAC at the time of diagnosis. In fact, a large number of PDAC patients faced tumor recurrence post-surgical resection (Onoue et al., 2004). Nevertheless, the therapeutic strategies for PDAC have improved in the last decades, which has led to an increased 5-year survival from 11 % to 21 % post-surgery and chemotherapy (Strobel et al., 2019).

Gemcitabine is the most commonly used chemotherapeutic drug in the clinical settings for the treatment of PDAC patients (Burris et al., 1997). At the biochemical level, deoxycytidine, which is an active molecule of gemcitabine, converts into active metabolite that interferes with DNA synthesis and consequently inhibits tumor growth (Mini et al., 2006). Notably, American Society of Clinical Oncology (ASCO) recommended gemcitabine, together with capecitabine for resectable tumors (Khorana et al., 2017). A clinical study by the European Study Group for PDAC (ESPAC)-4 reported that the overall

5-year survival rate of resected PDAC patients improved from 25.5 to 28.0 months with gemcitabine and capecitabine combined therapy compared to gemcitabine alone (Neoptolemos et al., 2017). However, the clinical outcome of adjuvant chemotherapeutic agents for the borderline resectable or unresectable tumors remain disappointing. Thus, neoadjuvant therapy emerged as an option for the borderline resectable or unresectable tumors, i.e. FOLFIRINOX treatment led to a conversion from unresectable stage to borderline or even resectable tumors (Nitsche et al., 2015; Petrelli et al., 2015).

For unresectable patients, chemotherapies remain the only option. For instance, combination of gemcitabine and nab-paclitaxel clinically applied as the first-line therapy for PDAC patients (Goldstein et al., 2015). An alternative to gemcitabine plus nab-paclitaxel for clinically fit patients is the FOLFIRINOX regimen, which is a combination therapy consisting of 5-FU, leucovorin, irinotecan, and oxaliplatin (Vaccaro et al., 2011). Notably, this combination significantly improves the outcome of metastatic patients when compared with monotherapy gemcitabine (11.1 vs 6.8 months) (Conroy et al., 2011). A phase III clinical trial reported that nanoliposomal irinotecan in combination with 5-FU/FA significantly improved the survival rate (6.1 vs 4.2 month) of those metastatic PDAC patients who had previously received gemcitabine-based therapy (Wang-Gillam et al., 2016). It is worth noting that, the second-line therapeutic option is determined based on the treatment applied in the first-line therapy as well as the patient performance (Ellenrieder et al., 2016).

Recently, the phase III POLO clinical trial reported that PARP inhibitor Olaparib improved progression-free survival. It is now recommended for the patients with germline BRAC mutation (Golan et al., 2019). Besides, immune therapy studies have shown significant improvement in survival rate in several cancer types. For instance, blockage of immune checkpoint T lymphocyte-associated antigen 4 (CTLA4) has been approved for clinical application in advanced melanoma (Hodi et al., 2010). Anti- programmed death 1 (PD1) and PD1 ligand (PDL-1) therapies were reported to be successfully established in multiple cancers including melanoma, lung cancer, and kidney cancer (Brahmer et al., 2015; Garon et al., 2015; Larkin et al., 2015; Motzer et al., 2015; Topalian et al., 2014). Nonetheless, PDAC is refractory to all these approaches, probably due to the negative

immune regulation in the pancreatic tumor microenvironment (TME) (Neoptolemos et al., 2018).

Taken together, it is still very challenging to treat PDAC. Hence, extensive studies in the molecular subtyping are urgently needed to understand aggressive features and chemoresistance of PDAC. As in breast and lung cancer, subgrouping patients by molecular characteristics may benefit PDAC patients through optimized/personalized therapeutic approaches (Andre and Pusztai, 2006; Rudin et al., 2019; Tsao et al., 2015).

1.2 Molecular subtypes of PDAC

In recent years, considerable progress has been made in identifying molecular subtypes of PDAC, which remarkably improved the molecular insights of this grave disease (**Table 1**). In 2011, Collisson *et al.* defined three molecular subtypes of PDAC known as classical (CLA), quasi-mesenchymal (QM) and exocrine-like subtypes (Collisson et al., 2011), which is a landmark study that contributes to uncover the heterogeneity of PDAC. By performing microarray gene expression analysis in resected PDAC patient tumors, they identified a 62 gene signatures that allows clustering of tumors into certain subtypes (Collisson et al., 2011). The CLA subtype is found to be associated with high levels of epithelial gene signatures, while QM subtype has a high expression of mesenchymal genes and exhibit poor survival rate compared to CLA subtype. Multiple human and murine PDAC cell lines were able to delineate the CLA and QM subtypes (Collisson et al., 2011), which, in future, could be utilized as a model for studying subtype-specific therapeutic strategies.

After 4 years, another work in PDAC subtyping was conducted by Moffitt et al. (Moffitt et al., 2015). In their study, stroma compartment was taken into consideration and virtual microdissection approach was utilized in primary and metastatic tumors to distinguish between stromal and tumor-specific gene sets. Tumor epithelial compartment can be characterized into classical (CLA) and basal-like (BL) subtypes, which have been shown to overlap with the previous Collisson subtypes (Collisson et al., 2011). In contrast to the CLA subtype, BL subtype has worse prognosis (Moffitt et al., 2015). Besides molecular

subtyping of epithelial-tumor compartments, Moffitt et al. molecularly characterized stromal compartments into two different subtypes: the normal and activated stroma. The so-called normal stroma corresponds to better prognosis, while activated stroma shows inflammatory signature and links to poor prognosis. In comparison to Collisson et al., the Moffitt et al. study has higher prognostic relevance since stroma subtypes were included and showed distinct tendencies.

In 2016, Bailey et al. performed RNA sequencing (RNA-seq) analysis in 96 bulk tumors to explore the transcriptional network and revealed four subtypes called progenitor, immunogenic, aberrantly differentiated endocrine exocrine (ADEX), and squamous (Bailey et al., 2016). The progenitor subtype is linked to the transcriptional programs, which are essential for endoderm fate determination. The immunogenic subtype shares high similarities with progenitor, and regulates pathways involving in antigen presentation and B cell signaling. While ADEX tumors exhibit molecular signatures associated with pancreatic differentiation and development (Bailey et al., 2016). The most aggressive squamous subtype is associated with metabolic reprogramming, hypoxia, as well as inflammation. Furthermore, The Cancer Genome Atlas (TCGA) research network confirmed a significant overlap of the squamous to the BL subtype (Cancer Genome Atlas Research Network, 2017), previously identified by Moffitt et al. Besides, previously defined CLA subtype (Collisson et al., 2011 and Moffitt et al., 2015) that largely overlapped with the progenitor subtype (Bailey et al., 2016). However, ADEX and immunogenic subtypes were found to have less tumor purity, i.e. a high degree of contamination with non-neoplastic cells.

Puleo et al. conducted a microarray analysis in a large cohort of patient samples from 309 paraffin embedded PDAC tissues (Puleo et al., 2018). An unsupervised analysis concluded five subtypes: pure classical, immune classical, desmoplastic, stroma activated, and pure basal-like. With a high cellularity, tumors were classified into pure classical and pure basal-like subtypes. Notably, they identified a significant association of pure classical to well differentiated/low grade tumors. In contrast, pure basal-like subtype is linked to poorly differentiated/high grade tumors. The overall survival rate of pure basal-like patients represent significantly lower compared to pure classical subtype.

In addition, most recent work from Chan-Seng-Yue et al. suggested the intra-subtype heterogeneity within the previously existing CLA and BL PDAC subtypes (Chan-Seng-Yue et al., 2020). Overall, this study overcomes the limitation of the previous studies that only have access to resected tumor tissues where the genomic signatures from high-grade tumors or advanced stage tumors could be underrepresented. The transcriptomic based analysis of the primary and metastatic PDAC tumors identified classical-A, classical-B, hybrid, basal-like A, and basal-like B subtypes (Chan-Seng-Yue et al., 2020). Interestingly, this study suggested that basal-like A subtype is the most aggressive phenotype, which occurs in very late stage tumors, conferring high resistance to chemotherapy and consequently worse prognosis. Basal-like B was found predominantly in the resectable PDAC tumors. However, CLA and BL subtypes were coexisted intratumorally (Chan-Seng-Yue et al., 2020), suggesting the highly heterogeneous phenotype of PDAC.

Table 1. PDAC subtypes.

Study	Samples	Methodology	Subtypes	Significance/implications
Collisson et al. 2011	63 resected PDAC tumors (27 microdissected; 35 whole PDAC), and 19 PDAC cell lines	microdissection transcriptome (microarray)	•Classical •QM •Exocrine-like	•QM has poor survival compared to classical subtype
Moffitt et al. 2015	206 tumors (145 primary; 660 metastatic), and 134 normal pancreas	Virtual microdissection transcriptome (microarray)	•Tumor compartment: classical and basal-like •Stromal compartment: activated and normal	•Basal-like and activated stroma subtype are correlated with worse prognosis •Basal-like tumors seems to benefit more from adjuvant therapy
Bailey et al. 2016	266 primary PDAC tumors	Transcriptome (RNA-seq)	•Pancreatic progenitor •Immunogenic • ADEX •Squamous	•Squamous is associated with poor survival

TCGA 2017	150 PDAC tumors	Transcriptome (RNA-seq)	Overlap of existed subtypes (high-purity tumors): •Classical/progenitor •Basal-like/ squamous	•Inhibition of MTOR pathway might be beneficial for *KRAS* wild-type patients
Puleo et al. 2018	309 resected primary PDAC tumors	Transcriptome (microarray)	•Pure classical •Immune classical •Desmoplastic •Stroma activated •Pure basal-like	•Pure basal-like is associated with poor survival
Chan-Seng-Yue et al. 2020	248 PDAC tumors (primary and metastatic)	Laser capture microdissection transcriptome (RNA-seq)	•Classical-A •Classical-B •Hybrid •Basal-like-A •Basal-like-B	•Basal-like-A is highly resistant to chemotherapy, associated with extremely poor prognosis

ADEX, Aberrantly differentiated endocrine exocrine; QM, Quasi-mensenchymal; RNA-seq, RNA sequencing; TCGA, The Cancer Genome Atlas.

Altogether, these transcription-based studies suggest the two most clinical-relevant PDAC molecular subtypes: the CLA subtype, characterized by expression of epithelial markers and corresponding to favorable prognosis, and the BL subtype, associated with high levels of epithelial-to-mesenchymal (EMT) signatures and correlating to unfavorable prognosis (**Figure 2**). Indeed, these subtypes show different vulnerabilities to chemotherapy: in particular, BL tumors show a high degree of chemoresistance, promoting a poor patient prognosis. The COMPASS trial reported by Aung et al. showed that the CLA subtype patients respond better to either modified FOLFIRINOX or gemcitabine/ plus nab-paclitaxel chemotherapy, while BL subtype still continuously progress under treatment (Aung et al., 2018).

CLA subtype

BL subtype

- Well differentiated
- Chemoresponsive
- **Better prognosis**

- Poorly differentiated
- Chemoresistant
- **Poor prognosis**
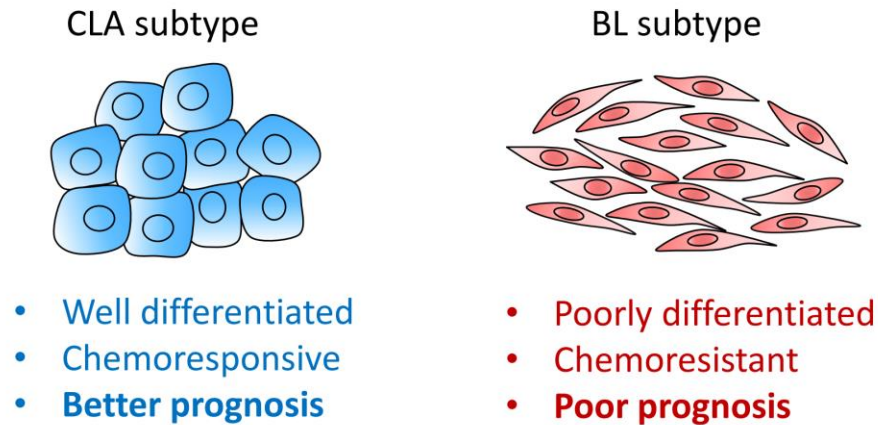
Figure 2. Characteristics of CLA and BL PDAC subtypes. PDAC can be robustly characterized into two subtypes: CLA and BL subtype. They display distinct tumor histology features, chemoresistance as well as prognosis.

1.3 Subtype-specific regulatory network

Despite having defined the prognostically relevant CLA and BL subtypes, the regulatory networks within tumor cells, especially the key transcription factors (TFs) that control subtype-specific gene programs and maintain their cellular identity, remain largely unknown. An initial study comprehensively addressed the subtype-specific transcriptional regulation as well as control of lineage-specific markers in PDAC phenotypic identity (Diaferia et al., 2016). By performing RNA-seq analysis in established human PDAC cell lines, they identified a set of genes corresponding to high- and low-grade tumors, reflecting CLA and BL tumors respectively. Among those, KLF5, ELF3, HNF1B, as well as JUNB were mainly expressed in low-grade tumors. In contrast, high-grade tumors showed abundant expression of ZEB1, GATA2 and ETV5 (Diaferia et al., 2016). Besides these grade-specific markers, 'GATA6' emerged as a potential biomarker for the CLA subtype identity in PDAC patient tumors (Aung et al., 2018; Chan-Seng-Yue et al., 2020). PDAC patients with high-grade tumors expressed significantly low GATA6, supporting by RNA *in situ* hybridization assay in the tumors (Aung et al., 2018). Further, to determine the role of GATA6 in the regulation of cell identity, Martinelli et al. employed shRNA-

mediated GATA6 silencing in multiple low-grade PDAC cell lines (Martinelli et al., 2017). Intriguingly, genetic inactivation of GATA6 led to loss of epithelial-lineage markers (e.g. E-cadherin) and gain of the EMT-related markers such as vimentin in the GATA6-depleted PDAC cells. Furthermore, cells acquired significantly more invasive and BL phenotypic identity upon GATA6 silencing. Furthermore, patients with low expression of GATA6 have shorter survival and a poor response to chemotherapy compared to those who have medium or high levels of GATA6 (Martinelli et al., 2017, Aung et al 2018). Recently, HNF4A, a low-grade lineage TF found to be an essential player in maintaining CLA subtype identity (Brunton et al., 2020). NHF4A depleted cells showed induction of BL phenotype gene signature, with upregulation of gene sets involved in WNT, insulin, as well as phosphatidylinositol 3-kinase (PI3K)-AKT signaling pathways. Besides, loss of HNF4A led to activation of BL-associated metabolic signatures (Brunton et al., 2020).

Overall, identification of low-grade/CLA-specific TF (i.e. GATA6) turned out to be a significant tool for PDAC patient stratification. Similarly, several studies have focused on deciphering the gene regulatory network underlying BL phenotype. Notably, it has recently been shown that TFs such as GLI2 and TP63 (ΔNp63) maintain BL subtype identity (Adams et al., 2019; Somerville et al., 2018). GLI2 alone is sufficient to cause a switch from CLA to BL subtype in PDAC cells (Adams et al., 2019). Similarly, TP63 was also identified as a key factor that controls a transcription regulatory network supporting the squamous/BL phenotypic state. Moreover, ectopic expression of TP63 was shown to be sufficient to induce the reprogramming of TFs for the maintenance of a squamous differentiation in PDAC (Somerville et al., 2018). Whether and how lineage-specific TFs recruit chromatin regulators to shape PDAC subtype plasticity remain poorly understood. Recent studies have shown that chromatin regulator lysine demethylase 6A (KDM6) is required to maintain the CLA PDAC subtype identity both *in vitro* and *in vivo* (Andricovich et al., 2018). Pancreas specific loss of *Kdm6a* (*Kras-Kdm6a*$^{-/-}$ mice) displayed poorly differentiated histological features. Mechanistically, global gene expression profile showed that depletion of *Kdm6a* led to enrichment of EMT, pro-inflammatory, and response to hypoxia pathways, corresponding to BL phenotypic identity (Andricovich et al., 2018).

Altogether, these studies have provided evidence for the mechanisms of regulation of PDAC subtypes. Here, we propose a model of lineage TFs determined subtype identity (**Figure 3**). By exploring the specific lineage markers, it will be possible to exploit clinical diagnostic markers as well as tailored therapeutic approaches.
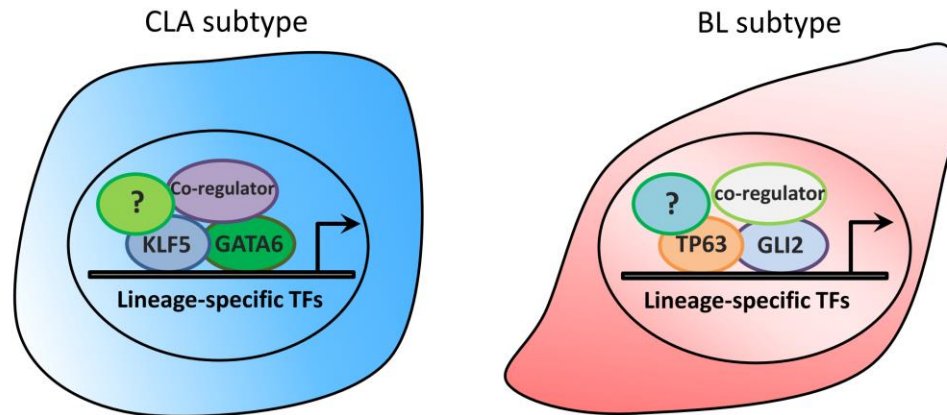
Figure 3. Proposed model of tumor-specific TFs in PDAC subtype maintenance. Lineage-specific TFs and coregulators shape CLA and BL subtype identity.

1.4 The tumor microenvironment

The TME of PDAC has a significant impact on tumor initiation, progression, and metastasis (Hessmann et al., 2020). PDAC has a complex TME that consists of endothelial cells, cancer-associated fibroblasts (CAFs), tumor cells, extracellular matrix (ECM), immune cells, and soluble factors such as growth factors, cytokine, and chemokine (**Figure 4**). CAFs and Tumor-associated macrophages (TAMs) are two prominent components of the inflammatory TME. In most of the solid tumors, the existence of TAMs is associated with an unfavorable prognosis (Komohara et al., 2014; Zhang et al., 2012). In PDAC, high expression of macrophage signatures are associated with poor prognosis (Bailey et al., 2016). Single-cell analysis performed by Hosein et al. revealed that the population of TAMs dramatically increased at the late stage of the disease compared to the initial phase, indicating the correlation between macrophage and aggressive PDAC phenotype (Hosein et al., 2019). Moreover, Candido et al. showed

that macrophage represses T cell activity to allow for tumor growth and is associated with the squamous phenotype (Candido et al., 2018). A subtype switch from squamous to progenitor could be seen upon macrophage depletion. In addition, the macrophage is found to inhibit the efficiency of gemcitabine by releasing pyrimidine nucleosides (Halbrook et al., 2019). Targeting macrophage via inhibitor against the colony stimulating factor 1 receptor (CSF1R) could restore the effect of gemcitabine (Candido et al., 2018).
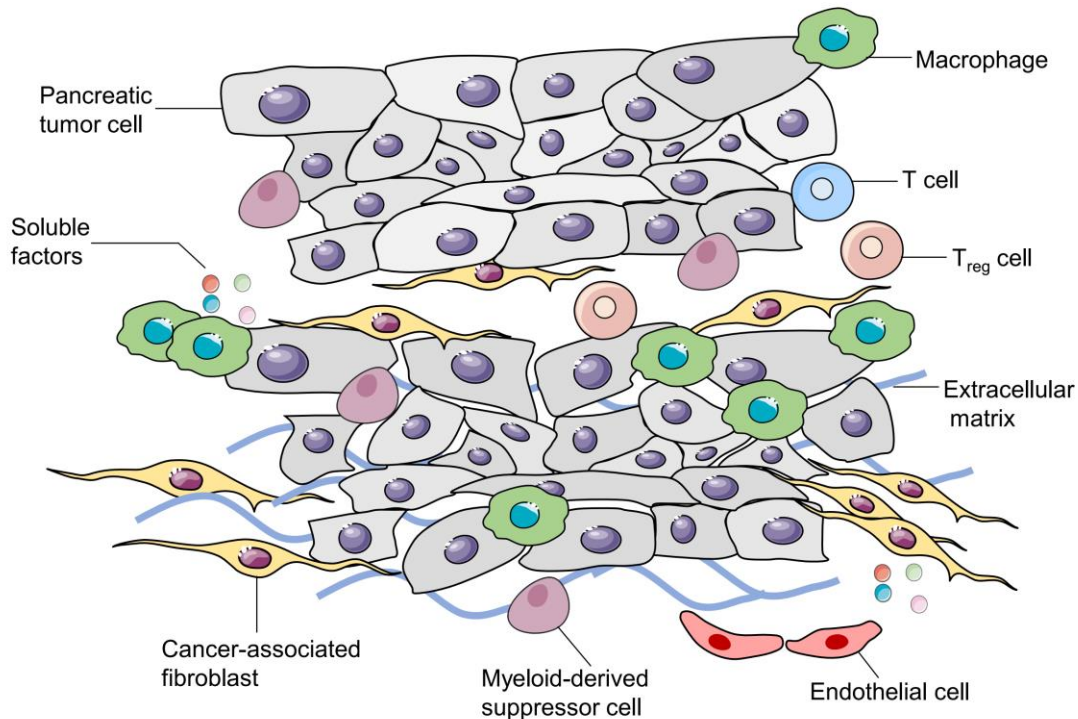
Figure 4. Stromal immune microenvironment of PDAC. The TME of PDAC comprises diverse cell types including tumor cell, endothelial cell, CAFs, extracellular matrix, soluble factors, as well as immune cells, such as T cell, T_{reg} cell, TAMs and myeloid-derived cell.

1.4.1 Inflammatory tumor stroma microenvironment

1.4.1.1 Role of inflammation in tumor progression

Inflammatory microenvironment is evidenced to be an essential content for almost all types of tumors (Mantovani et al., 2008). It is well established that inflammation-linked

diseases increase the risk of cancer development, as in prostate cancer, ovarian cancer, gastric cancer, intestinal cancer, as well as bladder cancer (Grivennikov et al., 2010; Mantovani et al., 2008). Inflammation has a significant impact on PDAC tumor development and progression (Guerra et al., 2007; Rhim et al., 2012., Singh et al 2015). Apart from smoking and alcohol consumption, chronic pancreatitis is considered the main risk factor for developing PDAC (Yadav and Lowenfels, 2013). Inflammation is initially induced in the context of pancreatitis to prevent the loss of homeostasis and promote tissue regeneration. For example, acinar cells transform into duct-like architecture termed acinar-to-ductal metaplasia (ADM) in response to inflammatory cues (Liou et al., 2013). Normally, ADM is highly plastic and reversible to allow the repair of pancreatic injury (Rooman and Real, 2012; Stanger and Hebrok, 2013). However, in the context of cancer, with the constitutively activation of oncogene *KRAS* and chronic presence of inflammatory cytokines, acinar cell displays a high degree of abnormalities and develops into full-blown PDAC (Logsdon and Ji, 2009).

Rihm et al. have unveiled a significant role of inflammation in pancreatic tumor formation and dissemination (Rhim et al., 2012). In the metastatic PDAC mouse model, EMT and invasiveness were extensively surrounded by inflammatory cells. Cerulein-induced inflammation in mice resulted in accelerated formation of PanIN lesions and increased circulating cells. For the confirmation of inflammation induced EMT, mice received anti-inflammatory drug, which showed a general reduction of inflammation and feebly developed PanIN lesions (Rhim et al., 2012). Based on these data, we proposed a model that the external stimulus (e.g. cytokines or chemokines) from the inflammatory microenvironment might induce PDAC subtype switch, which, in turn, lead to disease aggressiveness (**Figure 5**).
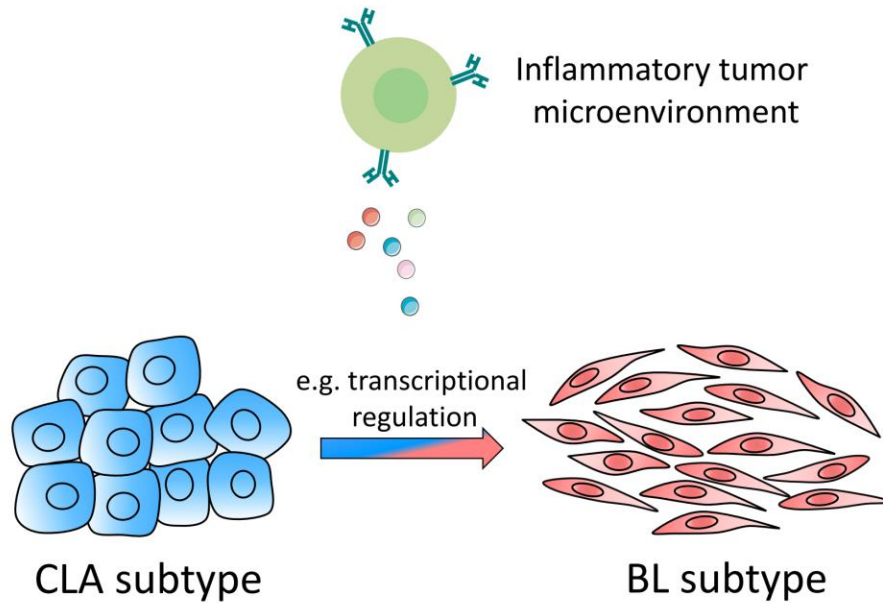
Figure 5. Inflammation-driven subtype shaping in PDAC. Inflammatory cytokines and chemokines secreted from the TME might induce formation of an aggressive subtype.

A recent study by Cobo et al. showed cell-autonomous reprogramming driven by inflammation that regulated the differentiation of acinar cells and contributed to the development of PDAC (Cobo et al., 2018). The orphan nuclear receptor NR5A2 is involved in pancreatic embryonic development and controls acinar cell differentiation (Hale et al., 2014). In PDAC patients, there is a strong correlation of low NR5A2 expression to the patients who had chronic pancreatitis previously (Cobo et al., 2018). In *Nr5a2* wild type mice, NR5A*2* binds on genes that maintain acinar cell differentiation. Interestingly, NR5A2 shifts its binding from acinar-related genes to inflammatory genes in *Nr5a2$^{+/-}$* pancreata, via interaction with cJUN/AP-1 transcription factor. Caerulein-treated (induce pancreatitis) wild type mice also exhibited a similar inflammatory profile. Notably, inhibition of cJUN TF led to abrogation of this transcriptional switch, thus, inflammatory gene expression was halted. Mechanistically, NR5A2 cooperates with *Nr0b2* to represses cJUN activity to maintain low inflammation and favorable outcome (Cobo et al., 2018). Therefore, NR5A2 loss leads to high induction of cJUN and further facilitate the acinar-to-inflammatory switch, which leads to unfavorable outcome.

1.4.1.2 Tumor stroma microenvironment in disease progression

Cytokines are key soluble factors in connecting inflammation to cancer (Grivennikov et al., 2010). They play a crucial role in modulating cellular components in TME, especially the interactions between epithelial and stromal immune compartment (Shadhu and Xi, 2019). In PDAC microenvironment, the dynamic cross-talk between tumor cells and inflammatory cells is largely determined by cytokines. Inflammatory cells (e.g. TAMs and CAFs) are the main source of cytokine production, secreting IL-1, IL-6, IL-10, TGF-β and TNFα to influence tumor cell behavior and promote PDAC progression (Biffi et al., 2019; Huang et al., 2019; Ikemoto et al., 2000; Karakhanova et al., 2015; Zhao et al., 2016).

TNFα is a well-known master regulator of inflammation and immune response. It is a type II transmembrane protein and is released by the cleavage of a converting enzyme at the site between Ala^{76}-Val^{77} (Wajant, 2009). TNFα can be produced in multiple cell types including macrophage, activated monocyte, activated T cell, dendritic cell, nature killer (NK) cell, microglia, as well as astrocyte (Zidi et al., 2010). TNFR1 (p55) and TNFR2 (p75) were identified as receptors for TNFα. TNFR1 is expressed ubiquitously on all cell types; however, TNFR2 is restricted to endothelial and immune cells (Sethi et al., 2008). While extensive efforts have been made to study the role of TNFα in regulating inflammation and inflammatory disease, the functional relevance of TNFα in tumor progression and drug resistance have not been fully addressed.

Lind et al. revealed a significant role of TNFR1 in skin cancer development (Lind et al., 2004). Squamous carcinoma mouse model develops rather quickly microscopically skin changes in 3 weeks, with massive immune cell infiltration. However, *Tnfr1-/-* mice do not give rise to skin tumor and inflammation (Lind et al., 2004), suggesting that TNFR1-mediated signaling pathway is involved in the development of skin cancer. In breast cancer, over half of the studied patients (105 patients in total) were found to have TNFα abundance in their tumor tissues characterized by immunohistochemistry staining. Tumor cells isolated from patients with high- and low- expression of TNFα were subjected to doxorubicin (DOX) treatment. It showed that TNFα-high expressing cells confer more resistance to DOX compared to TNFα-low expressing cell lines (Zhang et al., 2018). In

PDAC, TNFα induces invasive capacities of the PDAC cells and secretions of IL-8 and MMP9 (Egberts et al., 2008). Administration of TNFα *in vivo* leads to increased tumor growth and metastasis. However, blocking TNFα in combination with chemotherapy reduces tumor volume and metastasis in PDAC models (Egberts et al., 2008). Moreover, Zhao et al. has reported that high levels of TNFα is associated with an unfavourable prognosis in PDAC patients (Zhao et al., 2016).

1.4.2 Reciprocal interaction between stromal and tumors cells in PDAC prognosis

In the TME, studies have shown that the co-existence of stromal cells within tumor cells linked to distinct prognosis in PDAC. Moffitt et al. showed that coexisting activated stroma within BL tumors are linked to poor prognosis (Moffitt et al., 2015). However, Puleo et al., showed that activated stroma within BL tumors led to better survival of PDAC patients (Puleo et al., 2018). Therefore, further studies are required to address the stromal immune determined PDAC subtype identity and prognosis. It is known that tumor cells are capable of changing their phenotype in response to certain inflammatory factors secreted by the stromal compartment, and vice versa (Mantovani et al., 2008). TME can determine the tumor cell differentiation, as implanting identical patient-derived organoids directly into ducts or interstitial space of the pancreas, which induces either an intraductal or a stroma TME, respectively (Miyabayashi et al., 2020). It turned out that the EMT marker vimentin (VIM) was highly elevated in the tumors that grow in a stromal TME compared to the ones grown in intraductal TME. Interestingly, those organoids were also showed to transform stromal cells to gain more invasive properties with the induction of EMT, and specifically, TGF-β and WNT (Miyabayashi et al., 2020). Similarly, another study evidenced that TME shapes the phenotypic status of organoids regardless of the genotype (Raghavan et al., 2020). In addition, the soluble factors from TME induce cell identity shift concordant to gain of BL genes and loss of organoid-related genes (Raghavan et al., 2020).

In summary, these studies highlighted the importance of the dynamic interplay between stromal and epithelial compartments. How the two major PDAC subtypes act to shape

and interact with its microenvironment remains poorly understood. Hence, molecular understanding of the heterotypic interactions within TME could provide a novel insight into the development of specific therapeutic strategies.

1.5 Aims of the study

Recent studies have invested tremendous efforts in molecular classification of PDAC. In particular, the transcriptional profiling of TME indicates a significant correlation of stroma inflammatory gene signatures to distinct clinical outcomes (Singh et al., 2019; Moffitt et al., 2015; Maurer et al., 2019; Puleo et al., 2018). Markedly, the stromal immune compartment within differential epithelial tumor subtypes determine the therapeutic response and prognosis in PDAC (Singh et al., 2019; Moffitt et al., 2015).

Inflammatory cytokines are mediators of the cross talk between tumor cells and microenvironment. For instance, TNFα expression has been shown to be negatively associated with PDAC patient survival (Zhao et al., 2016). Studies have shown that PDAC tumor cells can change the plasticity through transcriptional reprogramming particularly in response to inflammatory cue (Rhim et al., 2012; Singh et al 2015). Therefore, we proposed that TNFα might change the plasticity of PDAC cells and mediate subtype switch from CLA to BL to accelerate the progression of PDAC.

In this study, we aimed to characterize the role of TNFα in PDAC subtype switch as well as examine the underlying mechanisms and the potential of selective pathway interference in PDAC therapy. Our specific aims were as follow:

1. To investigate the role of TNFα in PDAC subtype maintenance and disease aggressiveness;
2. To elucidate the mechanism of TNFα-dependent transcriptional reprogramming in PDAC subtype switch;
3. To explore the intrinsic factors which contribute to PDAC subtype identity and aggressiveness;
4. To identify TNFα-induced subtype-specific chromatin regulators for pharmacological interventions;

5. To evaluate the therapeutic interventions against TNFα-mediated inflammation-regulatory network in a PDAC subtype-specific therapy.

2. Material and methods

2.1 Material

2.1.1 Lab equipment

Table 2. Lab equipment.

Equipment	Company
Agarose electrophoresis chamber	Peqlab Biotechnologie, Erlangen, Germany
Anesthetic vaporizer-Sigma delta	Penlon, Abingdon, UK
Arium pro ultrapure water system	Sartorius, Göttingen, Germany
Aspirator with trap flask (Grant bio FTA-1)	Grant Instruments, Cambridge, UK
Bioanalyzer 2100	Agilent Technologies, Santa Clara, USA
Bioruptor Pico sonication device	Diagenode, Liege, Belgium
Centrifuge-Perfectspin 24R (refrigerated)	Peqlab Biotechnologie, Erlangen, Germany
Centrifuge-Heraeus Megafuge 16 / Multifuge X1R	Thermo Fisher Scientific, Waltham, USA
CO_2 incubator (HERAcell 240i)	Thermo Fisher Scientific, Waltham, USA
Cold plate-Histocore Arcadia c	Leica Biosystem, Wetzlar, Germany
Fluid Aspiration System – BVC Control	Vacuubrand, Wertheim, Germany
Fluoview F1000 Confocal Microscope	Olympus, Shinjuku, Japan
Freezer 4 ºC	Liebherr, Bulle, Switzerland
Freezer -20 ºC	Liebherr, Bulle, Switzerland
Freezer -80 ºC	Sanyo Electric, Japan
Heated Paraffin Embedding Module – EG1150 H with cold plate	Leica Biosystems, Nussloch, Germany
gentleMACS dissociator	Miltenyi Biotec, Bergisch Gladbach, Germany
Ice flaker-AF80	Scotsman, Edinburgh, UK
INTAS UV System	Intas Science Imaging Instruments, Göttingen, Germany
Liquid nitrogen cell storage canister-Biocane 47	Thermo Fisher Scientific, Waltham, USA

Light microscope "BX43"	Olympus, Shinjuku, Japan
Microplate reader PHOmo / LUmo	Autobio Labtec Instruments, Zhengzhou, China
Microscope-Axiovert 25	Carl Zeiss, Oberkochen, Germany
Microwave heat pad for animals-snuggleSafe	SnuggleSafe Lenric C21, West Sussex, UK
Nano Photometer-P330	Intas Science Imaging, Göttingen, Germany
Nalgene Mr. Frosty freezing container	Thermo Fischer Scientific, Waltham, USA
Neubauer counting chamber	Brand, Wertheim, Germany
Paraffin tissue embedder (EG1150H)	Leica Biosystems, Wetzlar, Germany
Perfect Spin 24Plus Microcentrifuge	VWR/Peqlab, Erlangen, Germany
Perfect Spin 24R Refrigerated Microcentrifuge	VWR/Peqlab, Erlangen, Germany
pH meter-FiveEasy Plus FEP20	Mettler Toledo, Schwerzenbach, Switzerland
Plate Spinner-PerfectSpin P	Peqlab Biotechnologie, Erlangen, Germany
PowerPac HC High-Current Power Supply	Bio-Rad Laboratories, Hercules, USA
Qubit Fluorometer-Q32854	Invitrogen, Karlsruhe, Germany
StepOnePlus real-time PCR system	Applied Biosystems, Foster City, USA
Rotary Microtome-RM2265	Leica Biosystems, Nussloch, Germany
Shaker-Duomax 1030	Heidolph Instruments, Schwabach, Germany
Shaver-ER-PA10	Panasonic Corporation, Osaka, Japan
StepOnePlus Real-Time PCR System	ThermoFisher Scientific, Waltham, USA
Tissue dehydration machine	Leica Biosystems, Nussloch, Germany
Trans-Blot Turbo Transfer System	Bio-Rad Laboratories, Hercules, USA
Tube Rotator	Stuart, Staffordshire, UK
Ultrasound scanner Vevo 2100	Fujifilm VisualSonics, Toronto, Candada
Vacuum pump: BVC Control	Vacuumbrand, Wertheim, Germay
VS120 virtual slide microscope	Olympus, Shinjuku, Japan
Vortexer Lab Dancer	Ika-Werke, Staufen, Germany
Vortexer Vornado	Benchmark Scientific, Edison, USA
Water bath WNB 14	Memmert, Schwabach, Germany

Weighing balance	Sartorius, Göttingen, Germany

2.1.2 Consumables

Table 3. Consumables.

Consumables	Company
Cell culture inserts – 8 µm pore size (BD 353097)	Sarstedt, Nümbrecht, Germany
Cell scraper 25 cm	Sarstedt, Nümbrecht, Germany
Centrifuge tube (15/50 mL)	Sarstedt, Nümbrecht, Germany
Cryotube 1.5 mL	Sarstedt, Nümbrecht, Germany
Embedding cassettes	Th. Geyer, Renningen, Germany
Eye and nose ointment - Bepanthen	Bayer Vital, Leverkusen, Germany
Glass coverslips (24×32, 24×60)	Menzel, Braunschweig, Germany
Hair removal cream-Veet	RB Healthcare UK, Hull, UK
Injection needle (sterile)	B.Braun, Melsungen, Germany
Insulin syringes 30G-BD Micro-Fine + Demi	Becton, Dickinson and Company, Franklin Lakes, USA
Membrane filter 0.45 µm	Merck Millipore, Billerica, USA
MicroAmp optical 96-well reaction plate	Applied Biosystems, Foster City, USA
Microtome blade	Feather, Osaka, Japan
Microtube (0.5/1.5/2 mL)	Sarstedt AG & Co., Nuembrecht, Germany
Nitrocellulose membrane	GE Healthcare Life Sciences, Marlborough, USA
Optical adhesive covers	Applied Biosystems, Foster City, USA
Parafilm	Pechiney Plastic Packaging, Menasha, USA
PCR tubes	Sarstedt, Nümbrecht, Germany
Scalpel	Feather, Osaka, Japan
Serological pipette (2/5/10/25 mL)	Greiner Bio-One, Frickenhausen, Germany
Syringe (1 mL)	BD Plastic, Madrid, Spain
Syringe (5/10/20 mL)	B.Braun, Melsungen, Germany

Labsolute Sterile syringe Filter (0.2 µm)	Th.Geyer Ingredients, Höxter, Germany
TC dish 100	Sarstedt, Nümbrecht, Germany
TC flask (T25/75/175)	Sarstedt, Nümbrecht, Germany
TC multiwell plates (6/12/24 wells)	Greiner Bio-One, Frickenhausen, Germany
Thick blot filter paper	Bio-Rad, Hercules, CA, USA
Tissue cassette	Sanowa, Leimen, Germany
Ultrasond gel	Asmuth Medizintechnik, Minden, Germany
Wound clips-Reflex 9	CellPoint Scientific, Gaithersburg, USA

2.1.3 Chemicals and reagents

Table 4. Chemicals and reagents.

Chemical / Reagents	Company
6x DNA Loading Dye	Thermo Fisher Scientific, Waltham, USA
Acrylamide solution (30%/0.8%)	AppliChem, Darmstadt, Germany
Acetic acid 100% p.A.	AppliChem, Darmstadt, Germany
Agarose	Nippon Genetics Europe, Düren, Germany
Agarose protein A beads, fast flow	Merck Millipore, Billerica, USA
Ampicillin	Carl Roth, Karlsruhe, Germany
β-Mercaptoethanol	Merck, Darmstadt, Germany
Bromophenol blue	Sigma-Aldrich, St. Louis, USA
Bradford protein assay	Bio-Rad, Hercules, USA
Bovine serum Albumin	Sigma-Aldrich, St. Louis, USA
Chloroform p.a.	Th. Geyer, Renningen, Germany
Citric acid monohydrate	Carl Roth, Karlsruhe, Germany
Collagen I, rat tail	Enzo Life Sciences, Lörrach, Germany
Dimethyl sulfoxide	Sigma-Aldrich, St. Louis, USA
Disodium phosphate	Carl Roth, Karlsruhe, Germany
Dithiothreitol	Sigma-Aldrich, St. Louis, USA

EDTA	Merck Millipore, Billerica, USA
EGTA	Sigma-Aldrich, St. Louis, USA
Eosin Y solution, aqueous	Sigma-Aldrich, St. Louis, USA
Epidermal growth factor	Sigma-Aldrich, St. Louis, USA
Ethanol absolute p.a.	Th. Geyer, Renningen, Germany
Formaldehyde (37%)	Sigma-Aldrich, St. Louis, USA
Formaldehyde solution (4%), buffered	Merck, Darmstadt, Germany
FastGene 100 bp DNA marker	Nippon Genetics Europe, Düren, Germany
GeneRuler 1 kb DNA ladder	Thermo Fisher Scientific, Waltham, USA
Glycine	Carl Roth, Karlsruhe, Germany
Glycerol	Carl Roth, Karlsruhe, Germany
HEPES	Carl Roth, Karlsruhe, Germany
Hematoxylin	Sigma-Aldrich, St. Louis, USA
Hydrochloric acid	Carl Roth, Karlsruhe, Germany
Hydrogen peroxide 30%	Carl Roth, Karlsruhe, Germany
Isopropanol	Sigma-Aldrich, St. Louis, USA
Isoflurane	AbbVie Deutschland, Wiesbaden, Germany
iTaq Universal SYBR Green Supermix	Bio-Rad, Hercules, CA, USA
Immu-Mount	Thermo Fisher Scientific, Waltham, USA
(+)-JQ1	MedChemExpress, Monmouth Junction, USA
Lipofectamine 2000 reagent	Invitrogen, USA
Lithium chloride	Sigma-Aldrich, St. Louis, USA
Matrigel	Abcam, Cambridge, UK
Monosodium phosphate	Merck, Darmstadt, Germany
NP-40	Thermo Fisher Scientific, Waltham, USA
Non-fat milk powder	Carl Roth, Karlsruhe, Germany
Normal goat serum	Abcam, Cambridge, UK
PageRuler Prestained Protein Ladder	Thermo Fisher Scientific, Waltham, USA
Paraffin	Engelbrecht, Edermünde/ Besse, Germany

Paraformaldehyde	Merck, Germany
PBS Dulbecco, powder	Biochrom, Berlin, Germany
Phenylmethylsulfonyl fluoride	Sigma-Aldrich, St. Louis, USA
Pierce TM ECL Western Blotting Substrate	Thermo Fisher Scientific, Waltham, USA
Ponceau S solution	Sigma-Aldrich, St. Louis, USA
Protease inhibitor cocktail cOmplete	Roche Diagnostics, Mannheim, Germany
Protein Assay Dye Reagent Concentrate (Bradford reagent)	Bio-Rad, Hercules, USA
Rotimount	Carl Roth, Germany
Roticlear	Carl Roth, Karlsruhe, Germany
RotiPhenol/chloroform/isoamylalcohol (25:24:1)	Carl Roth, Karlsruhe, Germany
Saline (0.9 % NaCl)	B.Braun, Melsungen, Germany
siLentFect Lipid reagent	Bio-Rad, Hercules, CA, USA
Sodium chloride	Merck, Darmstadt, Germany
Sodium dodecyl sulfate	Carl Roth, Karlsruhe, Germany
Sodium deoxycholate	Sigma-Aldrich, St. Louis, USA
Sodium fluoride	Sigma-Aldrich, St. Louis, USA
Sodium orthovanadate	Sigma-Aldrich, St. Louis, USA
Trans-Blot Turbo 5x transfer buffer	Bio-Rad Laboratories GmbH, Neuberg, Germany
Tetrasodium pyrophosphate	Sigma-Aldrich, St. Louis, USA
Tris-HCl	Carl Roth, Karlsruhe, Germany
Tris-base	Carl Roth, Karlsruhe, Germany
Triton X-100	Carl Roth, Karlsruhe, Germany
TRIzol	ThermoFisher Scientific, Waltham, USA
Tumor Necrosis Factor-α human	Sigma-Aldrich, St. Louis, USA
Tumor Necrosis Factor-α human	PeproTech, Hamburg, Germany
Tween-20	Sigma-Aldrich, St. Louis, USA
Western Lightning ECL plus	PerkinElmer, Waltham, USA
Western Lightning ECL ultra	PerkinElmer, Waltham, USA

Xylene	AppliChem, Darmstadt, Germany

2.1.4 Kits and plasmids

Table 5. Kits used in the study.

Kits	Company
Bioanalyzer High Sensitivity DNA Analysis Kit	Agilent Technologies, Santa Clara, California, USA
CellTiter-Glo Luminescent Cell Viability Assay Kit	Promega, Madison, USA
ChIP DNA Clean & Concentrator kit	Zymo Research Europe, Freiburg, Germany
Human Tumor Dissociation Kit	Miltenyi Biotec, Bergisch Gladbach, Germany
Human CCL2/MCP-1 Quantikine ELISA Kit	R&D Systems, Minneapolis, USA
Human TNFα Quantikine ELISA Kit	R&D Systems, Minneapolis, USA
iScript cDNA Synthesis Kit	Bio-Rad Laboratories, Hercules, USA
Mouse Cell Depletion Kit	Miltenyi Biotec, Bergisch Gladbach, Germany
Mouse TNFα Quantikine ELISA Kit	R&D Systems, Minneapolis, USA
Proteome Profiler Human Cytokine Array Kit	R&D Systems, Minneapolis, USA
Proteome Profiler Mouse Cytokine Array Kit, Panel A	R&D Systems, Minneapolis, USA
TruSeq RNA Library Prep Kit v2	Illumina, San Diego, USA

Table 6. Plasmids used in the study.

Plasmids	Company
pMD2.G	Addgene, Watertown, USA
psPAX2	Addgene, Watertown, USA
pCDH-TNFα	Addgene, Watertown, USA
pLKO.1	Addgene, Watertown, USA
pMSCV-cJUN	Addgene, Watertown, USA

pMSCV	Addgene, Watertown, USA

2.1.5 Drugs

Table 7. Therapeutic drugs.

Drug	Company
Carprieve	Norbrook Laboratories, Newry, UK
Gemcitabine hydrochloride	Sigma-Aldrich, St. Louis, USA
Oxaliplatin	Sigma-Aldrich, St. Louis, USA
SN38	Sigma-Aldrich, St. Louis, USA
Buprenorphine	Bayer Vital, Leverkusen, Germany

2.1.6 Nucleic acids

2.1.6.1 siRNA oligonucleotides

Table 8. siRNA used in the study.

siRNAs	Catalogue number	Company
Negative control siRNA	AM4611	Thermo Fisher Scientific, Waltham, USA
cJUN #1	AM16704	Thermo Fisher Scientific, Waltham, USA
cJUN #2	AM16708	Thermo Fisher Scientific, Waltham, USA
BRD4 #1	J-004937-06-0002	Dharmacon, Lafayette, USA
BRD4 #2	J-004937-07-0002	Dharmacon, Lafayette, USA

2.1.6.2 Primers

Table 9. Primers used for qRT-PCR (human).

Gene	Forward primer	Reverse primer
XS13	TGGGACAGAACACCATGATG	AGTTTCTCCAGAGCTGGGTTGT

cJUN	TCCAAGTGCCGAAAAAGGAAG	CGAGTTCTGAGCTTTCAAGGT
CCL2	CAGCCAGATGCAATCAATGCC	TGGAATCCTGAACCCACTTCT

Table 10. Primers used for ChIP-qPCR (human).

Gene	Forward primer	Reverse primer
CCL2 Promoter	GCTTAATGGCACCCCATCCT	GGGTCAGGACGAGACACTTTT
CCL2 Enhancer	CCACTCACTTCTCTCACGCC	CTGTCTGCCTCCCACTTCTG
JUN Enhancer 1	TGCTGCTGTAGTGCACATTCT	AGCACAGACCTTTCTGCTGG
JUN Enhancer 2	ATGGACACTCATACATCAGAGAGC	CTCAGCGTTCTCATCCGTGT
JUN Enhancer 3	AGATTTCTGGGATCCGGCTTG	CCGAGGAAAGCTCTTCGCAA
CDH1 Promoter	GGTGAACCCTCAGCCAATCAG	AGTTCCGACGCCACTGAGA
CDH1 Enhancer 1	GAGGCGGTATAGCCAGTTCC	CTGCTCCTAGAGGCTCCTGA
CDH1 Enhancer 2	GCTCGTGGAGGTTGTGTAGAA	CAAGCAGAAGCTGACAAGTTCAA
VIM Promoter	ATCTGGGAGGCCCACGTAT	TCTTTGCTCGAATGTGCGGA
VIM Enhancer 1	ATTCCAAACCCCTGGATGATGTC	GGATATGCTAGTGCTCTGACTGTT
VIM Enhancer 2	AAGTTGCCTAAGTAACATCAATGCC	GGGTCTGAAACCCAACACACT

2.1.7 Antibodies and enzymes

Table 11. Antibodies used for western blot.

Antibodies	Dilution	Catalogue number	Company
BRD4	1:1000	ab128874	Abcam, Cambridge, UK
CCL2	1:1000	MA5-17040	Invitrogen, Eugene, USA
cJUN	1:1000	9165S	Cell Signaling Technology, Danvers, USA
E-Cadherin	1:1000	610181	BD Bioscience, San Jose, USA
JUNB	1:1000	3753S	Cell Signaling Technology, Danvers, USA
JUND	1:1000	sc-74	Santa Cruz Biotechnology, Dallas, USA
β-actin	1:40000	A3854	Sigma-Aldrich, St. Louis, USA

Anti-mouse IgG (HRP)	1:6000	7076S	Cell Signaling Technology, Danvers, USA
Anti-rabbit IgG (HRP)	1:6000	7074S	Cell Signaling Technology, Danvers, USA

Table 12. Antibodies used for flow cytometry analysis.

Antibodies	Dilution	Catalogue number	Company
TNFα	1:20	502908	BD Bioscience, San Jose, USA
IgG1, κ isotype control	1:20	553973	BD Bioscience, San Jose, USA

Table 13. Antibodies used for immunofluorescence staining.

Antibodies	Dilution	Catalogue number	Company
α-Amylase	1:100	3796	Cell Signaling Technology, Danvers, USA
CCL2	1:1000	MA5-17040	Invitrogen, Eugene, USA
CK19	1:100	ab52625	Abcam, Cambridge, UK
CD45	1:50	550539	BD Biosciences, San Jose, USA
CD68	1:50	ab955	Abcam, Cambridge, UK
cJUN	1:100	9165S	Cell Signaling Technology, Danvers, USA
JUNB	1:100	3753S	Cell Signaling Technology, Danvers, USA
KRT81	1:100	sc-100929	Santa Cruz Biotechnology, Dallas, USA
TNFα	1:50	ab1793	Abcam, Cambridge, UK
Goat anti-rabbit IgG-Alexa Fluor 488	1:500	A-11008	Thermo Fisher Scientific, Waltham, USA
Goat anti-mouse IgG-Alexa Fluor 568	1:500	A-21124	Thermo Fisher Scientific, Waltham, USA
Goat anti-rat IgG-Alexa Fluor 647	1:500	A-21247	Thermo Fisher Scientific, Waltham, USA

Table 14. Antibodies used for ChIP.

Antibodies	Catalogue number	Company
BRD4 antibody	C15410337	Diagenode, Liege, Belgium
cJUN antibody	9165S	Cell Signaling Technology, Danvers, USA
JUNB antibody	3753S	Cell Signaling Technology, Danvers, USA
H3K27ac antibody	GTX128944	GeneTex, Alton Pkwy Irvine, USA
Rabbit IgG	C15410206	Diagenode, Liege, Belgium

Table 15. Enzymes used in the study.

Enzymes	Catalogue number	Company
Proteinase K	A4392,0005	AppliChem, Darmstadt, Germany
SuperScript II Reverse Transcriptase	18064022	Thermo Fisher Scientific, Waltham, USA
RNase A	R6513	Sigma-Aldrich, St. Louis, USA

2.1.8 Buffers

2.1.8.1 Buffers for Western blot

Table 16. Whole cell lysates (WCL) buffer.

Name	Components	Final concentration
	HEPES (pH7.5)	50 mM
	NaCl	150 mM
	EGTA	1 mM
WCL buffer	Glycine	10 % (v/v)
	Triton X-100	1 % (v/v)
	NaF	100 mM
	Tetrasodium pyrophosphate	10 mM

Table 17. Laemmli buffer (5x).

Name	Components	Final concentration
Laemmli buffer	Tris (pH6.8)	225 mM
	Glycerin	50 % (v/v)
	SDS	5 % (v/v)
	DTT	100 mM
	Bromophenol blue	0.02 % (v/v)
	β-Mercaptoethanol	5 % (v/v)

Table 18. Separating gel buffer and stacking gel buffer stocks.

Name	Components	Final concentration
Separating gel buffer stock (pH 8.8)	Tris-base	1.5 M
	SDS	0.4 % (v/v)
Stacking gel buffer stock (pH 6.8)	Tris-base	0.5 M
	SDS	0.4 % (v/v)

Table 19. Separating and stacking buffer working solution.

Name	Components	Volume
Separating gel buffer 10%	Separating gel buffer stock	20 mL
	Acrylamide solution (30%/0.8%)	26.6 mL
	Glycerol	4 mL
	Aqua dest	29.3 mL
Separating gel buffer	Separating gel buffer stock	20 mL
	Acrylamide solution (30%/0.8%)	40 mL

15%	Glycerol	4 mL
	Aqua dest	16 mL

Table 20. Running buffer (10x).

Name	Components	Final concentration
Running buffer	Tris-base	250 mM
	Glycerin	1.92 M
	SDS	1 % (w/v)

Table 21. Transfer buffer (1L).

Name	Components	Final concentration
Transfer buffer	5x Transfer buffer	200 mL
	Ethanol	200 mL
	Aqua dest	600 mL

Table 22. TBS buffer (10x).

Name	Components	Final concentration
TBS buffer	Tris-base	121.4 g
(pH 7.6)	NaCl	400.31 g
	Aqua dest	5 L

Table 23. TBST buffer (10x).

Name	Components	Final concentration
TBST buffer	TBS	1X
	Tween	0.1 % (w/v)

Table 24. Blocking solution.

Name	Components	Final concentration
Blocking solution	TBST	1X
	Non-fat milk	5 % (w/v)

2.1.8.2 Buffers for immunofluorescence staining

Table 25. Citrate buffer.

Name	Components	Final concentration
Citrate buffer	Citric acid monohydrate	2.1 g
(pH 6.0)	Aqua dest	1L

Table 26. PB buffer.

Name	Components	Final concentration
PB buffer	Monosodium phosphate	2.4 g
(pH 7.4)	Disodium phosphate	11.31 g
	Aqua dest	1 L

Table 27. PBT buffer.

Name	Components	Final concentration
PBT buffer	PB	1X
	Triton X-100	0.4 % (v/v)

2.1.8.3 Buffers for Chromatin Immuno-Precipitation

Table 28. Nelson buffer.

Name	Components	Final concentration
Nelson buffer	NaCl	150 mM
	EDTA (pH 8)	20 mM
	Tris-HCl (pH 7.5)	50 mM
	NP-40	0.5 %
	Triton X-100	1 %
	NaF	20 mM

Table 29. Gomes wash buffer.

Name	Components	Final concentration
Gomes wash buffer	Tris–HCl (pH 8.5)	100 mM
	LiCl	500 mM
	NP-40	1 % (v/v)
	Sodium deoxycholate	1 % (w/v)
	NaF	20 mM
	EDTA	20 mM

Table 30. Weinmann lysis buffer.

Name	Components	Final concentration
Weinmann lysis buffer	Tris–HCl (pH 8.0)	50 mM
	EDTA	10 mM
	SDS	1 % (v/v)

2.1.9 Cell culture

Table 31. Cell culture components.

Components	Company
Bovine pituitary extract	Sigma-Aldrich, St. Louis, USA
Defined Keratinocyte-SFM Medium	ThermoFisher Scientific, Waltham, USA
Dulbecco's Modified Eagle Medium (DMEM)	ThermoFisher Scientific, Waltham, USA
Fetal calf serum (FCS)	BioWest, Nuaillé, France
Non-essential amino acids (NEAA)	ThermoFisher Scientific, Waltham, USA
Opti-MEM	ThermoFisher Scientific, Waltham, USA
PBS (-Ca/-Mg)	ThermoFisher Scientific, Waltham, USA
Penicillin-streptomycin solution	Sigma-Aldrich, St. Louis, USA
Roswell Park Memorial Institute (RPMI) 1640 Medium	ThermoFisher Scientific, Waltham, USA
Polybrene	Santa Cruz Biotechnology, Dallas, USA
Puromycin	Sigma-Aldrich, St. Louis, USA

2.2 Methods

2.2.1 Animal studies

Animal experiments conducted in this study were approved by the University of Göttingen Central Animal-experimental Facility.

$Kras^{G12D}$;$Trp53^{R172H}$;$PdxCre$ (KPC) tumor tissues used in this study were provided by D. Spyropoulou (Department of Gastroenterology, GI Oncology & Endocrinology, UMG, Germany). In this model, $Kras$ and $Trp53$ were both mutated specifically in the pancreas to induce PDAC as described previously (Hingorani et al., 2005). Histopathological classification of KPC tumors into well-to-moderately (W/M) (G1/G2), or poorly differentiated (G3/G4), was performed by expert pathologist P. Ströbel (Department of Pathology, UMG, Germany).

2.2.1.1 Orthotopic mouse models

10-week old male NMRI-*Foxn1^{nu/nu}* mice were used to generate orthotopic PDAC mouse models. Mice were injected with buprenorphine (0.1 mg/kg body weight) intraperitoneally (i.p.) 30 mins before transplantation. Mice were then kept on a warm plate and anesthetized by inhalation of 2.5 -3.5 % isoflurane in oxygen for surgery. Mice were subcutaneously injected with Carprieve (Norbrook Laboratories, Newry, UK; 5 mg/kg body weight) to ease the pain and inflammation immediately before surgery and one to two days after surgery if necessary. After confirming there was no stimuli reflection, skin was opened (~1 cm cut) on the left side of the mice where pancreas resides. 1×10^6 PDAC cells (CAPAN1, CAPAN2, MiaPaCa2, and PANC1) were suspended in 15 µL culture medium and injected into the tail of the pancreas with an insulin syringe.

For establishing the syngeneic KPC orthotopic mouse model, 10-week old male C57BL6J mice were anesthetized for hair removal before surgery, as described previously (Patzak et al., 2019). 3.5×10^4 KPC cells were injected into the tail of the pancreas. The rest of the procedures was carried out as above.

2.2.1.2 Sonography

Three weeks post transplantation, small animal high-resolution ultrasound was applied weekly to determine the tumor growth, as described previously (Patzak et al., 2019). Briefly, mice were put under isoflurane anesthesia and fixed with surgical tape so that each leg was restrained. Ultrasound gel was applied on the ventral body surface. Subsequently, ultrasound imaging was carried out using an Ultrasound scanner Vevo 2100 (Fujifilm VisualSonics, Toronto, Canada).

2.2.1.3 Treatment

For TNFα studies, CAPAN1-transplanted mice were randomized into two groups. TNFα (PeproTech GmbH, Hamburg, Germany; 0.4 mg/kg body weight) was administrated via i.p. injection three times a week for in total three weeks. Aqua dest. was administrated in control mice.

For anti-TNFα studies, mice were randomized before treatment and administrated with anti-TNFα antibody (Hölzel Biotech, Köln, Germany; 10 µg/g body weight) or IgG isotype control (Hölzel Biotech, Köln, Germany; 10 µg/g body weight) three times a week after 10 days of transplantation.

For JQ1 studies, mice were randomized before treatment. 10 days after transplantation, JQ1 (MedChemExpress, Monmouth Junction, USA; 50 mg/kg body weight,) was administrated via i.p injection daily for three weeks. DMSO was administrated in control mice.

2.2.1.4 Tissue harvesting

Mice were euthanized by inhalation of CO_2 and subsequent cervical dislocation. Whole pancreas, spleen, liver, and blood samples were collected. Samples of pancreatic tumor tissue were snap-frozen and stored at -80 ℃ for further analysis. The rest of tissues were fixed in 4 % formaldehyde solution overnight. Blood samples in heparin tubes were centrifuged at 4000 X g for 10 min at room temperature. Serum was transferred to a microtube and stored at -80 ℃.

2.2.1.5 Paraffin embedding and tissue sectioning

Formaldehyde-fixed tissues were processed with an automatic tissue processer (Leica Biosystems, Nussloch, Germany) prior to paraffin embedding. The dehydration protocol is as follow: 75 min formaldehyde solution, 30 min 55 % ethanol, 45 min 85 % ethanol, 60 min 96 % ethanol, 75 min 99 % ethanol, 70 min 99 % ethanol, 90 min 99 % ethanol, 20 min xylene, 30 min xylene, 70 min xylene, 30 min paraffin, 45 min paraffin, 90 min paraffin. Tissues were then embedded in paraffin blocks. A microtome was used to section tissues at a thickness of 4 µm. Sections were kept at 37 ℃ overnight before further staining.

2.2.1.6 Hematoxylin and Eosin Staining

Tissue sections were deparaffinized in xylene (twice for 30 min). After rehydration in and ethanol series (99 %, 95 %, 70 %, each 1 min), slides were kept in aqua dest. for 3 min.

Subsequently, slides were incubated in hematoxylin solution for 8 min followed by a washing step in running tap water for 7 min. Slides were then transferred shortly (5 s) in aqua dest. containing 0.2 % acetic acid followed by incubation in eosin solution (in 0.2 % acetic acid) for 15 s. Next, slides were dehydrated in increasing concentrations of ethanol (70 % for 30 s, 95 % for 1.5 min, 100 % for 2 min). Finally, slides were cleared in Roticlear and fixed with Rotimount.

2.2.1.7 Tile image

Whole tile image scans of H&E and IF staining were carried out using a VS120 virtual slide microscope (Olympus, Shinjuku, Japan), and resulting images were evaluated using cellSens Dimension software (Olympus, Shinjuku, Japan).

2.2.1.8 Immunofluorescence (IF) staining and quantification

IF was carried out as previously described (Singh et al., 2016). After deparaffinization with two times washing of xylene for 30 mins, sections were rehydrated in a descending order of ethanol (99 %, 96 %, 80 %, each 4 min). Antigen retrieval was achieved by keeping slides boiling in citrate buffer (pH 6.0) for 6 minutes in a microwave, then cooling down for 10 min at room temperature. Subsequently, sections were kept on ice for 20 min and washed five times for 5 min with PB. Afterwards, sections were blocked in 10 % normal goat serum (NGS; Abcam, Cambridge, UK) diluted in PBT buffer for 1.5 h at 4°C. Primary antibodies (**Table 13**) were diluted as indicated in PBT buffer containing 2 % NGS and added onto each slide (100-200 µL), keeping in a humid box overnight at 4°C. Next day, sections were washed five times for 5 min each with PB and subjected to secondary antibodies staining (**Table 13**) for 2 h at 4°C. Secondary antibodies were diluted in PBT buffer containing 2 % NGS. DAPI was diluted to 20 µg/mL in PB and added to sections for 10 min at room temperature. In the end, slides were fixed in Immu-Mount (Thermo Fisher Scientific, Waltham, MA, USA) with a coverslip. IF images were acquired via FluoView 1000 confocal microscopy (Olympus FluoView 1000) and quantified either manually by counting positive cells or by measuring staining intensity (as integrated density above a set threshold, given as arbitrary units (A.U.)) using ImageJ Fiji software (Schindelin et al., 2012).

2.2.2 Cell culture

2.2.2.1 Cell culture for established PDAC cell lines

Human PDAC cell lines (CAPAN1, CAPAN2, PANC1, and MiaPaCa2) were obtained from the ATCC. PT45P1 cell line was kindly provided by G. Natoli (Humanitas University, Malian, Italy). CAPAN1, CAPAN2, and PT45P1 were cultured in Roswell Park Memorial Institute (RPMI) 1640 Medium (ThermoFisher Scientific, Waltham, USA) supplemented with 10% fetal calf serum (FCS; BioWest, Nuaillé, France). PANC1 and MiaPaCa2 were cultured in Dulbecco's modified Eagle's Medium (DMEM; ThermoFisher Scientific, Waltham, USA) supplemented with 10% FCS. The primary PDAC cell line derived from $Kras^{G12D}$; $Trp53^{R172H}$; $PdxCre$ (KPC) mice has been described previously (Patzak et al., 2019). KPC cells were maintained in DMEM supplemented with 10% FCS and 1% non-essential amino acids (NEAA; ThermoFisher Scientific, Waltham, USA). All cell lines were kept at 37 °C and 5 % CO_2.

For thawing cells, stocks were immediately defrosted in a 37 °C water bath and then mixed with 8 mL complete culture medium, followed by centrifugation at 1200 rpm for 3 min. The cell pellet was resuspended in 10 mL culture medium and transferred into a culture flask. Cells were passaged at least once after thawing before conducting any functional experiment.

For making cell stocks, cells pellets were resuspended in freezing medium [90 % FCS plus 10 % dimethyl sulfoxide (DMSO)] and aliquoted into cryotubes. Cells were stored in Mr. Frosty containers in a -80 °C freezer overnight and then transferred into liquid nitrogen for long term storage.

2.2.2.2 Generation of primary PDAC cells from patient-derived xenografts

The used patient-derived xenograft (PDX) model was established by S. Hahn (Ruhr-University Comprehensive Cancer Center, Bochum, Germany). Surgically resected PDAC tissues collected from patients were implanted subcutaneously in NMRI $Foxn1^{nu/nu}$ mice. Resulting xenograft tumors were isolated and re-implanted in both flanks of mice for at least three generations. The PDX tumors were harvested and subsequently

dissociated by gentleMACS dissociator (Miltenyi Biotec, Bergisch Gladbach, Germany). For the isolation of primary PDX tumor cells, the human tumor dissociation kit and mouse cell depletion kit (Miltenyi Biotec, Bergisch Gladbach, Germany) were utilized according to the manufacturer's protocol. Selected primary PDX tumor cell lines (GCDX5, GCDX57, and GCDX62) were cultured in type I collagen-coated dishes for several passages, and then transferred to normal culture vessels for further experiments. Xenografting and generation of PDX cell lines was performed by S.K. Singh, E. Hessmann and W. Kopp (Department of Gastroenterology, GI Oncology & Endocrinology, UMG, Germany). The study was approved by the ethics committee of the Ruhr University Bochum (permission no. 3534-9, 3841-10, 16-5792) and the University Medical Center Göttingen (permission no. 70112108). All animal experiments were performed according to the guidelines of the local Animal Use and Care Committees at the Ruhr University Bochum (8.87-50.10.32.09.018) and the Central Animal-experimental Facility at the University of Göttingen (14/1634, 15/2057, 18/2953).

GCDX cell lines were maintained in a 3:1 mixture of Keratinocyte-SFM (KSF) and RPMI media, supplemented with 2% (v/v) FCS, 1% (v/v) Penicillin-streptomycin, bovine pituitary extract (BPE), and epidermal growth factor (hEGF).

2.2.2.3 Generation of lentiviral and retroviral transduced stable cell lines

For the preparation of virion, 2×10^6 HEK-293T (clone 17) cells (ATCC, Manassas, Virginia, USA) were seeded in a 10 cm dish. The next day, HEK-293T cells were transfected with gene of interest (GOI)-containing plasmid (10.67 µg), envelope vector (5.33 µg) with either 8 µg of lentiviral psPAX2 or retroviral pKAT (Finer et al., 1994) packaging vectors using Lipofectamine 2000 (Invitrogen, USA). The cell supernatant containing virus was collected and filtered through 0.45 µm membrane filter (Merck Millipore, Billerica, USA). The virus-containing media and polybrene were then used to transduce target cells (Santa Cruz Biotechnology, Dallas, USA). 24 h post transduction, fresh culture medium was added to replace the virus-containing medium. After 72 h, cells were selected by 2 µg/mL puromycin (Sigma-Aldrich, St. Louis, USA) and maintained subsequently in 0.5-1 µg/mL culture medium. All the constructs used are listed in **Table**

6. All the transduced stable cell lines were kindly generated by K. Bojarczuk and B. Chapuy (Department of Hematology and Medical Oncology, UMG, Germany).

2.2.2.4 Cell viability assay for chemosensitivity experiments

The CellTiter-Glo Luminescent Cell Viability Assay (Promega, Madison, USA) was performed to quantify cell viability according to the manufacturer's instructions. For individual experiments, 6 x 10^3 cells were seeded in 96-well plates in 100 µL per well 24 h prior to treatment. Gemcitabine, SN38 (an active Irinotecan metabolite) or oxaliplatin were diluted to different concentrations as indicated in the figures and applied to individual wells. After 72 h, plates were equilibrated to RT for 30 min. Cells were subsequently incubated with 30 µL CellTiter-Glo solution and kept on a shaker (400-600 rpm) for 2 min, and incubated in the dark for 10 min. The mixture was then transferred into a 96-well white plate and subjected to measurement of the luminescence via a LUmo Luminometer at an integration time of one second per well.

2.2.2.5 Flow cytometry analysis

1 x 10^6 cells were taken freshly for the cell surface staining of TNFα or TNFα-mCherry reporter gene. Firstly, cells were transferred into a 96-well plate (round bottom) at a concentration of 1 x 10^5 cells/well. Subsequently, cells were centrifuged at 300 X g for 5 min and washed once with FACS buffer (10% knock out serum in -Ca/-Mg PBS; ThermoFisher Scientific, Waltham, USA). PDAC cells were either stained with primary antibodies or untreated control for 30 min at RT. Cells were then washed with 200 µL FACS buffer twice prior to flow cytometry analysis. For endogenous TNFα expression, 488 nm laser was used to detect established PDAC cell lines (CAPAN1, CAPAN2, PANC1, and MiaPaCa2). For the mCherry expression, 561 nm laser was used to detect TNFα-mCherry overexpressing cells (TNFα-OE). Antibodies used for this study are listed in **Table 12**.

2.2.2.6 siRNA transfection

2.5 x 10^5 cells were seeded in 6-well plates (2 mL per well). The next day, culture media was freshly changed to 1 mL 30 min prior to transfection. For each well, transfection

mixture was prepared by adding 6 µL siLentFect lipid reagent (Bio-Rad, Hercules, CA, USA) and 6 µL of 20 µM si*cJUN*, si*BRD4* or non-targeting siRNA to 200 µL Opti-MEM medium (ThermoFisher Scientific, Waltham, USA). The lipid-siRNA mixture was incubated at room temperature for 15 min and then added into wells. Cells were incubated with siRNA for 24 h, after which the medium was exchanged. Protein or RNA was harvested 48-72 h after transfection. siRNA sequences used for this study are listed in **Table 8**.

2.2.2.7 Trans-well invasion assay

16 µL type I collagen stock was diluted in 984 µL 0.1 M HCl in a microtube. The bottom of 8 µm porous inserts for 24-well plates were coated with 50 µL diluted collagen, which solidifies after 1-2 h. Matrigel (Abcam, Cambridge, UK) was thawed on ice and 50 µL were mixed with 10 µL medium containing 1×10^5 cells. The solution was seeded in coated inserts in duplicates and incubated at 37°C for 30 min. Subsequently, 250 µL culture medium was added to inserts and 750 µL to the wells. After 48 h, Matrigel was removed from the inserts with cotton swabs. Invaded cells on membranes were fixed with 4% PFA, followed by three times washing of PBS. The membranes of inserts were removed and stained with 20 µg/mL DAPI for 1 min. Pictures were acquired using a FluoView 1000 confocal microscope and FV10-ASW software version 4.2 (Olympus, Shinjuku, Japan). The invaded cells were counted manually per 20X field of view (F.o.V) from 10 pictures per replicate.

2.2.3 Molecular biology

2.2.3.1 RNA extraction

Cells were washed twice with PBS, scraped in 800 µL TRIzol (ThermoFisher Scientific, Waltham, USA) and collected in a 1.5 mL microtube. 200 µL chloroform were added to each sample, followed by vortexing and centrifugation at 13000 X g for 15 min at 4 °C. The aqueous phase was transferred into a new tube which allows RNA precipitation by incubation with 500 µL iso-propanol at room temperature for 10 min. Samples were then centrifuged at 13000 X g for 30 min at 4 °C and subsequently washed twice with 1 mL

75% ethanol. Dried pellets were ultimately dissolved in 30 µL aqua dest. and stored at - 80 ºC.

2.2.3.2 cDNA synthesis

RNA concentration was measured using a Nano Photometer-P330 (Intas Science Imaging, Göttingen, Germany). 1 µg RNA was used for cDNA synthesis using the iScript cDNA synthesis kit (Bio-Rad Laboratories, Hercules, USA) as per manufacturer's instructions. cDNA synthesis was performed in a thermal cycler as follows: 25 ºC for 5 min, 46 ºC for 20 min, 95 ºC for 1 min. The 20 µL reaction volume was finally diluted with 80 µL aqua dest.

2.2.3.3 qRT-PCR

Quantitative real-time PCR (qRT-PCR) reaction was prepared as shown in **Table 32**:

Table 32. qRT-PCR reaction volume.

Reactions	Volume per single 10µL reaction
SYBR green mix	5 µL
Aqua dest.	3.5 µL
Forward primer	0.25 µL
Reverse primer	0.25 µL
cDNA	1 µL

qRT-PCR primers used in this study are listed in **Table 9**. All samples were pipetted in triplicates and performed by StepOnePlus Real-Time PCR System (Applied Biosystems, Foster City, USA) with the program shown in **Table 33**:

Table 33. qRT-PCR program.

Program	Temperature	Time	Cycle number
Initiating phase	95 ºC	10 min	
	95 ºC	15 s	40 cycles (mRNA qPCR) or 55 cycles (ChIP-qPCR)
	60 ºC	1 min	

	95 ⁰C	15 s
Melting curve	60 ⁰C	1 min
	95 ⁰C	15 s

2.2.3.4 Chromatin immunoprecipitation

Cells were cultured in 15 cm culture dishes until they reached 80-90 % confluency and then fixed with 1 % formaldehyde at room temperature for 15-20 min. 1.25 M glycine (Carl Roth, Karlsruhe, Germany) was added for 5 min to quench the reaction. Nelson buffer containing protease and phosphatase inhibitors (1 mM PMSF, 1 mM NaO, 10 mM NaF, and 1 X cocktail cOmplete) was used to lyse the cells to release nuclei. After centrifugation at 12000 X g for 2 min at 4 ⁰C, nuclei pellet was suspended in Gomes lysis buffer containing 0.1 % SDS, protease and phosphatase inhibitors (1 mM PMSF, 1 mM NaO, 10 mM NaF, and 1 X cocktail cOmplete). The suspension was aliquoted into sonication tubes as 250 µL per tube prior to sonication, which was performed by Diagenode Biorupter-Pico with 30 seconds ON/OFF pulse for 10-15 cycles. 30 µL sheared chromatin was incubated with RNase A (0.75 µL from 30 mg/ml stock; 55 °C, 30 min; Sigma-Aldrich, St. Louis, USA) and proteinase K (1 µL from 20 mg/mL stock; 65 °C, overnight; AppliChem, Darmstadt, Germany) and then loaded on a 1.5 % agarose gel for the confirmation of fragment size. Properly sheared chromatin (from 200 to 600 bp) was then pre-cleared by incubation with 100 µL 50 % slurry protein A agarose beads on a rotator for 1 h at 4 ⁰C. Subsequently, samples were centrifuged at 12000 X g for 2 min at 4 ⁰C and the supernatant aliquoted for the gene of interest, IgG isotype control, and input. If not processed immediately, samples were snap-frozen and kept at -80 ⁰C. ChIP-grade primary antibodies were incubated with samples on rotator overnight at 4 ⁰C. Agarose beads were blocked in BSA (1 µg/µL) diluted in Gomes lysis buffer. The next day, the protein-antibody complex solution was incubated with blocked beads for 2 h at 4 ⁰C. Immune complex was washed as follow: 1 time Gomes lysis buffer, 2 times Gomes wash buffer, 2 times Gomes lysis buffer, and 2 times TE buffer to remove unspecific binding. Washed chromatin was then incubated with RNase A (0.2 µg/µL; 55 °C, 30 min; Sigma-Aldrich, St. Louis, USA) and proteinase K (1 µL from 20 mg/mL stock; 65 °C, overnight;

AppliChem, Darmstadt, Germany) prior to DNA extraction. DNA was extracted by phenol/chloroform/isoamyl alcohol solution and washed once with 70 % ethanol. Final DNA was resuspended in 20-30 µL aqua dest. and stored at -20 ºC for further analysis.

2.2.3.5 Protein sample preparation

For the preparation of whole cell lysates, cells were washed twice with ice-cold PBS and lysed in WCL buffer on ice for 30 min. Lysates were then centrifuged at 12000 X g for 20 min and supernatant was collected for Western blot analysis.

2.2.3.6 Bradford assay

Protein concentration/content was determined using Bradford reagent (Bio-Rad, Hercules, CA, USA). Briefly, BSA was diluted to different concentrations for the establishment of a standard curve. 1 µL of each protein sample was added to 200 µL Bradford reagent. The absorbance value was measured by PHOMO plate reader at 595 nm. The absorbance of samples was then used to calculate the protein concentration using the standard curve.

2.2.3.7 Western blot analysis

Sodium dodecyl sulfate-polyacrylamide gel electrophoresis (SDS-PAGE) was carried out to separate proteins with different molecular masses. Equal amount of protein (20 µg) was loaded on SDS-PAGE gel and electrophoresis was conducted at 100 V for 30 mins followed by 120 V for 1 h 40 min. The protein was transferred onto nitrocellulose (NC) membranes using a semi-dry blotting system (25V, 1.0 A). 10 % separation gel was used for the detection of the proteins more than 30 kDa. 15 % gel was used for proteins less than 30 kDa. Proteins on NC membrane were visualized by short incubation with Ponceau S solution. Subsequently, membrane was blocked with 5% (w/v) milk powder in TBST buffer for 1 h at room temperature, followed by incubation with primary antibodies overnight at 4°C. Secondary HRP-linked antibodies were incubated for 1 h at room temperature. All antibodies were diluted in 5 % milk powder in TBST buffer. Protein was detected by an Intas ChemoCam Imager using ECL substrate (Bio-Rad, Hercules, USA). Antibodies used for this study are listed in **Table 11**.

2.2.3.8 Proteome profiler cytokine array

Cells were seeded in a 6-well plate in 2 mL medium and grown to 80-90 % confluency. 48 h after a medium change the supernatant was collected and centrifuged at 5,000 X g for 5 min prior to cytokine detection using Proteome Profiler Human Cytokine Array Kit (R&D Systems, Minneapolis, USA) following the manufacturer's instructions.

2.2.3.9 ELISA

Cells were seeded in a 24-well plate in 500 µL medium. 48 h after medium change the supernatant was collected and centrifuged at 5,000 X g for 5 min prior to detection. The levels of secreted human TNFα were measured by Quantikine ELISA kit (R&D Systems, Minneapolis, USA). For *in vivo* detection, blood samples were collected and centrifuged at 4000 X g for 10 min. Plasma of control and TNFα treated mice were measured for human and murine TNFα by Quantikine ELISA kit (R&D Systems, Minneapolis, USA).

2.2.4 Next generation sequencing

2.2.4.1 RNA-seq and data processing

5×10^5 CAPAN1 cells were seeded in 6-well plates. The next day, cells were treated with either TNFα (10 ng/mL; Sigma-Aldrich, St. Louis, USA) or vehicle control for 18 h. Next, cells were harvested in TRIzol (Ambion, Kaufungen, Germany) for RNA isolation (three biological replicates). The RNA quality was checked by agarose gel electrophoresis. cDNA library was prepared using 500 ng of total RNA and the TruSeq RNA Library Prep kit (Illumina, San Diego, USA) as per manufacturer's instructions. cDNA concentration was measured via Qubit dsDNA high sensitivity assay (Thermo Fisher Scientific, Waltham, USA). Fragment sizes were confirmed by Bioanalyzer high sensitivity DNA analysis (Agilent Technologies, Santa Clara, California, USA) prior to sequencing (single-end 50 bp) on a HiSeq2000 (Illumina, San Diego, USA). Sequencing was performed at the core facility of NGS Integrative Genomics Unit at the UMG, Göttingen.

For data analysis, the read-outs were quality-checked using FastQC v0.11.5 (https://www.bioinformatics.babraham.ac.uk/projects/fastqc/). Reads were mapped

against reference human genome hg38 by STAR v2.5.2b (Dobin et al., 2013), Next, aligned reads were assigned to individual genes for transcript quantification by HTSeq-count version 0.10.0 (Anders et al., 2015). Differential expression analysis was performed by DESeq2 (Love et al., 2014). Genes were considered differentially expressed between treatments if they had an absolute log2-fold change of > 0.58 and an adjusted p-value of < 0.05. Principle component analysis (PCA) was determined by prcomp function in R and plotted by ggplot2 in R. pheatmap package in R was utilized for generating heatmaps. Gene set enrichment analysis (GSEA) was performed using R package clusterProfiler (Yu et al., 2012). Bioinformatic analysis was performed by X. Li (Developmental Biology, University of Göttingen, Germany).

2.2.4.2 ChIP-seq library preparation and data processing

10-15 x 10^6 cells were cross-linked in 1% PFA (PBS-diluted) for 10 min at room temperature. Subsequently, cells were quenched in ice-cold glycine (0.125 M) for 5 min. The preparation of ChIP materials was followed by the protocol from Ford et al. (Ford et al., 2014). A Bioruptor sonicator was utilized to generate a size of 300-500 bp DNA fragments (https://ethanomics.files.wordpress.com/2012/01/chip_covaris4.pdf). For the immunoprecipitation, antibodies used are listed in **Table 14**. Immunoprecipitated DNA was purified using the ChIP DNA Clean & Concentrator kit (Zymo Research Europe, Freiburg, Baden-Württemberg, Germany), following the manufacture's instruction. Next-generation sequencing (single-end) was conducted on a HiSeq4000 platform (Illumina, San Diego, USA) to obtain at least 20 million reads per sample. Raw sequencing reads (~100 bp) were mapped to the reference human genome (hg19) using BWA (Li and Durbin, 2010). Peak calling was performed by MACS2 (Zhang et al., 2008) to identify signal enrichment over input. Next, genes were assigned to peaks through GREAT (http://great.stanford.edu/public/html/). ChIP-seq analysis was performed by T. Georgomanolis (Cologne Center for Genomics, University of Cologne, Germany).

2.2.5 Tissue microarray (TMA) staining and analysis

Human PDAC tissue microarray (TMA) slides were obtained from the Departments of Pathology as well as General, Visceral and Pediatric Surgery of the University Medical Center Göttingen following the ethical regulations of the institute (70112108). In total, 46 matched PDAC patient samples were evaluated, with one to three cores per patient. IF staining, TMA evaluation, and data acquisition were performed as described above.

2.2.6 Publicly available PDAC microarray data analysis

For patient microarray expression analysis, data from Puleo et al. (Puleo et al., 2018) was downloaded from the ArrayExpress database (E-MTAB-6134). For genes associated with multiple probes, the probe with the highest average expression across all patients were used for the analysis. For gene set overrepresentation analysis in squamous and pancreatic progenitor PDAC patient tumors (Bailey et al., 2016), the differential expression was performed on the R2 platform (https://hgserver1.amc.nl/cgi-bin/r2/main.cgi) using the default parameters and enrichment analysis conducted using clusterProfiler as described above. Publicly available patient data analysis was performed by Lukas Klein (Department of Gastroenterology, GI Oncology & Endocrinology, University Medical Center Göttingen, Germany)

2.2.7 Statistical analysis

GraphPad Prism version 8.0.2 was used for statistical analysis (GraphPad Software, San Diego, USA). Mann-Whitney test, or unpaired Student's t-test was performed for the comparison of two groups. Log-rank test was applied for survival data. For gene expression correlation of published microarray data, the Pearson's correlation coefficient with a two-tailed P value was calculated. Results were considered significant with a P value below 0.05, as indicated in the figures.

3 Results

3.1 High level of TNFα is associated with BL phenotype in PDAC

In order to investigate the role of TNFα in PDAC progression, we first examined whether there was any correlation between TNFα expression and a certain tumor phenotypic identity. Therefore, we utilized a genetically engineered $Kras^{G12D}$;$p53^{R172H}$;$PdxCre$ (KPC) mouse model, which is widely used in PDAC studies as it recapitulates human pancreatic carcinogenesis (Hingorani et al., 2005). KPC tumor sections were subjected to H&E staining. KPC tumors were highly heterogeneous and contained both well-to-moderately differentiated (W/M) and poorly differentiated tumor contents. As shown in **Figure 6A**, G1 and G2 tumors presented W/M tumor features, with glandular, duct-like structures, whereas G3 and G4 tumors were lacking cellular differentiation, forming extremely poorly differentiated histological features. We then probed TNFα and cytokeratin-19 (CK19) on these W/M (G1-G2) and poorly differentiated (G3-G4) KPC tumor tissues. CK19 is a surrogate marker for tumor cells. Notably, TNFα was found to be highly expressed in poorly differentiated tumors (G3-G4) when compared with W/M (G1-G2) differentiated tumors (**Figure 6B**), indicating an association between TNFα and the poorly differentiated phenotypic state.

To further evaluate the tumor phenotype-dependent expression of TNFα, human CLA and BL orthotopic mouse models were generated to investigate whether TNFα was highly expressed in BL tumors, which are associated with poorly differentiated tumors. To this end, immunodeficient mice were selected to allow human PDAC cells (CLA and BL) to grow inside the pancreas. The established CLA (i.e. CAPAN1 and CAPAN2) and BL (i.e. PANC1 and MiaPaCa2) cell lines were orthotopically transplanted into the pancreas of immunodeficient mice NMRI-Foxn1$^{nu/nu}$. Notably, the CLA subtype-derived tumors maintained glandular structures and formed well differentiated tumors, and the liver tissues did not form any visible metastases. In comparison, as expected, the BL tumors formed poorly differentiated tumors and liver metastases (**Figure 6C**). Double immunofluorescence (IF) staining of TNFα and CK19 was performed again in the CLA

and BL orthotopic tumors. In line with the observation in KPC mice, TNFα was found to be highly expressed in the BL tumors compared to CLA tumors (**Figure 6D**).
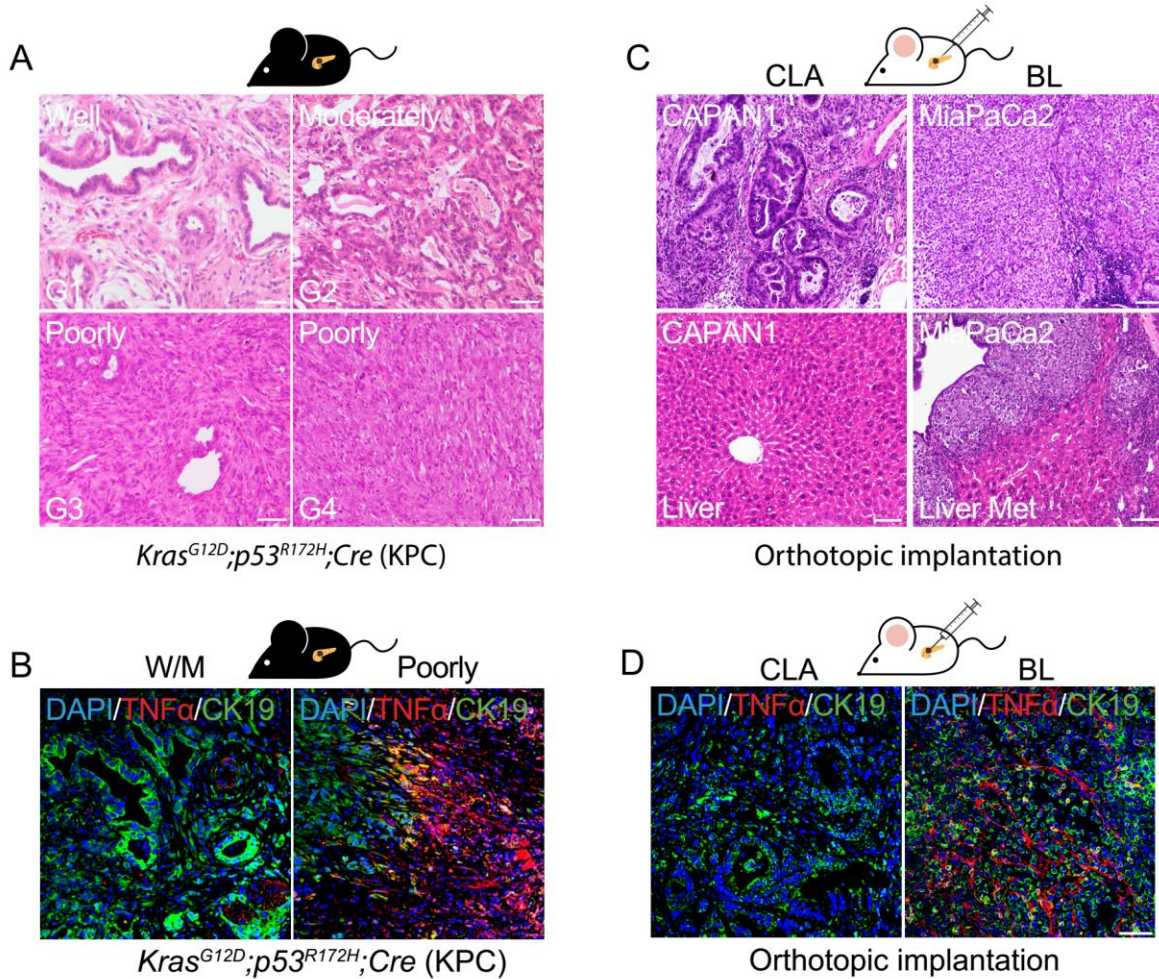

Figure 6. Phenotype-dependent expression of TNFα in PDAC. (A) Representative H&E images of graded (G1 to G4) $Kras^{G12D}$;$p53^{R172H}$;$PdxCre$ (KPC) tumor tissues. Scale bar: 20 μm. (B) Immunofluorescence (IF) staining of TNFα (red) and cytokeratin 19 (CK19) in well-to-moderately differentiated (W/M) as well as poorly differentiated tumors of KPC mice. Scale bar: 50 μm. n=5 in W/M; n=5 in poorly. (C) Representative images of H&E staining in pancreatic tumors and liver tissues derived from orthotopically implanted classical (CLA) CAPAN1 as well as basal-like (BL) MiaPaCa2 mouse models. Scale bar: 20 μm. (D) IF staining of TNFα (red) and CK19 (green) in the tumor tissues as indicated in (C). Scale bar: 50 μm. n=9 in CLA; n=10 in BL.

To further validate whether high levels of TNFα determines subtype-specificity, we used histologically characterized W/M and poorly differentiated resected PDAC patient tumors. Notably, we observed high TNFα levels particularly in the poorly differentiated tumors compared to W/M PDAC (**Figure 7A and 7B**). Collectively, these data indicate that high levels of TNFα are associated with highly aggressive BL phenotypic state.
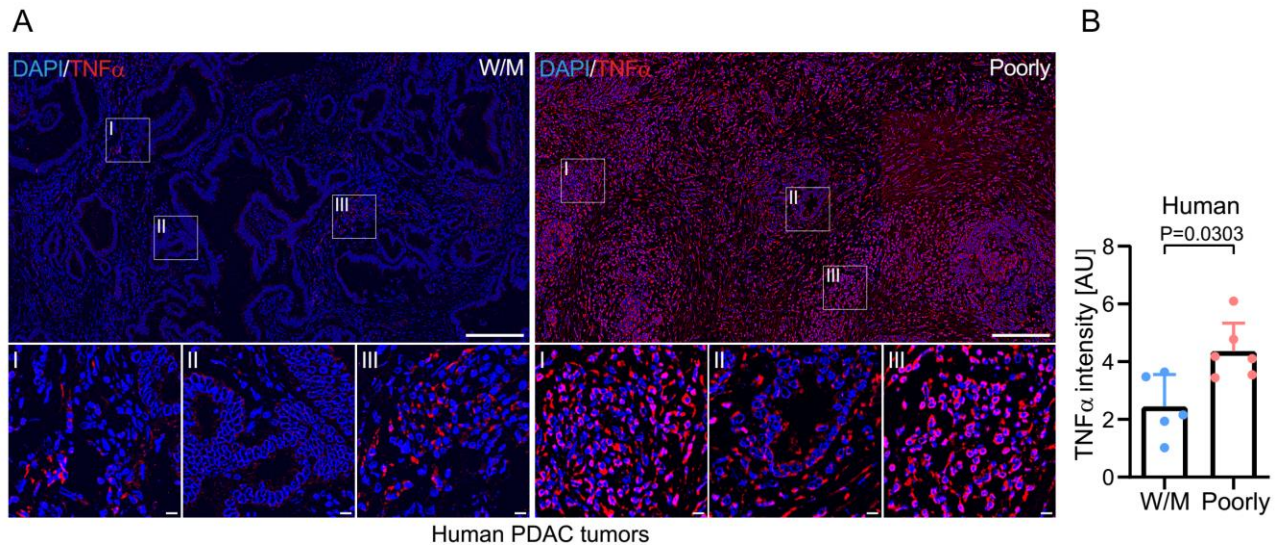
Figure 7. TNFα is highly expressed in poorly differentiated PDAC patient tumors. (A) representative tile scan images of IF staining of TNFα in W/M and poorly differentiated PDAC patient tumors. I-III show higher magnification images. Scale bar: whole section (top): 2 mm; higher magnification images (bottom): 10 µm. (B) Quantification of TNFα intensity in (A). Scatter plots show values in arbitrary units (AU) of each patient, as well as means ± s.d. as bar graphs. Mann-Whitney test was used for statistical analysis. n=5 in W/M; n=6 in poorly.

3.2 TNFα promotes CLA to BL phenotypic switch in PDAC

3.2.1 TNFα promotes poorly differentiated phenotypic state *in vivo*

Next, we sought to investigate whether TNFα promotes tumor aggressiveness in PDAC. Therefore, CLA (i.e. CAPAN1) subtype cells were orthotopically implanted in mice and treated with exogenous TNFα. As detailed in **figure 8A**, immunodeficient NMRI Foxn1$^{nu/nu}$

mice were implanted with CAPAN1 cells into the pancreas. Three weeks after transplantation, as it approached the time that tumor started to form, 3D ultrasound was used weekly to evaluate the tumor growth until mice developed a decently sized tumor (approx. 6 mm in diameter) (**Figure 8B**). Mice were administrated TNFα or vehicle control intraperitoneally (i.p.) three times per week. At the endpoint (three weeks of TNFα treatment), mice were sacrificed for tissue isolation.
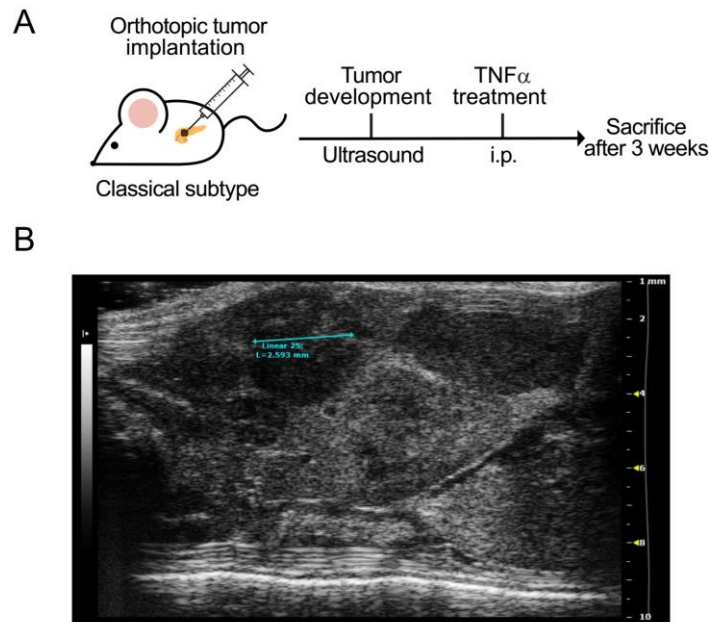

Figure 8. Schematic of orthotopically implanted PDAC cells into the pancreas. (A) An illustration of the experimental design. 10-weeks old male immunodeficient NMRI-Foxn1$^{nu/nu}$ mice were orthotopically implanted with 1 x 10^6 CLA cell line CAPAN1 into the pancreas. Three weeks after transplantation, (B) ultrasound was performed weekly to evaluate the tumor growth. Treatment began when the tumor diameter reaches approx. 6 mm. TNFα (0.4 mg/kg body weight) was injected intraperitoneally (i.p.) three times a week, using aqua dest. as control. Mice were sacrificed after three weeks of treatment. Tissues were collected including entire pancreatic tumor, spleen, liver, lung, and blood samples.

Next, tumor tissues harvested from vehicle control (VC) and TNFα-treated mice were subjected to H&E staining. In order to have an overview of the tumor histology, whole slide scans of the H&E sections were performed. Representative tile images as well as

selected tumor areas at a higher magnification are shown in **Figure 9A**. In general, control tumors exhibited a W/M differentiated phenotype that fully recapitulates the CLA PDAC subtype identity. However, the proportion of poorly differentiated tumor area significantly increased in TNFα-treated mice, which is a sign for the BL subtype, as quantified in **Figure 9B**. Duct-like structures were prominent in the VC tumors compared to more separated and irregular structures in the TNFα-treated tumors, suggesting that TNFα switched CLA to the highly aggressive BL phenotypic state.
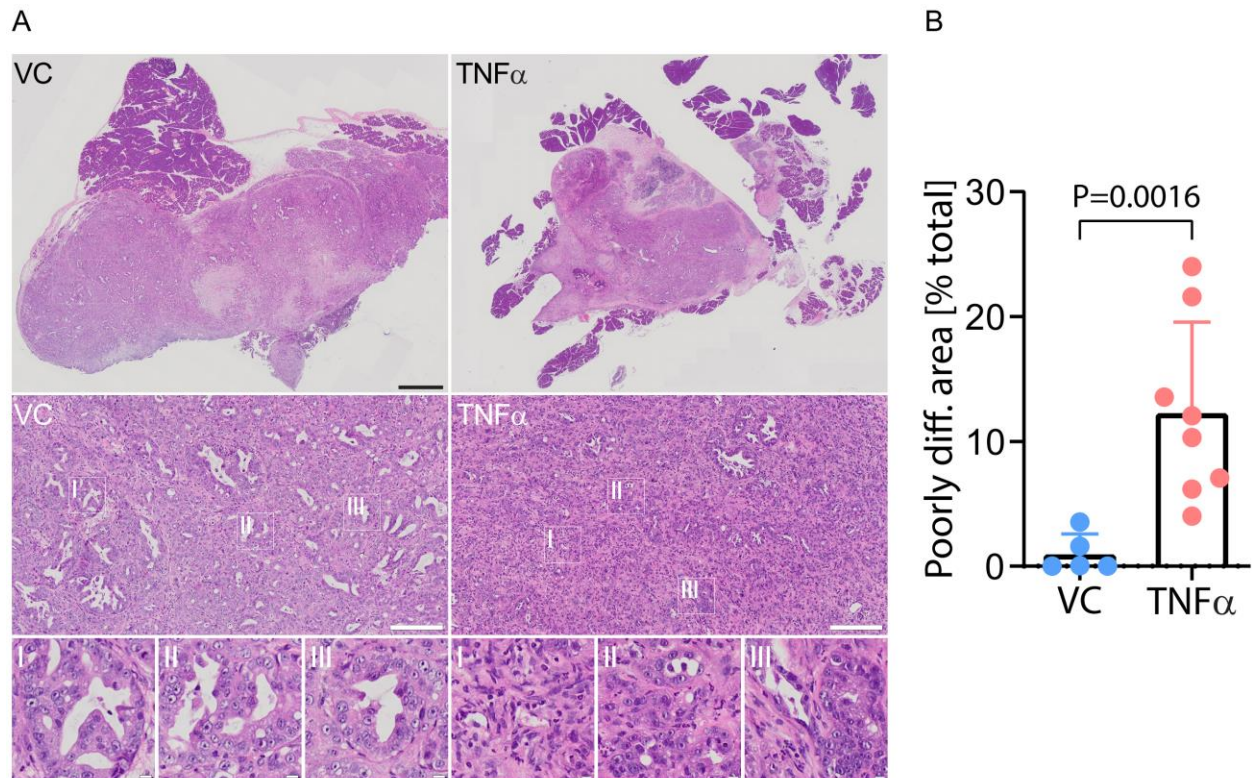
Figure 9. TNFα promotes W/M to poorly differentiated phenotype. (A) Representative tile scan images of H&E staining in pancreatic tumor tissues from vehicle control (VC) and TNFα-treated orthotopically implanted mice (CAPAN1). I-III show higher magnification images. Scale bar: whole section (top): 2 mm; representative images (middle): 200 μm; higher magnification images (bottom): 10 μm. (B) Scatter plots show quantification of poorly differentiated tumor area as a percentage of total tumor area in VC and TNFα-treated mice, as well as means ± s.d. as bar graphs. n=5 in VC; n=8 in TNFα. Mann-Whitney test was used for statistical analysis.

To further validate our observations, IF staining was performed for Keratin-81 (KRT81) and amylase in the tumors developed from VC and TNFα-treated mice. Of note, KRT81 is an established clinical marker that is specifically expressed in the BL tumors (Noll et al., 2016). Additionally, PDAC patients showing high levels of KRT81 have a lower survival rate (Noll et al., 2016). Amylase was used to stain for normal pancreatic acinar cells, which allowed us to distinguish tumor cells from normal tissue. We observed a significant induction of KRT81 expression in the tumor core as well as peritumoral regions (amylase⁺) following TNFα treatment (**Figure 10**), consistent with the tumor histology.

Interestingly, except for the induced BL invasive phenotype, abundant infiltration of CD45⁺ immune cells were found in the TNFα-treated tumors. In contrast, VC tumors barely have CD45⁺ cells present (**Figure 11**). Collectively, these data suggest that TNFα promotes a poorly differentiated/BL phenotype and immune cell infiltration in PDAC.
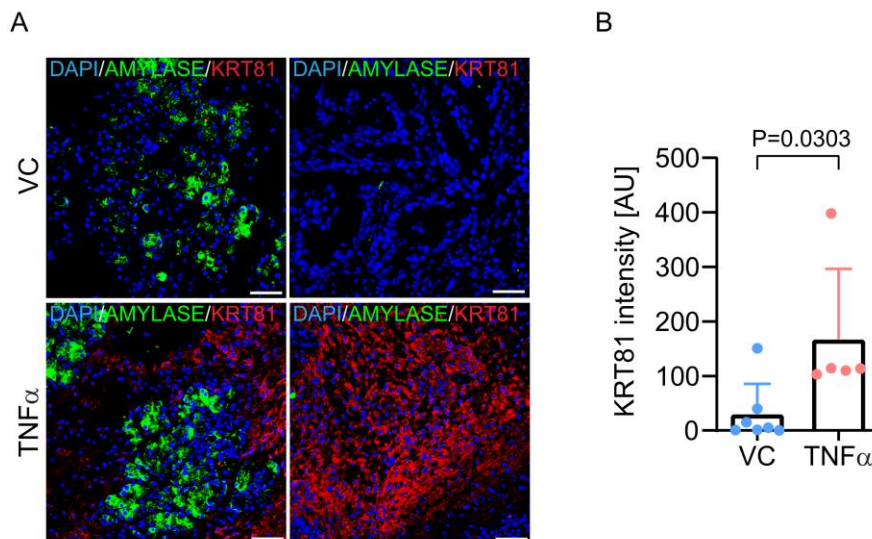
Figure 10. TNFα treatment leads to high level of of KRT81 *in vivo*. (A) Representative IF images of KRT81 (red) and amylase (green) in orthotopic CAPAN1 VC and TNFα treated pancreatic tumor tissues. scale bar: 50 μm. (B) Quantification of KRT81 in (A). Scatter plots show values in arbitrary units (AU) as an average per animal, as well as means ± s.d. as bar graphs. 10 images were evaluated per animal. Mann-Whitney test was used for statistical analysis. n=7 in VC; n=5 in TNFα.
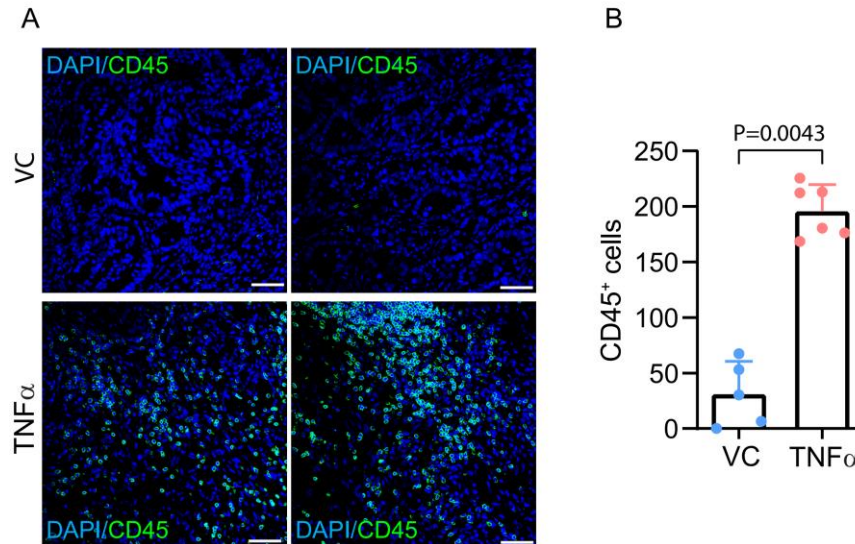
Figure 11. TNFα treatment induces CD45$^+$ immune cell infiltration. (A) Representative IF images of CD45 (green) in orthotopic CAPAN1 VC and TNFα treated tumor tissues. Scale bar: 50 μm. (B) Quantification of CD45$^+$ cells in (A). Scatter plots show average values per animal of counts per field of view as well as means ± s.d. as bar graphs. 10 images per animal were evaluated. Mann-Whitney test was used for statistical analysis. n=5 in VC; n=6 in TNFα.

3.2.2 TNFα promotes invasive behavior of CLA PDAC cells

To understand the mechanism underlying the observed phenotypic switch *in vivo*, we performed a 3D-transwell invasion assay in CLA cells following TNFα treatment. The number of invading cells was significantly induced in presence of TNFα in both CLA cell lines, i.e. CAPAN1 and CAPAN2 (**Figure 12A and 12B**). Additionally, the increased invasive capacity was associated with an induction of EMT marker ZEB1, concomitant with a reduction of differentiation marker KLF5. The most prominent effect was seen after 48 h of the TNFα treatment (**Figure 12C**).
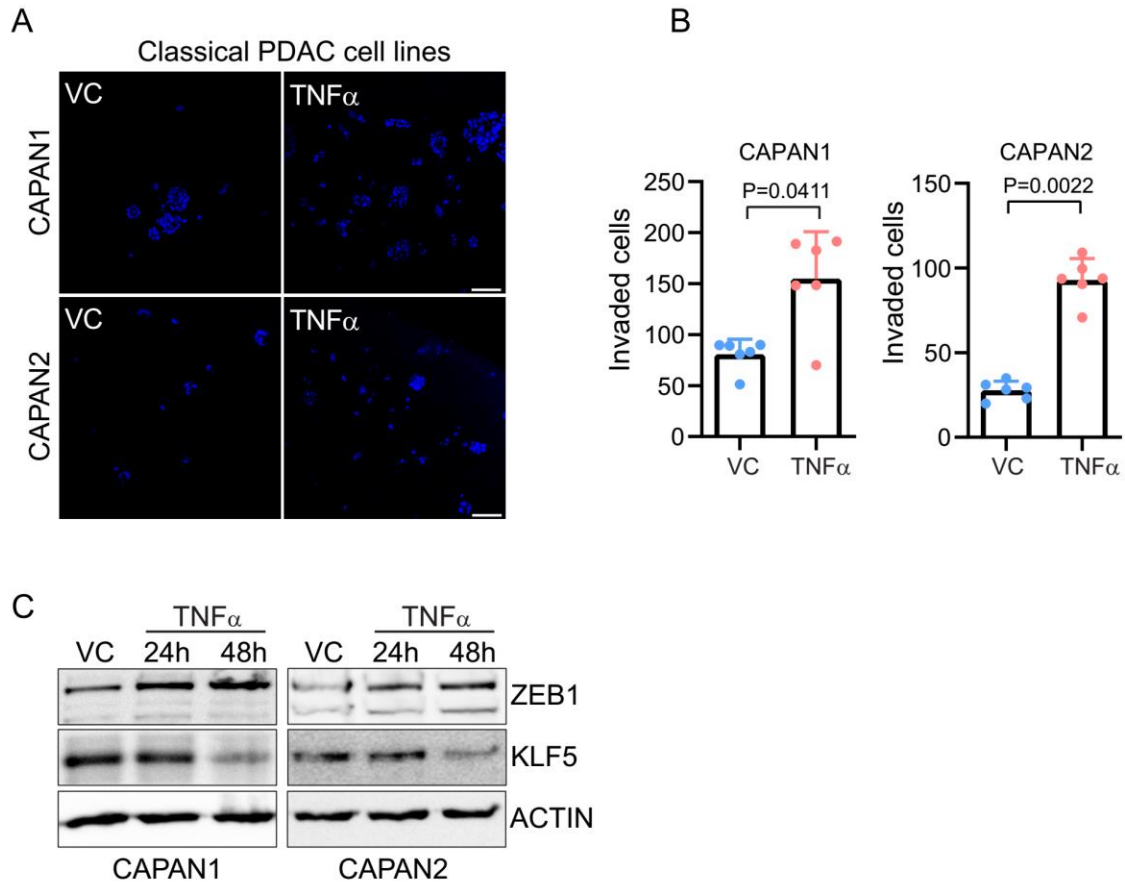
Figure 12. TNFα increases the invasive capacity of CLA cells. (A) 3D-transwell invasion assay of CLA cell lines (CAPAN1 and CAPAN2) treated with TNFα (10 ng/mL), or aqua dest. as vehicle control (VC). Representative images of DAPI-stained invaded CAPAN1 and CAPAN2 cells. Scale bar: 50 μm. (B) Quantification of invaded cells as shown in (A). Scatter plots show average values per technical replicate of counts per F.o.V. as well as means ± s.d. as bar graphs. Mann-Whitney test was used to determine the statistical significance. n=3. (C) Western blot analysis of ZEB1, KLF5 upon TNFα or VC treatment for 24 h and 48 h in CLA cells CAPAN1 and CAPAN2. Actin was used as a loading control. Representative of three independent experiments.

3.2.3 TNFα induces CLA to BL subtype switch by transcriptional reprogramming of lineage-specific genes

To gain further insight into the molecular mechanisms underlying the TNFα-mediated subtype switch, we performed RNA sequencing using CLA CAPAN1 cells treated with

TNFα or vehicle control. Gene set enrichment analysis (GSEA) revealed a significant enrichment of EMT and inflammatory response hallmarks in TNFα-treated samples (**Figure 13A**), consistent with our previous observations of TNFα-treated orthotopic tumors as well as *in vitro* experiments (**Figure 9, Figure 11, and Figure 12**). Additionally, gene sets linked to the invasive PDAC subtype such as 'KRAS signaling down' and 'Myogenesis' (Miyabayashi et al., 2020) were also found to be enriched in the TNFα-treated samples (**Figure 13B**), whereas gene sets involved in 'Fatty acid metabolism', 'Adipogenesis', and 'Myc targets V1' were enriched in control samples (**Figure 13B**). To determine whether TNFα-altered gene signatures associated with a particular PDAC subtype, we utilized the publicly available CLA-related gene sets, as previously reported (Maurer et al., 2019). We found that TNFα treatment led to a reduction in the expression of most CLA-specific genes (**Figure 13C**). The genes that were upregulated coinciding with a known BL signature, as well as downregulated genes coinciding with CLA were shown in volcano plot (**Figure 13D**). Taken together, these data suggest that TNFα promotes a BL phenotype in PDAC cells.
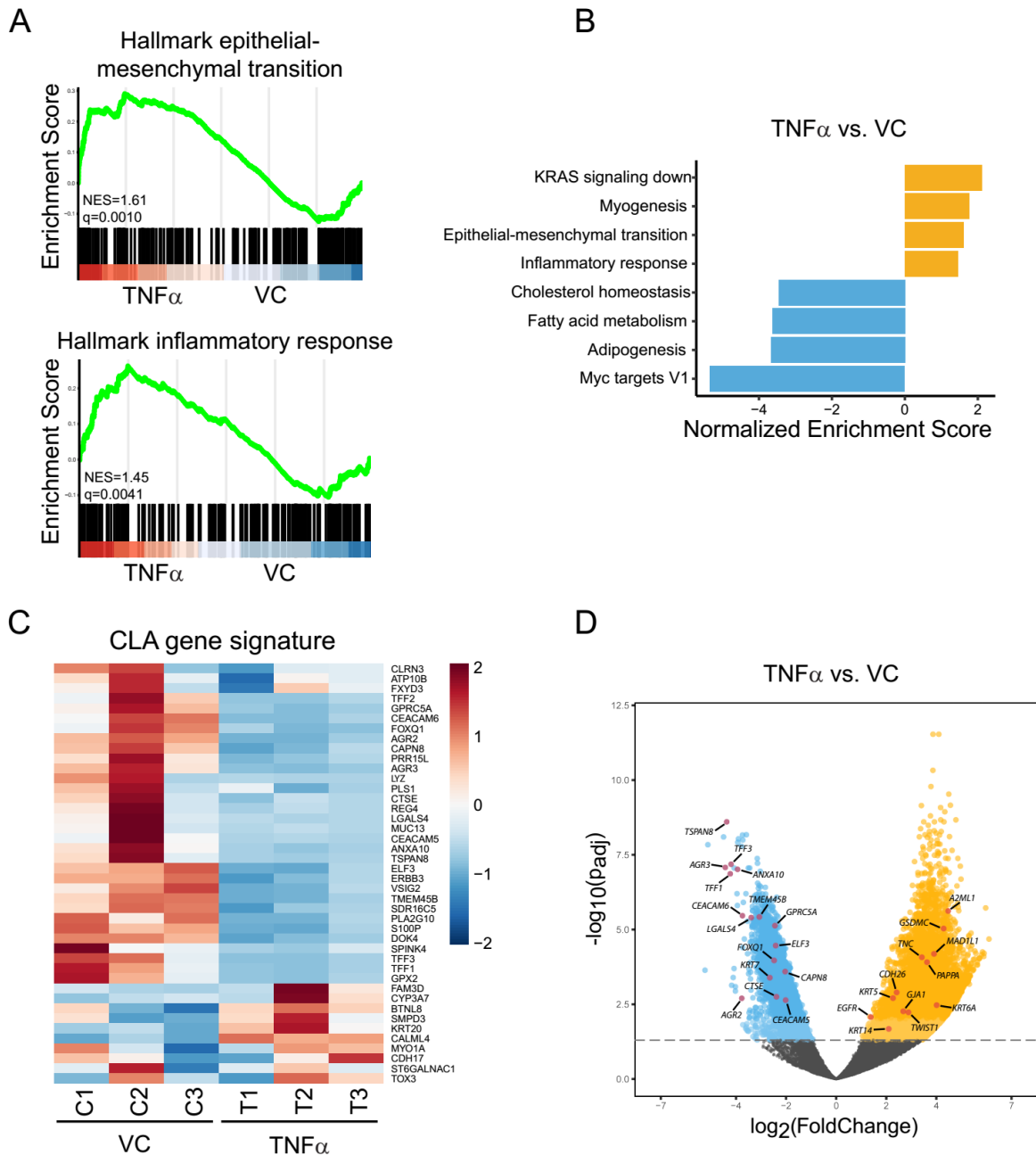
Figure 13. TNFα induced PDAC subtype-specific gene regulatory network. (A) Enrichment plots from gene set enrichment analysis (GSEA) in 18h TNFα-treated (10 ng/mL) versus vehicle control (VC) samples in CLA CAPAN1 cells. Normalized enrichment scores (NES) and q-values are indicated. (B) Normalized enrichment scores of selected Hallmark gene sets from the Molecular Signature Database in CAPAN1 cells with TNFα versus VC treatment. (C) Heatmap displays expression of CLA-associated genes as defined by Maurer et al. (Maurer et al., 2019) in CAPAN1 cells in the presence or absence of TNFα. (D) Volcano plot of differential expression

analysis. Upregulated genes coinciding with known BL markers and downregulated genes coinciding with CLA are plotted in red.

3.3 Molecular subtypes of PDAC determine distinct tumor microenvironment

3.3.1 BL-specific immune cells are source of TNFα in PDAC TME

Based on the earlier observation that TNFα was preferably expressed in the poorly differentiated tumors (**chapter 3.1**), we initially hypothesized that the BL PDAC cells might be the source of TNFα. Thus, TNFα expression was examined in CLA and BL cells by flow cytometry. Despite the pivotal role of TNFα *in vivo*, we did not find significant levels of TNFα in either CLA (i.e. CAPAN1 and CAPAN2) or BL cells (i.e. PANC1 and MiaPaCa2) (**Figure 14A**). For further validation, human-specific TNFα ELISA was performed in the supernatant from these cells. Consistently, TNFα expression was not detected in all the cell lines (**Figure 14B**).
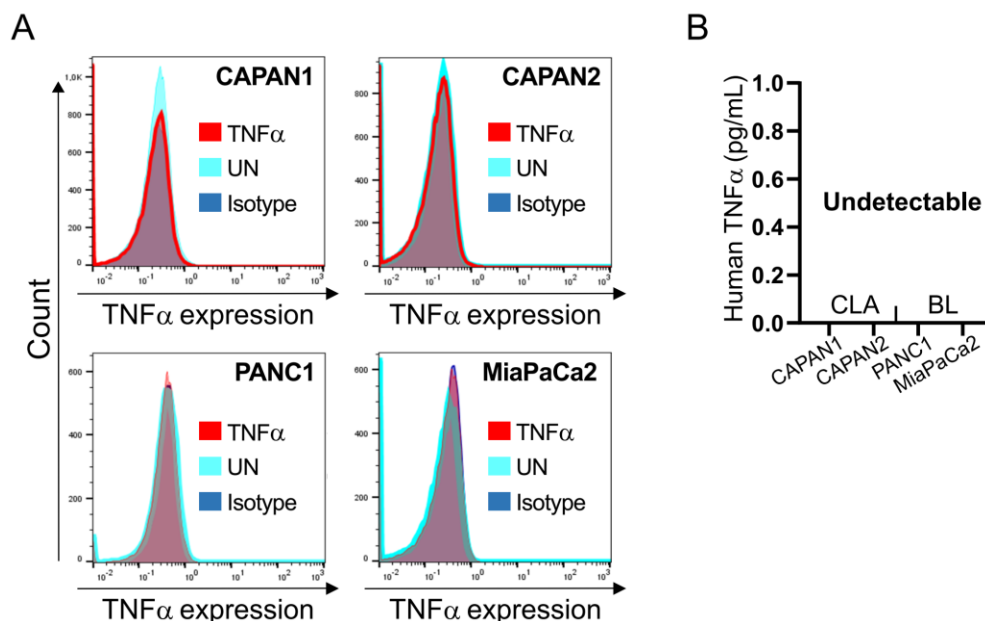
Figure 14. TNFα is not produced by PDAC cell lines. (A) Flow cytometry analysis was performed for TNFα in CLA cells CAPAN1 and CAPAN2, as well as BL cells PANC1 and

MiaPaCa2, using anti-TNFα antibody, without any staining (UN), and isotype control (IgG1κ). Counts of gated cells are shown against fluorescence intensity, which is linked to TNFα expression. n=3. (B) Concentrations of TNFα in cultured CLA CAPAN1 and CAPAN2 as well as BL PANC1 and MiaPaCa2 cells as measured by human-specific ELISA. n=2.

Given that none of the PDAC cell lines produced TNFα, we considered that inflammatory TME might be the source of TNFα production in PDAC tumors. Thus, human- and murine-specific ELISA in was carried out in the plasma-derived from the above-mentioned CLA and BL orthotopically transplanted mice (**Figure 6**). Notably, human TNFα secretion was not detected in either CLA or BL plasma samples (**Figure 15A**). Strikingly, murine TNFα was detected only in BL plasma (**Figure 15B**). Additionally, TNFα expression was measured in the previously mentioned TNFα-treated CLA mouse model (**Figure 8**). Human TNFα was able to be detected in the TNFα-treated mice as expected (**Figure 15C**), since human recombinant TNFα was administrated in these mice. Besides, we noted that murine TNFα could be detected as well in the TNFα treated mice (**Figure 15D**).

Together, human TNFα was not detectable in the PDAC cell lines as well as in the plasma from CLA and BL tumor bearing mice. However, murine TNFα was detectable in the BL and induced the TNFα-treated CLA plasma samples, suggesting that TNFα originated from the host inflammatory TME.
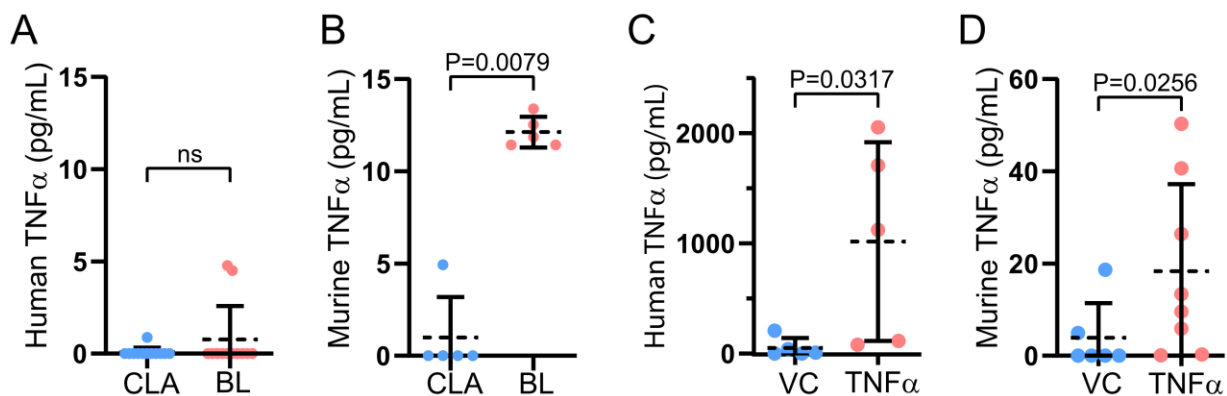

Figure 15. Host immune inflammatory tumor microenvironment produces TNFα in the BL PDAC subtype. (A and B) Human-specific (A) and murine-specific (B) TNFα ELISA in plasma samples isolated from mice orthotopically implanted with CLA and BL cells. Scatter plots show

values of each animal as well as means ± s.d. as bar graphs. Mann-Whitney test was used to determine the statistical significance. (A) n=12. (B) n=5. (C and D) Human-specific (C) and murine-specific (D) TNFα ELISA in plasma samples isolated from VC and TNFα-treated CLA mice. Scatter plots show values of each animal as well as means ± s.d. as bar graphs. Mann-Whitney test was used to determine the statistical significance. (C) VC, n=5; TNFα, n=5. (D) VC, n=6, TNFα, n=8.

3.3.2 Subtype-dependent immune cell infiltration

To find out whether immune cells in the inflammatory TME were the source of TNFα, we performed IF staining of CD45 in the CLA and BL orthotopic tumors. Notably, CD45^{+} cells were highly present in the BL orthotopic tumors compared to the CLA ones (**Figure 16A**). Since macrophages are known to be abundant in the PDAC TME and associated with poor survival (Bailey et al., 2016; Hessmann et al., 2020; Puleo et al., 2018), we sought to further examine the expression of the macrophage marker CD68 in these tumor tissues as well as the TNFα-treated tumors where an induction of CD45^{+} cells was seen (**Figure 11**). Notably, BL orthotopic tumors showed higher recruitment of CD68^{+} cells compared to CLA orthotopic tumors (**Figure 16B**). Similarly, CD68^{+} cells were found to be strongly induced upon TNFα treatment compared to VC (**Figure 16C**). Since these CD45^{+}/CD68^{+} cells and TNFα are both more prominent in the BL tumors, indicating that TNFα is most likely produced by the immune cells, especially CD68^{+} macrophages.
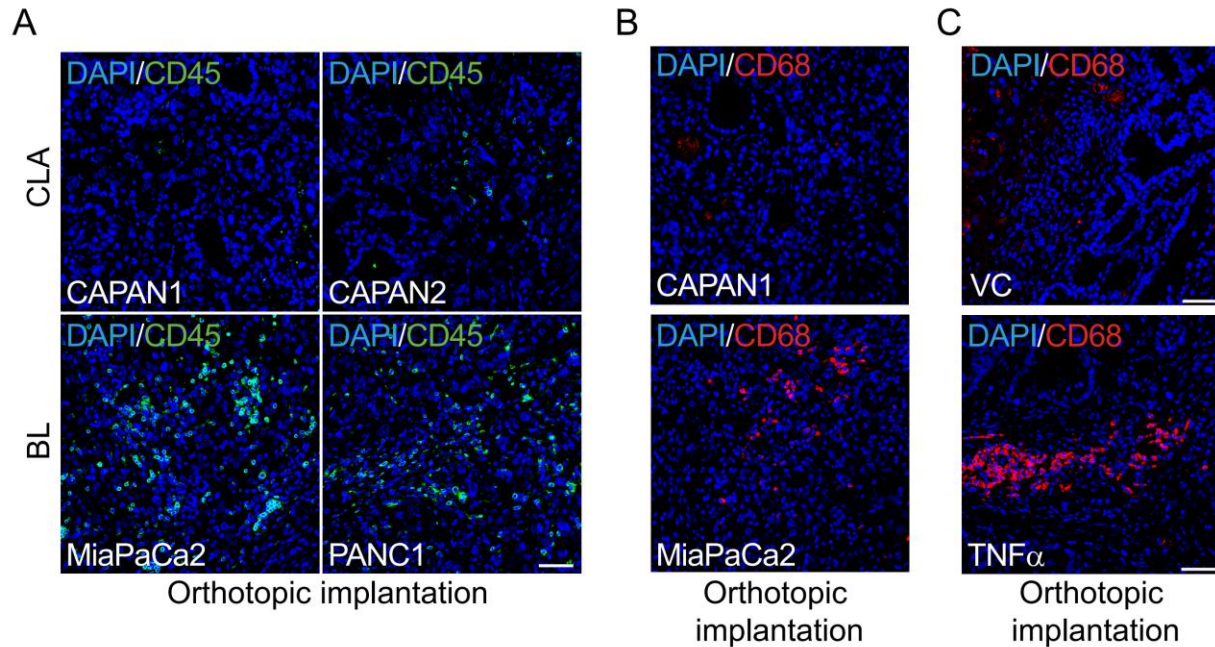
Figure 16. CD45+ and CD68+ cells are highly infiltrated in the BL orthotopic tumors. (A) Representative IF staining of CD45 (green) in CLA (CAPAN1 and CAPAN2) and BL (PANC1 and MiaPaCa2) orthotopic tumors. Scale bar: 50 μm. n=5 in CLA; n=5 in BL. (B) IF analysis of CD68 (red) in CLA (CAPAN1) and BL (MiaPaCa2) orthotopic tumors. n=5 in CLA; n=5 in BL. (C) representative IF images of CD68 (red) in VC and TNFα-treated CLA CAPAN1 orthotopic tumors. Scale bar: 50 μm. n=6 in VC; n=6 in TNFα-treated.

3.3.3 Subtype-specific intrinsic factors determine immune cell recruitment

To understand the mechanism of how immune cells were recruited into the BL TME and its potential mediators, we first compared the cytokine expression profile between CLA and BL cell lines by utilizing publicly available RNA-seq data (GSE64560). Several cytokines were found to be upregulated in the BL cells, including CCL2, which is known to be associated with macrophages recruitment (Nagarsheth et al., 2017) (**Figure 17A**). Next, we used an unbiased approach via the Proteome Profiler Human Cytokine Array Kit to detect cytokine production in human CLA and BL PDAC cell lines. Consistently, CCL2 was observed to be highly upregulated in BL PANC1 and PT45P1 cell lines compared to CLA CAPAN1 and CAPAN2 cells (**Figure 17B**).

As CCL2 expression correlated with the BL subtype in PDAC cell lines, we next sought to elucidate whether there was a correlation between CCL2 and subtype identity in PDAC patient tumors. Hence, we analyzed CCL2 status in the Bailey-defined pancreatic progenitor (or CLA) and squamous (or BL) subtypes (Bailey et al., 2016). In line with the association of CCL2 to the BL PDAC cells, CCL2 was found to be highly enriched in the squamous (i.e. BL) subtype compared to pancreatic progenitor (i.e. CLA) tumors (**Figure 17C**). Next, the association of CCL2 and CD68+ macrophages was verified in a publicly available microarray dataset of PDAC patient tumors (Puleo et al., 2018). We found that CCL2 correlated positively with CD68 (**Figure 17D**). Taken together, these results indicate that high expression of CCL2 correlates with CD68+ macrophage infiltration in BL tumors.
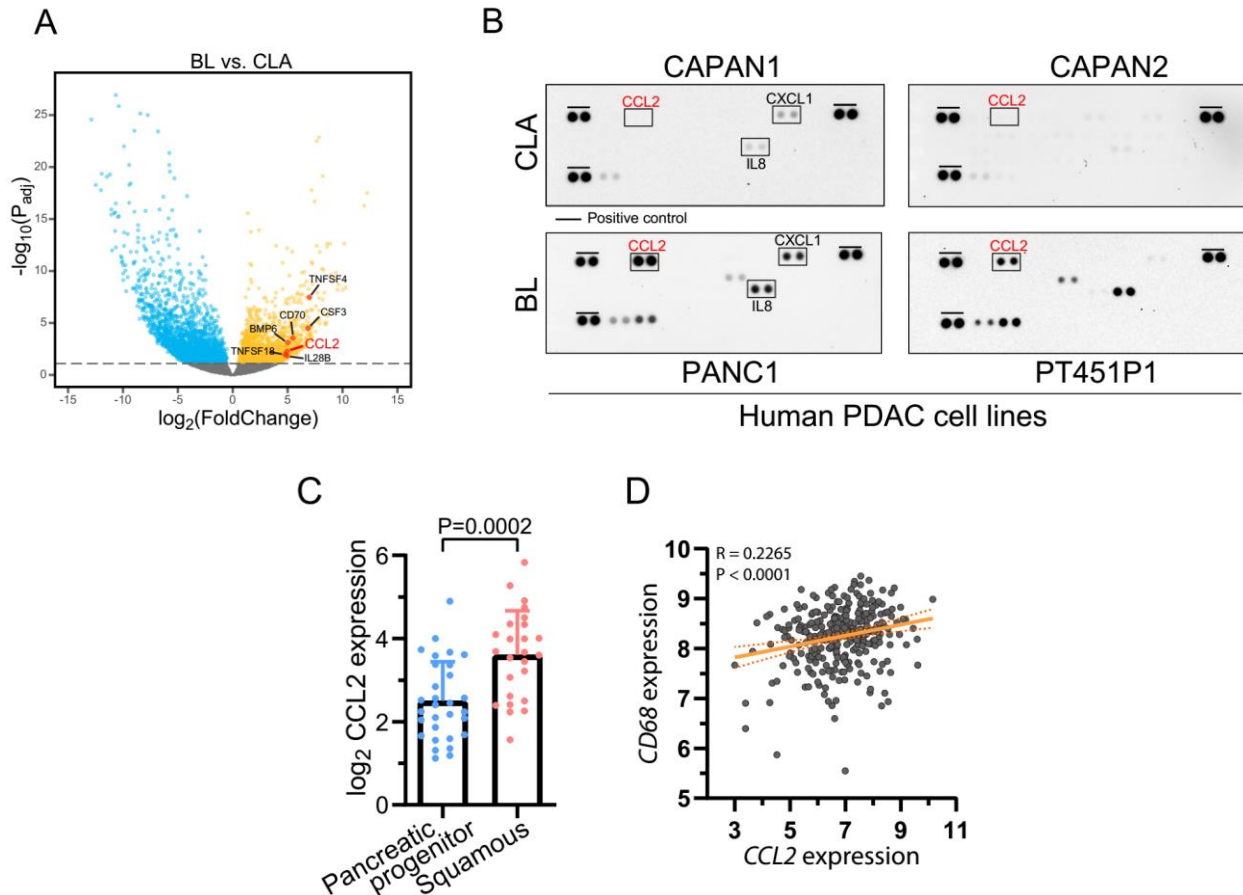
Figure 17. CCL2 is linked to BL PDAC subtype and associates with CD68+ macrophages.
(A) Volcano plot of differential gene expression between CLA (CAPAN1 and CAPAN2) and BL

(PANC1 and MiaPaCa2) PDAC cell lines. Publicly available RNA sequencing data (GSE64560; Diaferia et al., 2016) was reanalyzed by F. Wegwitz (Department of Gynecology and Obstetrics, UMG). Cytokines significantly upregulated in BL cells compared to CLA cells are highlighted. (B) Expression of cytokines detected by Proteome Profiler Human Cytokine Array Kit. CLA CAPAN1 and CAPAN2 as well as BL cells PANC1 and PT45P1. Unlabeled black spots with lines indicate for positive control. (C) Expression of CCL2 in well-defined pancreatic progenitor (n=30) and squamous (n=25) patients (Bailey et al., 2016). Data was retrieved by L. Klein (Department of Gastroenterology, GI Oncology & Endocrinology, UMG) using R2, an online platform for genomic dataset analysis (https://hgserver1.amc.nl/cgi-bin/r2/main.cgi). Mann-Whitney test was used to determine the statistical significance. (D) Correlation analysis of CCL2 and CD68 in 309 PDAC patient tumors (Puleo et al., 2018). Data was obtained from the ArrayExpress database (E-MTAB-6134). RMA normalized probe intensity were plotted. A linear regression with 95 % CI is shown in orange.

3.4 Distinct AP1 transcription factors determine PDAC subtype identity

3.4.1 Mutually exclusive expression of JUNB/AP1 and cJUN/AP1 in PDAC

To elucidate the mechanism of the observed cytokine upregulation, we analyzed publicly available patient microarray data (Puleo et al., 2018), and found a significant enrichment of the TNFα signaling pathway and inflammatory AP1 signaling exclusively in BL patients (**Figure 18A**). Therefore, we speculated that there might be a relevance of the AP1 pathway to the observed inflammatory BL phenotype. Hence, we examined the expression of JUN/AP-1 family transcription factors (TFs) in CLA and BL cell lines. Strikingly, JUNB was found to be highly enriched in CLA cell lines, whereas cJUN was restricted into BL cells (**Figure 18B**). This data was further confirmed by IF staining of JUNB and cJUN in CLA and BL orthotopic tumors. **Figure 18C** shows high level of JUNB in CLA tumors, while cJUN was enriched in BL tumors. Next, we sought to examine whether the exclusivity of JUNB and cJUN was also reflected in patient tumors. Thus, we performed double IF staining of cJUN or JUNB together with E cadherin (ECAD) in tissue microarrays (TMA) of 46 PDAC patients. ECAD is an important molecule for cell adhesion

and highly expressed in the CLA subtype. Of note, cJUN was abundant in the area where ECAD was negative. Conversely, JUNB was highly co-localized with ECAD⁺ cells in the differentiated areas, whereas cJUN was absent (**Figure 18D, 18E, and 18F**). Collectively, our results show that JUNB is highly expressed in the CLA well-differentiated compartment, while cJUN is enriched in BL tumors.
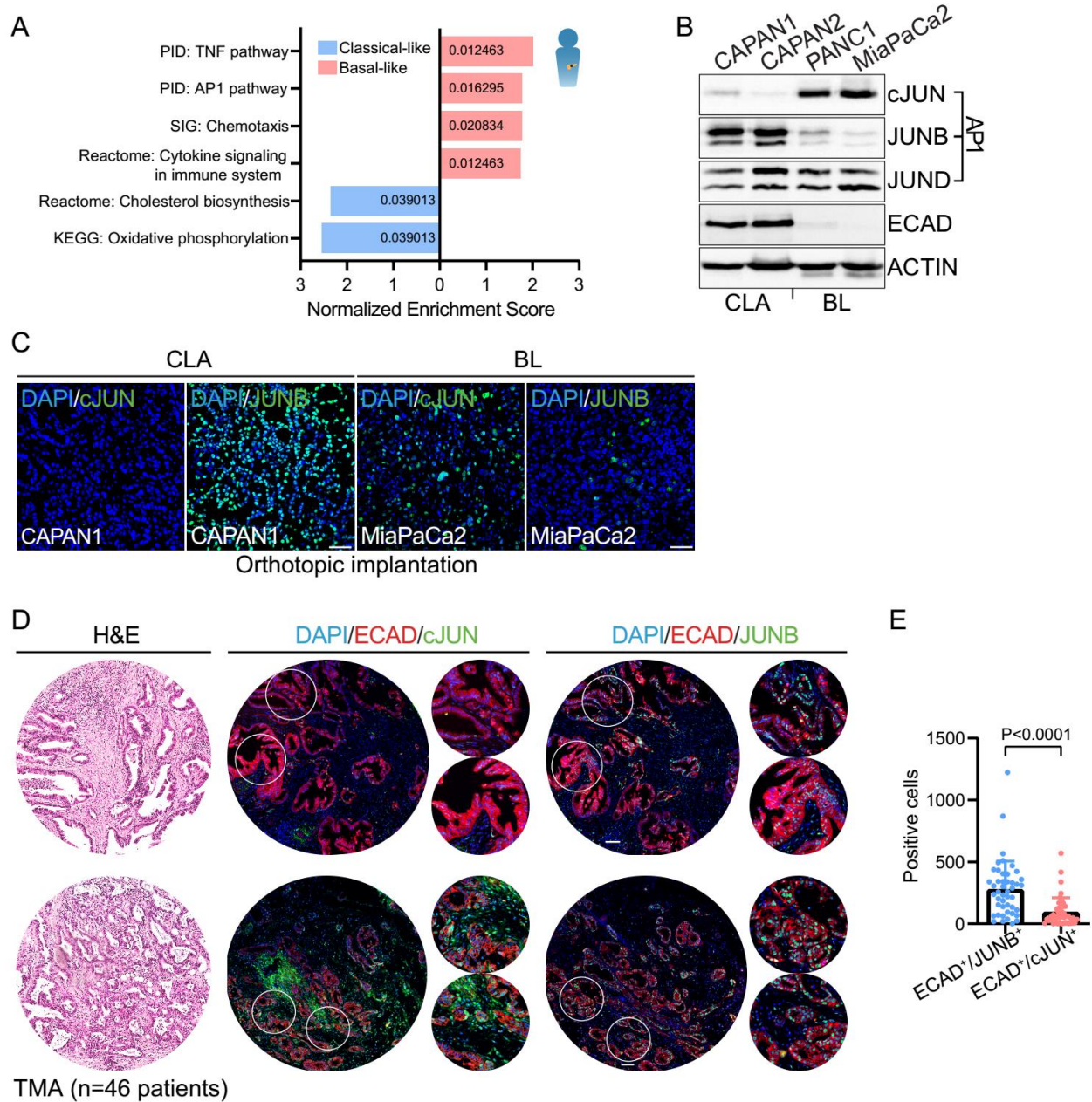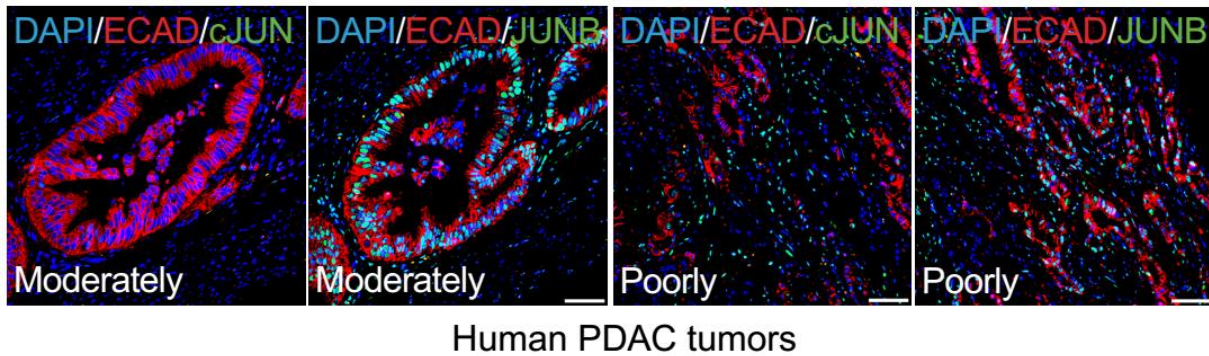

Figure 18. *Continued on following page.*

F

Human PDAC tumors

Figure 18. Subtype-restricted AP1 transcriptional program in PDAC. (A) Bar graph shows the normalized enrichment score and adjusted P values of selected pathways in CLA and BL subtypes based on RNA microarray analysis of 309 PDAC patients (Puleo et al., 2018). (B) Western blot analysis of JUN/AP1 family (cJUN, JUNB and JUND), and ECAD in CLA (CAPAN1 and CAPAN2) and BL (PANC1 and MiaPaCa2) PDAC cells. Actin was used as a loading control. Representative of three independent experiments. (C) Representative IF images of cJUN and JUNB staining in CLA and BL orthotopic tumors. Scale bar: 50 µm. (D) Representative H&E (left panel) and IF staining of cJUN/ECAD (middle panel) as well as JUNB/ECAD (right panel) in tissue microarray (TMA) spots of 46 PDAC patients, with identical patients in each row. Scale bar: 100 µm. (E) Number of JUNB$^+$/ECAD$^+$ as well as cJUN$^+$/ECAD$^+$ cells in TMA described in (D). Scatter plot shows average value per patient of all evaluated TMA spots (1-3 per patient), with means ± s.d. as bar graphs. Mann-Whitney test was used to determine the statistical significance n=46. (F) Representative IF images of cJUN/ECAD and JUNB/ECAD in moderately differentiated area as well as poorly differentiated primary PDAC tissues. Scale bar: 50 µm.

3.4.2 Differential genome binding profile of CLA-JUNB and BL-cJUN

Since JUNB and cJUN were found to be restricted in the specific PDAC subtype, we sought to explore the underlying molecular mechanism and whether they contributed to PDAC subtype identity. Thus, chromatin immunoprecipitation followed by sequencing (ChIP-seq) for JUNB and cJUN was carried out in CLA and BL cells, respectively. The genome binding profiles of JUNB and cJUN were clearly separated by principal component analysis (**Figure 19A**). CLA cells could be easily distinguished from BL cells

by the differential binding profile (**Figure 19B**). To specify the potential role of cJUN and JUNB in PDAC, the genes linked to regions which were JUNB bound and gained openness as identified by assay for transposase-accessible chromatin followed by sequencing (ATAC-seq) (data not shown) in the CLA (CAPAN1) cells over the BL (PANC1) cells were used for Gene Ontology analysis (GO). Similarly, the genes bound by cJUN and gained openness in the BL PANC1 over the CLA CAPAN1 were selected. This analysis revealed that CAPAN1/JUNB-specific genes were involved in lipid biosynthesis, cell-cell adhesion regulation, and epithelial cell differentiation (**Figure 19C**). However, PANC1/cJUN-specific genes were correlated with vasculature development, leukocyte migration, and cytokine production (**Figure 19D**). These data suggest that JUNB- or cJUN-controlled loci are linked to the subtype-specific phenotypic state.
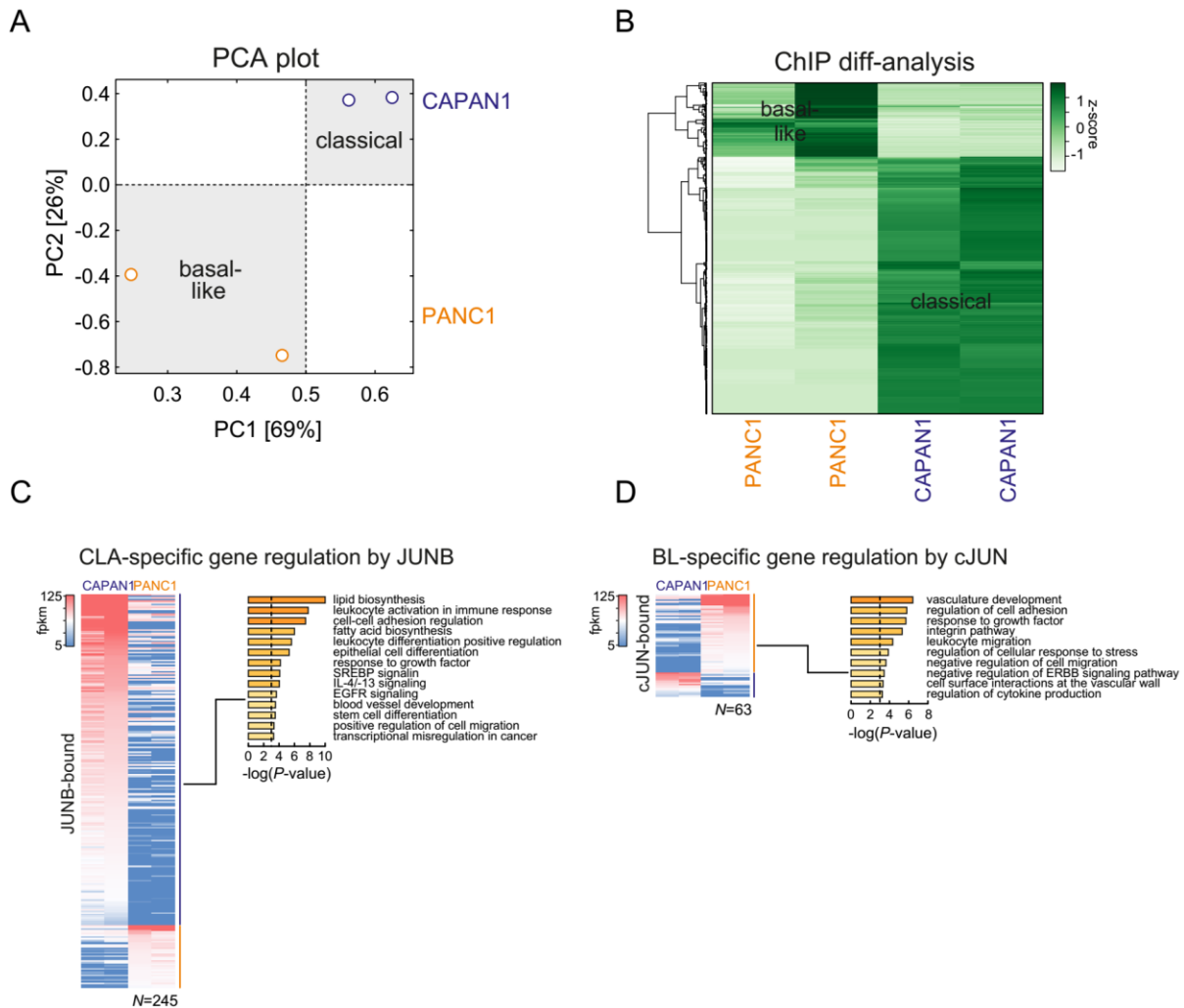
Figure 19. Differential genome binding profile of cJUN and JUNB. (A) Principal component analysis (PCA) of JUNB and cJUN ChIP-seq profiles from CLA (CAPAN1) and BL (PANC1) cell lines. Two biological repeats were included for each cell line. (B) Heatmap of differential binding profile of ChIP-seq data of JUNB and cJUN in the CLA (CAPAN1) and BL (PANC1) cells. (C and D) Heatmaps of JUNB- or cJUN-occupied regions intersected with ATAC-seq peaks in CAPAN1 (E) and PANC1 (F) respectively. Bar plots show gene ontology (GO) terms enriched for the genes assigned to each set of peaks.

In line with the GO analysis, JUNB specifically occupies the promoter and enhancer regions of *CDH1* (encodes the ECAD protein). Accordingly, high occupancy of H3K27ac which indicates for activate promoters and enhancers was seen in the CLA CAPAN2 cells

at the same loci, but not in BL PANC1 cells (**Figure 20A**). Conversely, cJUN bound the *VIM* promoter and enhancer loci, accompanied by occupancy of H3K27ac specifically in BL PANC1 cells (**Figure 20B**). These data suggest the positive regulation of the epithelial marker *CDH1* by JUNB, as well as the mesenchymal regulator *VIM* by cJUN. ChIP-qPCR validated that JUNB indeed bound on the promoter and one of the enhancer regions on *CDH1* with strong H3K27ac (**Figure 20C and 20D**), while cJUN occupied both promoter and enhancer regions of *VIM,* associated with H3K27ac occupancy (**Figure 20E and 20F**). These data indicate that JUNB might control cell differentiation via regulation of *CDH1*, on the other hand, cJUN may support the BL phenotype through *VIM*.
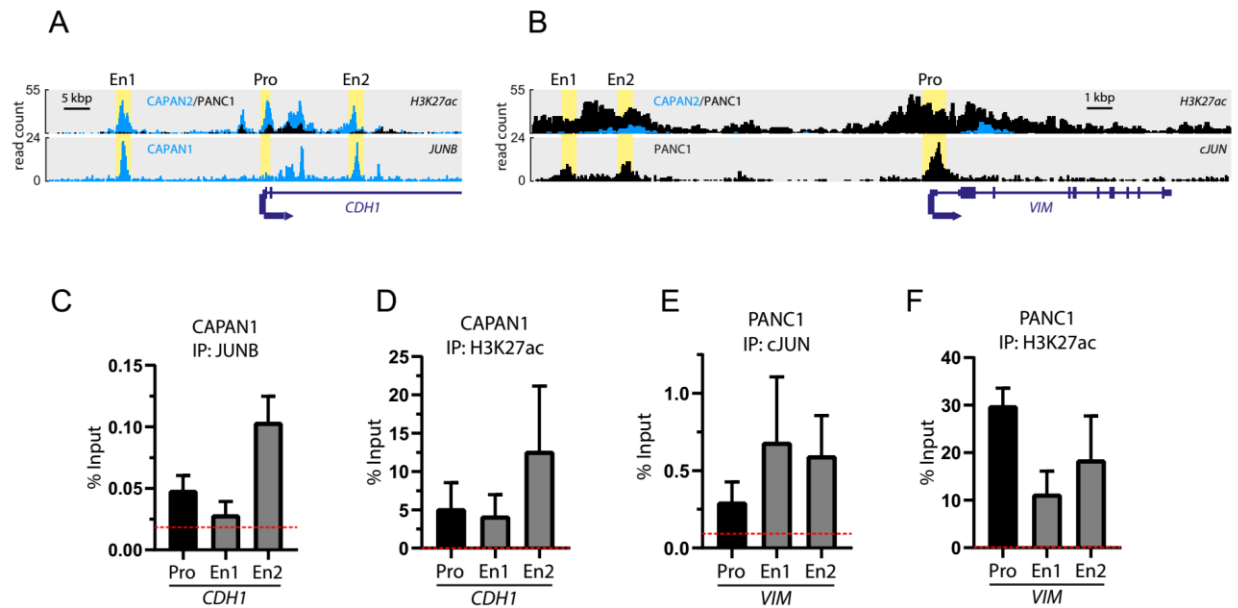

Figure 20. JUNB occupies *CDH1* active promoter and enhancer and loci whereas cJUN binds on *VIM*. Coverage plots of ChIP-seq for JUNB in CLA CAPAN1 cells, as well as H3K27ac in CLA CAPAN2 and BL PANC1 cells at *CDH1* locus. For H3K27ac ChIP-seq data, publicly available dataset was utilized (Diaferia et al., 2016). Enhancer (En) and promoter regions (Pro) are indicated. (B) Coverage plots of ChIP-seq for cJUN in BL PANC1 cells, as well as H3K27ac in CLA CAPAN2 and BL PANC1 cells at the *VIM* locus. Enhancer (En) and promoter regions (Pro) are highlighted. (C and D) qRT-PCR analysis following ChIP of JUNB (C) and H3K27ac (D) on *CDH1* promoter and enhancer regions indicated in (A). n=3. (E, F) qRT-PCR analysis following ChIP of cJUN (E) and H3K27ac (F) on *VIM* promoter and enhancer regions indicated in (B). n=3. For (C-F), IgG isotype control levels are indicated in red.

3.4.3 cJUN overexpression induces invasiveness of CLA PDAC cells

To explore the functional significance of cJUN in driving a PDAC BL subtype identity, we established retrovirally transduced CLA cells with constitutive cJUN overexpression. **Figure 21A** confirmed that cJUN was successfully overexpressed in the CLA CAPAN1 cells. Notably, cJUN overexpression led to a dramatic morphological change from well-clustered islands towards a more spindle-like shape (**Figure 21B**). 3D-transwell invasion assay was conducted to compare the invasiveness between CAPAN1 empty vector (EV) and cJUN overexpressing (cJUN-OE) cells. Interestingly, the number of invading cells was significantly induced following cJUN overexpression (**Figure 21C and 21D**), suggesting that cJUN promotes an invasive behavior of PDAC cells.
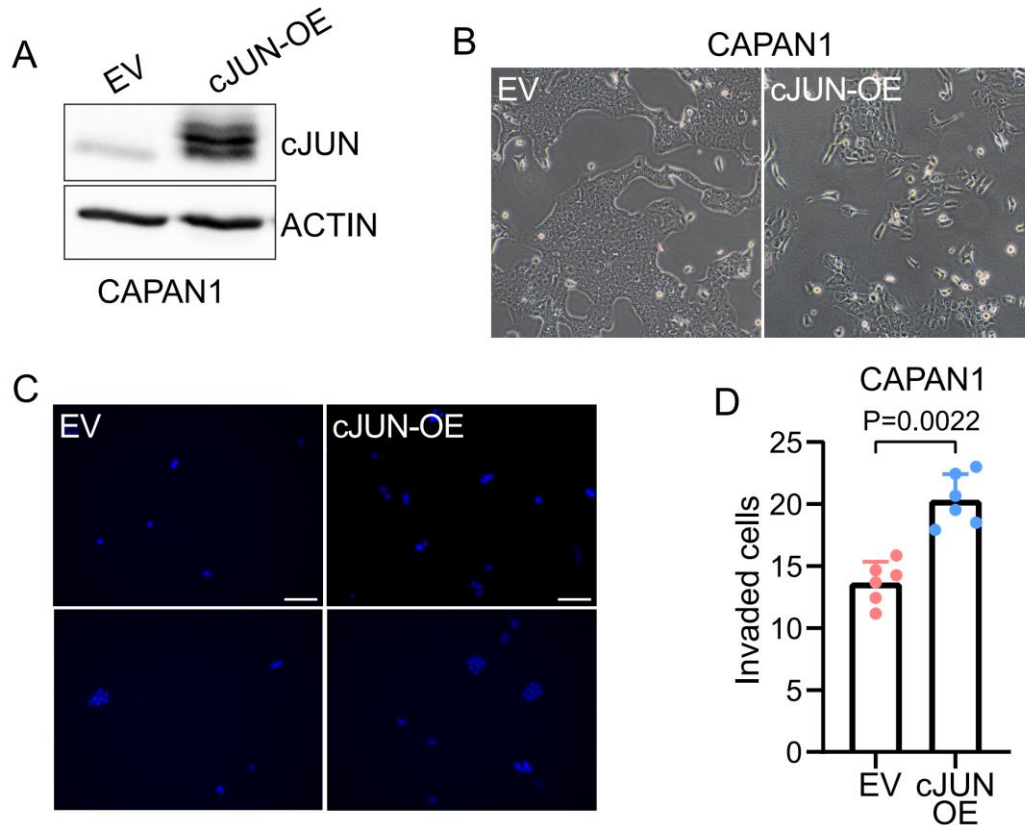

Figure 21. cJUN induces the invasive potential of CLA PDAC cells. (A) CLA CAPAN1 cells were transduced with either an empty vector (EV) or a stable cJUN overexpression (cJUN-OE) construct. Western blot analysis was performed to confirm the efficiency of cJUN overexpression. Actin was used as a loading control. Representative of three independent experiments. (B) Bright-

field images of (A). (C) 3D-transwell invasion assay of CAPAN1-EV and CAPAN1-cJUN-OE cells. Representative images show DAPI staining of invaded cells. Scale bar: 100 µm. (D) Quantification of invaded cells of (C). Scatter plot shows average values of count per field of view per individual technical replicate, as well as means ± s.d. as bar graphs. Mann-Whitney test was used to determine the statistical significance. n=3.

Since BL subtype is in general more resistant to chemotherapy treatment, we sought to investigate whether cJUN-OE cells lose sensitivity to chemotherapies. Cell viability of EV and cJUN-OE cells was examined upon gemcitabine, oxaliplatin, and SN38 treatment across a wide range of concentrations as indicated in **Figure 22**. cJUN-OE cells showed a decreased sensitivity to gemcitabine with IC_{50} values of 14.6 nM compared to EV of 10.92 nM (**Figure 22A**). A similar effect was seen following the treatment with oxaliplatin (cJUN-OE IC_{50} = 1458 nM vs EV IC_{50}= 744.5 nM) (**Figure 22B**) as well as the active irinotecan metabolite SN38 (cJUN-OE IC_{50} = 4.86 nM vs EV IC_{50}= 1.63 nM) (**Figure 22C**). These data suggest that cJUN contributes to chemoresistance in PDAC cell lines.
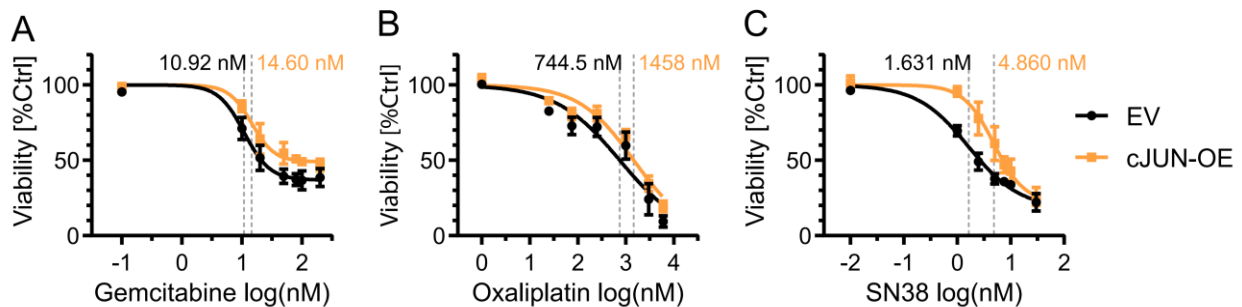

Figure 22. cJUN overexpression contributes to resistance to chemotherapeutics. CAPAN1-EV and cJUN-OE cells were seeded in 96-well plates and treated with gemcitabine, oxaliplatin, and SN38 at different concentrations indicated in the figure for 72 h. CellTiter-Glo was utilized to examine the cell viability. Dose response curves show cell viability of EV (black) and cJUN-OE (yellow) cells upon gemcitabine (A), oxaliplatin (B), and SN38 (C). IC_{50} values for each drug are indicated n=3.

3.4.4 cJUN-CCL2 regulation in BL PDAC cells

Since the BL subtype has high levels of CCL2 as well as cJUN/AP1, which is known as an inflammatory transcriptional factor, we hypothesized that cJUN may regulate CCL2 to recruit macrophages. Thus, we took advantage of our cJUN ChIP-seq data in BL PANC1 cells and visualized ChIP-seq tracks on Integrative Genomics Viewer (IGV). A significant enrichment of cJUN on both promoter and enhancer regions of CCL2 could be observed (**Figure 23A**), indicating that cJUN binds on the *CCL2* gene in PDAC. For further validation, we performed individual ChIP-qPCR analysis for cJUN and H3K27ac in PANC1 cells with primers designed on these regions, as indicated in **Figure 23A**. Consistently, we found a significant occupancy of cJUN on the *CCL2* promoter as well as enhancer accompanied with strong H3K27ac (**Figure 23B and 23C**), suggesting that cJUN might positively regulate CCL2 expression.
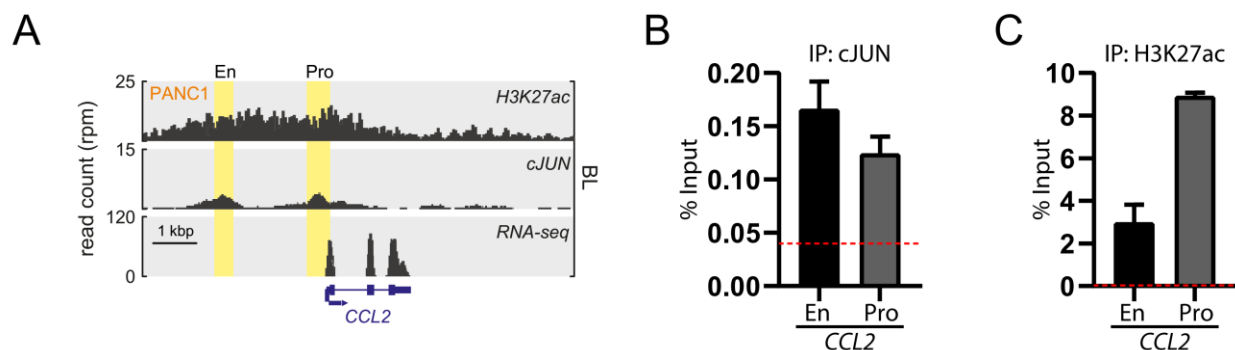

Figure 23. cJUN occupies active promoter and enhancer regions of CCL2 in BL cells. (A) Coverage plots of ChIP-seq for cJUN and H3K27ac, as well as RNA-seq in BL PANC1 cells at *CCL2* locus. For H3K27ac ChIP-seq and RNA-seq data in PANC1 cells, a publicly available dataset was utilized (Diaferia et al., 2016). Enhancer (En) and promoter regions (Pro) are highlighted. (B and C) qRT-PCR analysis following ChIP of cJUN (B) and H3K27ac (C) on *CCL2* promoter and enhancer regions indicated in (A) n=2.

3.4.5 Loss of cJUN leads to reduction of CCL2

To validate the regulation of cJUN on CCL2, we subjected BL PANC1 cells to cJUN-targeting siRNA transfection and tested cJUN expression on Western blot (**Figure 24A**).

siRNA #1 showed higher knockdown efficiency for cJUN. Therefore, it was used in all following experiments (**Figure 24A**). qRT-PCR confirmed siRNA-mediated knockdown on mRNA level. We observed that *CCL2* mRNA expression was significantly decreased upon cJUN silencing (**Figure 24B**). cJUN-dependent expression of CCL2 was further validated at the protein level by Western blot analysis using the established BL cell lines PANC1 and PT45P1 (**Figure 24C and 24D**). To test whether this effect was reproducible in the cells isolated from patient-derived xenografts (PDX), cJUN-high cell lines GCDX5 and GCDX57 were utilized for cJUN silencing. Consistently, CCL2 was considerably reduced following loss of cJUN (**Figure 24E and 24F**). These data strongly suggest that cJUN positively regulates CCL2 in BL PDAC cells.
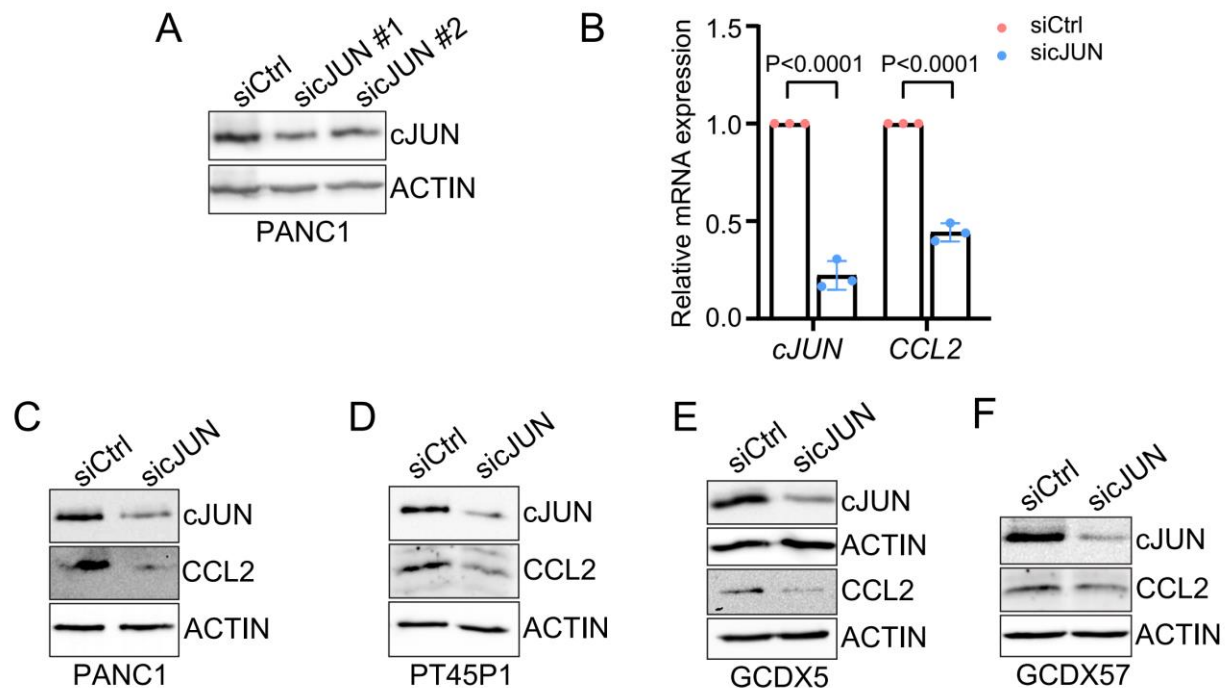

Figure 24. Effect of cJUN depletion on CCL2. (A) BL PANC1 cells were transfected with either siCtrl or different sicJUN sequences for 48 h. Cell lysates were subjected to Western blot analysis to test the efficiency of cJUN knockdown. Representative of three independent experiments. (B) qPCR analysis was performed for *cJUN* and *CCL2* in BL PANC1 cells upon 48 h transfection of either siCtrl or sicJUN. Bar graphs show means ± s.d. Unpaired student's t-test was used for statistical significance. n=3. (C-F) Western blot analysis of cJUN and CCL2 following cJUN silencing in established BL cells PANC1 (C), PT45P1 (D), as well as cell lines isolated from

patient-derived xenograft GCDX5 (E), and GCDX57 (F). Actin was used as loading control. Representative of three independent experiments.

3.4.6 TNFα upregulates cJUN and CCL2 expression

It is evident that TNFα is secreted from the TME and contributes to tumor progression as well as maintenance of the BL phenotypic state. Thus, we reasoned that TNFα might activate the inflammatory program in tumor cells to constitutively produce cytokines such as CCL2, in turn forming a positive loop for the recruitment of immune cells. To validate our hypothesis, we treated CLA (CAPAN1 and CAPAN2) as well as PDX-derived (GCDX62) cell lines with TNFα (10ng/µL) in a time dependent manner, as shown in **Figure 25**. Following the treatment with TNFα, expressions of cJUN as well as CCL2 were markedly induced, with robust effects seen at 8 h treatment (**Figure 25**).
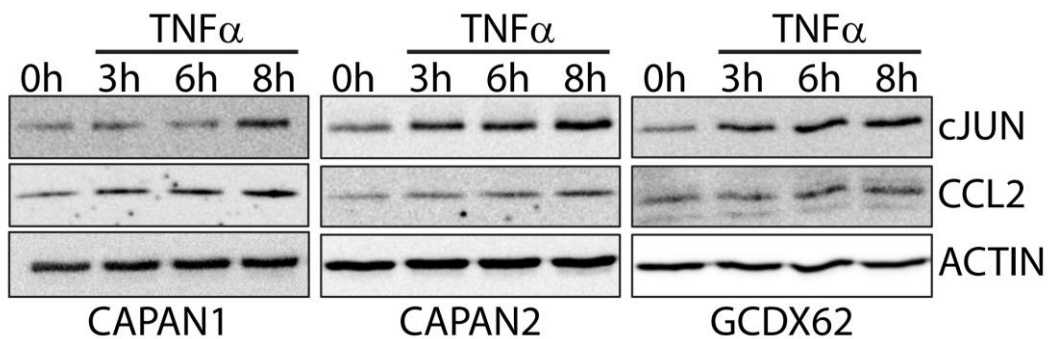

Figure 25. Exogenous TNFα treatment induces expression of cJUN and CCL2 in CLA cell lines. Western blot analysis of cJUN and CCL2 following TNFα treatment (10 ng/mL) for 3 h, 6 h, and 8 h in CAPAN1, CAPAN2, and GCDX62. Actin was used as loading control. Representative of three independent experiments.

For further validation, we engineered CLA PDAC cell lines to stably overexpress TNFα. Cells were transduced with either empty vector (EV) or lentiviral construct which carries a TNFα-mCherry insert. The expression of TNFα in these cells was confirmed by flow cytometry analysis (**Figure 26A**). CAPAN1- and CAPAN2-TNFα-OE cell lines displayed a significant induction of cJUN and CCL2 compared to their respective EV control (**Figure**

26B and 26C), along with a phenotypic switch from well-clustered toward a more spindle-like mesenchymal morphology in 2D culture (**Figure 26D**). This confirms that TNFα activates the expression of cJUN and CCL2 and promotes a more aggressive BL phenotype.
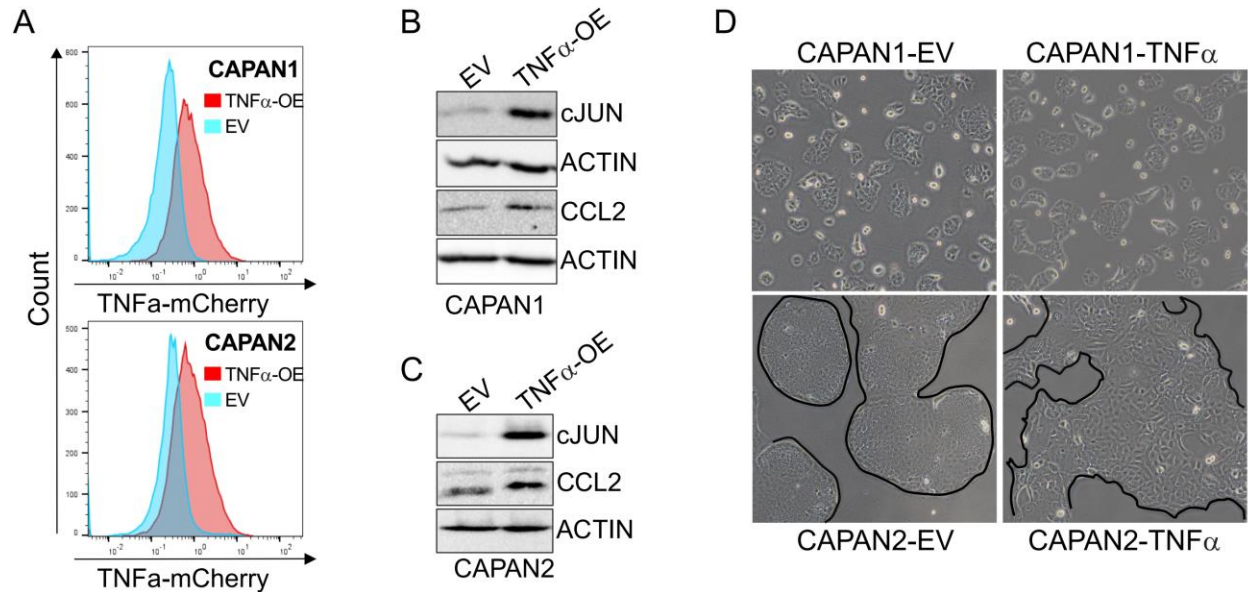

Figure 26. TNFα overexpression leads to induction of cJUN and CCL2. (A) Flow cytometric analysis of TNFα expression in CAPAN1-EV, CAPAN1-TNFα-OE, CAPAN2-EV, CAPAN2-TNFα-OE cells. 561 nm laser was used to detect TNFα-mCherry expression. Count of gated cells is shown against fluorescence intensity, which correlates to TNFα expression. n=3. (B and C) Western blot analysis of cJUN and CCL2 in CAPAN1-TNFα-OE cells (B) as well as CAPAN2-TNFα-OE cells (C). Actin was used as a loading control. Representative of three independent experiments. (D) Representative bright field images show morphology of CAPAN1-EV, CAPAN2-EV and their corresponding TNFα overexpression cell lines.

3.4.7 TNFα induces CCL2 expression via cJUN in PDAC

To determine whether cJUN was essential for TNFα-induced CCL2 expression, we utilized TNFα-OE cell lines and subjected them to *cJUN* siRNA transfection to test whether CCL2 expression is altered. Indeed, cJUN and CCL2 levels were significantly induced in both TNFα-OE cell lines. However, following siRNA-mediated depletion of

cJUN, the induction of CCL2 was alleviated (**Figure 27A and 27B**). This data suggests that TNFα induces CCL2 expression through a cJUN-dependent mechanism.
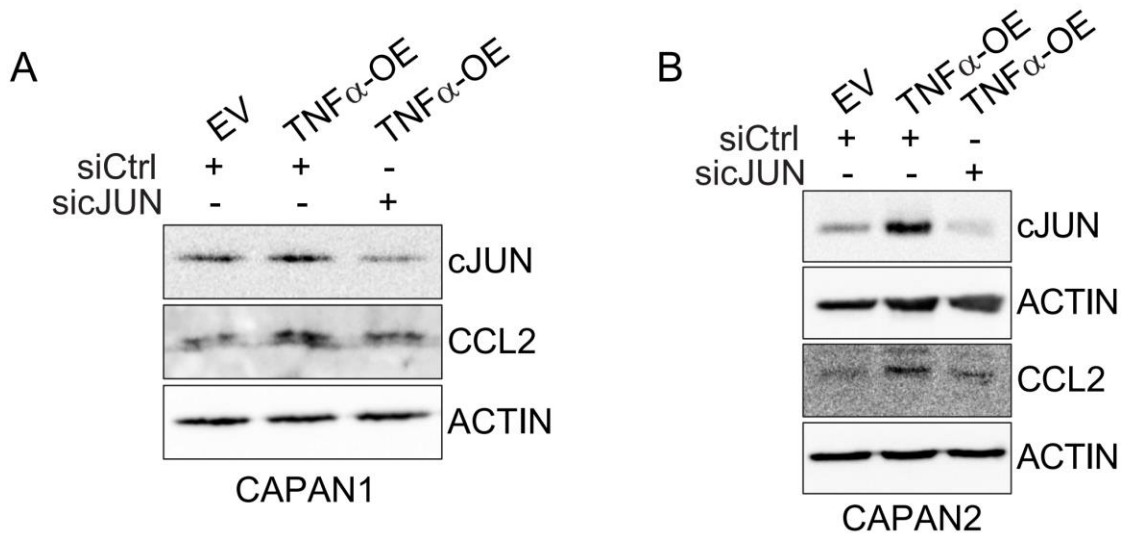

Figure 27. TNFα induced CCL2 is dependent on cJUN. (A and B) CAPAN1-TNFα-OE (A) and CAPAN2-TNFα-OE (B) cells were transfected with either siCtrl or sicJUN for 48 h. Cell lysates were subjected to Western blot analysis to test the expression of cJUN, CCL2. Actin was used as a loading control. Representative of three independent experiments.

3.5 TNFα monotherapy does not improve overall survival

So far, we identified a positive feed forward loop that TNFα+ producing macrophages induce cJUN-CCL2 signaling in tumor cells, further recruiting macrophages to sustain the BL subtype identity. Therefore, we investigated whether inhibition of TNFα alone was able to abrogate this feed forward loop and support a favorable prognosis. A syngeneic KPC mouse model was established by implanting KPCbl6 cells into C57BL/6J mice (**Figure 28A**). After tumor development, mice were administered anti-TNFα antibodies or IgG isotype control via i.p. injection. Survival was recorded when mice reached end point criteria, for example 20 % bodyweight lost, unkempt hair, looking dull or abnormal posture. However, the survival rate of IgG and anti-TNFα-treated mice did not differ significantly (**Figure 28B**).
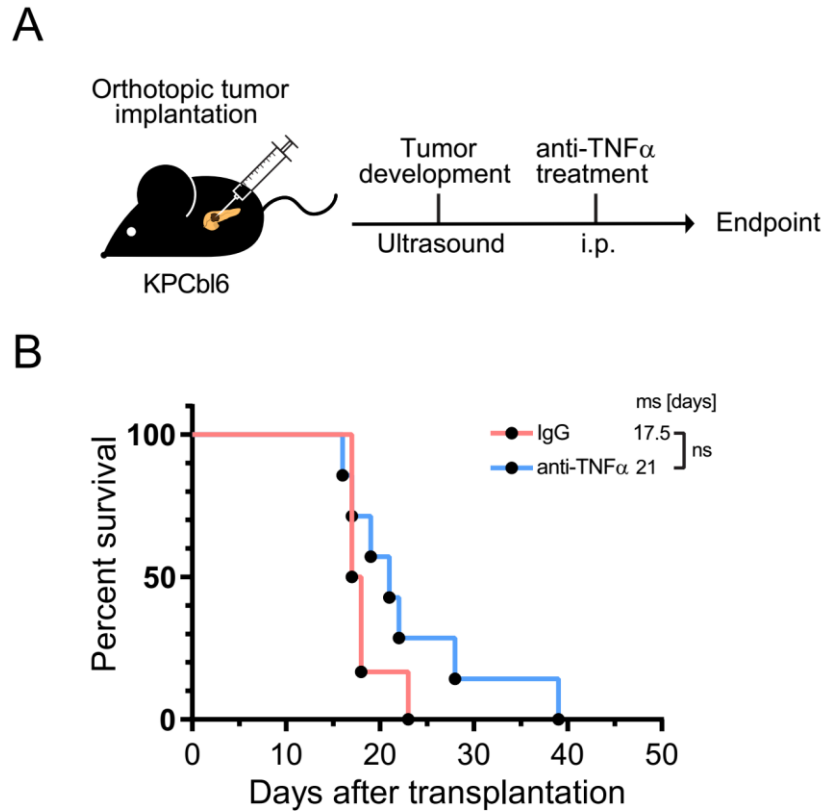
Figure 28. Inhibition of TNFα failed to improve the survival of syngeneic KPC mice. (A) illustration of experimental settings. 10-weeks old male C57BL/6J mice were orthotopically transplanted with 3.5 x 10^4 KPCbl6 cells. Tumor development was ensured by ultrasound. Anti-mouse TNFα antibody (10 µg/g body weight) was applied three times per week. (B) Kaplan-Meier plot indicating survival of IgG (red) and anti-TNFα-treated (blue) syngeneic KPC mice. Median survival (ms) as well as significance (as per log-rank test) are indicated.

H&E staining was performed in the IgG and TNFα-treated syngeneic KPC tumors. Tumor histology showed poor differentiation in general; however, we did observe any difference between control and treatment groups (**Figure 29A**). Histological quantification of well-differentiated tumors confirmed that there was no difference in well differentiated area between IgG and TNFα-treated tumors (**Figure 29B**). Additionally, blocking TNFα did not reduce the recruitment of CD45$^+$ cells (**Figure 29C and 29D**). These data suggest that TNFα inhibition is not an ideal therapeutic option.
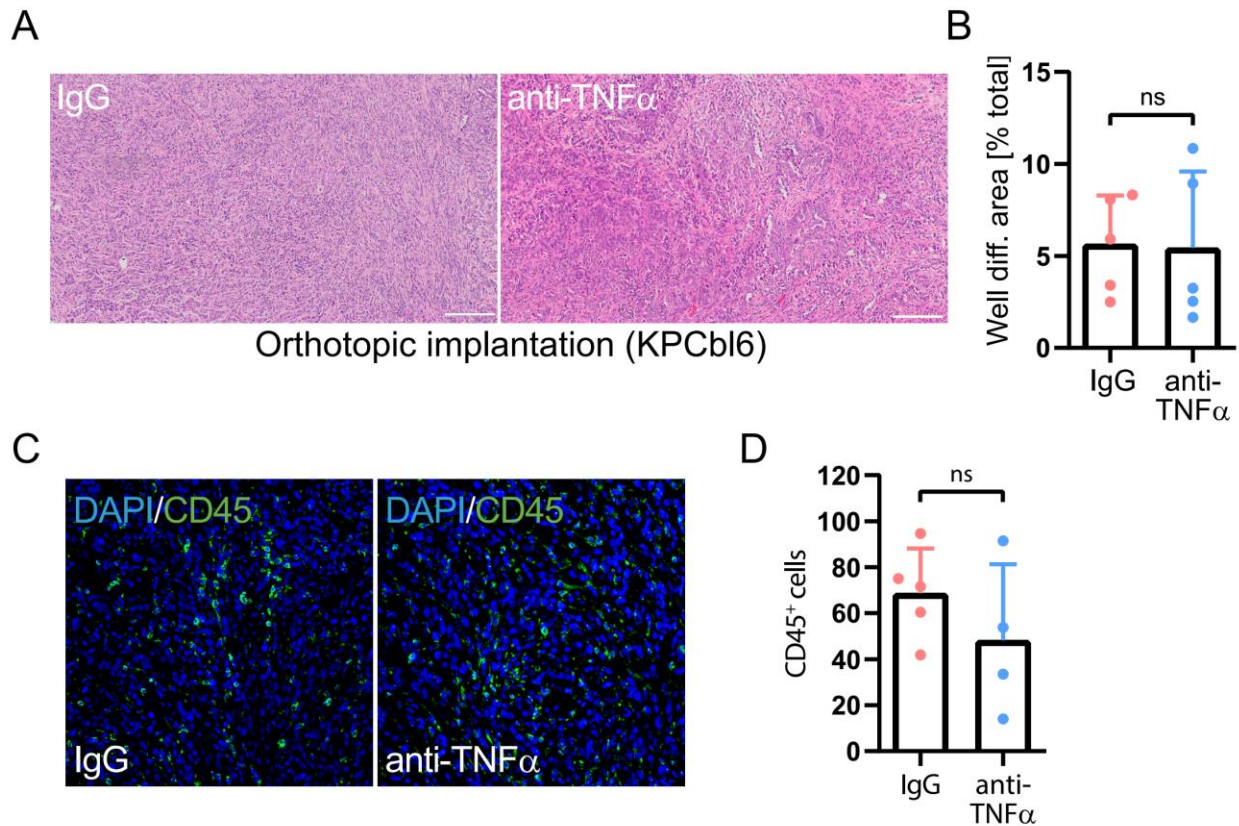
Figure 29. Inhibition of TNFα did not alter tumor differentiation or infiltration of CD45⁺ cells.
(A) Representative tile scan images of H&E staining in IgG and anti-TNFα-treated syngeneic KPC tumors. Scale bar: 200 µm. (B) Quantification of well differentiated tumor areas in (A). Scatter plots show well differentiated tumor area as percentage of total tumor area per animal, as well as means ± s.d. as bar graphs. Mann-Whitney test was used for statistical analysis. n=5 in IgG; n=5 in anti-TNFα. (C) Representative images of IF staining for CD45 in (A). (D) Quantification of CD45⁺ cells in (C). Scatter plots show average values per animal of counts per field of view as well as means ± s.d. as bar graphs. Mann-Whitney test was used for statistical analysis. n=5 in IgG; n=4 in anti-TNFα.

3.6 BRD4 controls cJUN expression via enhancer regulation

Since it is not feasible to block the cJUN-CCL2 signaling axis by TNFα inhibition, and there is no therapeutic drug available for specifically targeting TF cJUN, we sought to find

a potential chromatin regulator which may control cJUN expression in the BL subtype. Thus, we utilized a publicly available ChIP-seq dataset in PDAC cells (Diaferia et al., 2016) and examined differential occupancy of the active transcription mark Histone 3 lysine 4 trimethylation (H3K4me3) as well as H3K27ac between CLA and BL cell lines by the Enrichr tool (Chen et al., 2013; Kuleshov et al., 2016). Strikingly, we found not only cJUN binding regions to be significantly enriched (defined by H3K4me3 and H3K27ac), but also the bromodomain co-regulator BRD4 in the BL-specific active genomic regions (**Figure 30**).
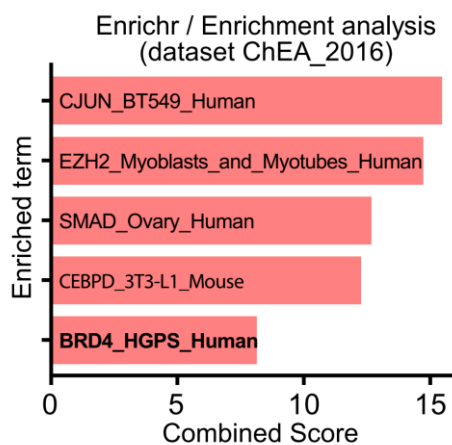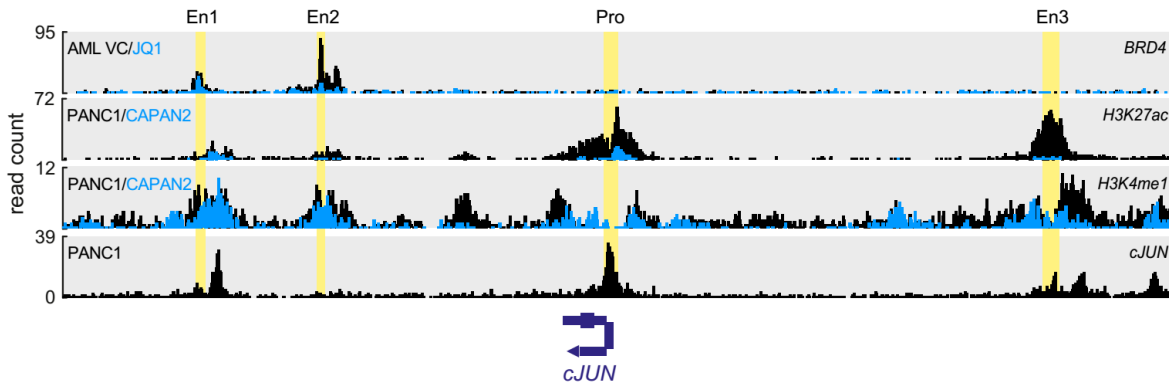

Figure 30. Enrichment score of cJUN and BRD4. Publicly available ChIP-seq dataset (Diaferia et al., 2016) was reanalyzed by F. Wegwitz (Department of Gynecology and Obstetrics, UMG, Germany) for the differential occupancy of H3K27ac and H3K4me3 (>2 fold change) between the BL and CLA PDAC cells using the Enrichr tool (Chen et al., 2013; Kuleshov et al., 2016).

To validate whether there was an association between cJUN and BRD4, we made use of a published dataset of BRD4 ChIP-seq in acute myeloid leukemia (AML) with DMSO and JQ1 treatment (Bhagwat et al., 2016). JQ1 is a small-molecule inhibitor for bromodomain and extra-terminal domain (BET) family with high affinity towards BRD4 (Filippakopoulos et al., 2010). This data revealed a significant occupancy of BRD4 on *cJUN* enhancer regions. ChIP-seq data of H3K27ac as well as enhancer marker Histone 3 lysine 4 monomethylation (H3K4me1) also displayed a strong enrichment at *cJUN* enhancer loci However, the enrichment was reduced upon JQ1 treatment (**Figure 31A**). Next, we

performed individual ChIP-qPCR experiments for BRD4 to confirm binding over the putative enhancer regions of *cJUN*. Indeed, these three loci were found to be strongly occupied by BRD4. As predicted, BRD4 lost its occupancies on these sites following 8 h JQ1 treatment (**Figure 31B**).

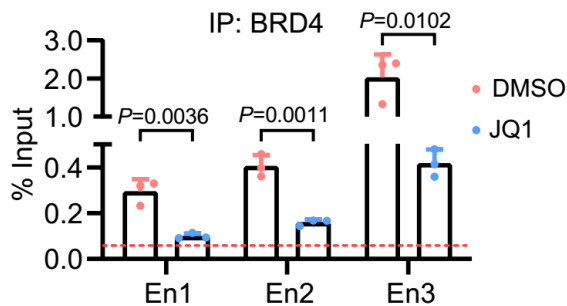**Figure 31. BRD4 occupies *cJUN* enhancer loci.** (A) Coverage of BRD4 ChIP-seq in acute myeloid leukemia (AML) in vehicle control (VC; black) and JQ1-treated (blue) conditions (Bhagwat et al., 2016), as well as H3K27ac and H3K4me1 ChIP-seq in CLA cells (CAPAN2; blue) and BL cells (PANC1; black) (Diaferia et al., 2016) at the *cJUN* gene locus. (B) ChIP for BRD4 was performed in BL PANC1 cells upon DMSO and JQ1 treatment for 8 h followed by qRT-PCR analysis. Red dashed line indicates average IgG isotype control. Bar graphs show means ± s.d. Mann-Whitney test was used for statistical analysis. n=3.

To validate the ChIP-qPCR results, which implies a regulation of cJUN by BRD4, we examined the expression of cJUN upon BRD4 depletion in BL cell lines. First, PANC1 cells were transfected with two different siRNAs to test the knockdown efficiency (**Figure**

32A). Accordingly, siBRD4 #1 was chosen to perform further analysis. Next, BL cell lines were tested for cJUN expression upon BRD4 silencing. We observed a significant reduction of cJUN following BRD4 silencing in both PANC1 and MiPaCa2 cell lines (**Figure 32B**), suggesting that BRD4 regulates cJUN expression.
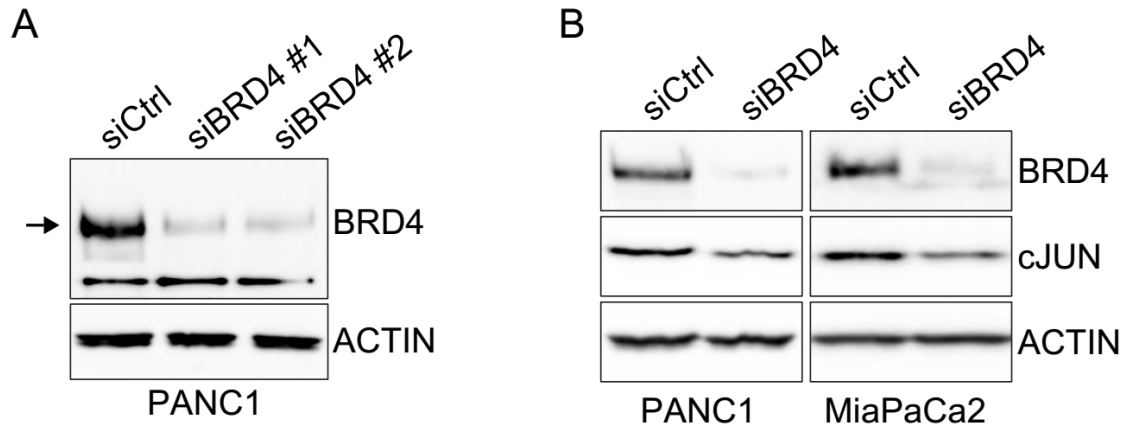

Figure 32. BRD4 positively regulates cJUN in BL cells. (A) Western blot analysis for BRD4 in BL PANC1 cells transfected with either siCtrl or siRNAs targeting BRD4 for 48 h. (B) Western blot analysis of BRD4 and cJUN in siBRD4 or siCtrl transfected BL PANC1 and MiaPaCa2 cells. Actin was used as loading control. Representative of three independent experiments.

3.7 Pharmacological inhibition of the BRD4-cJUN-CCL2 axis supports a favorable prognosis in preclinical mouse model

To elucidate the potential of pharmacological inhibition of BRD4, BL PANC1 cells were subjected to JQ1 treatment at different concentrations. As expected from siBRD4 experiments, JQ1 treatment led to a significant downregulation of cJUN at a concentration of 500 nM in BL PANC1 cells (**Figure 33**).
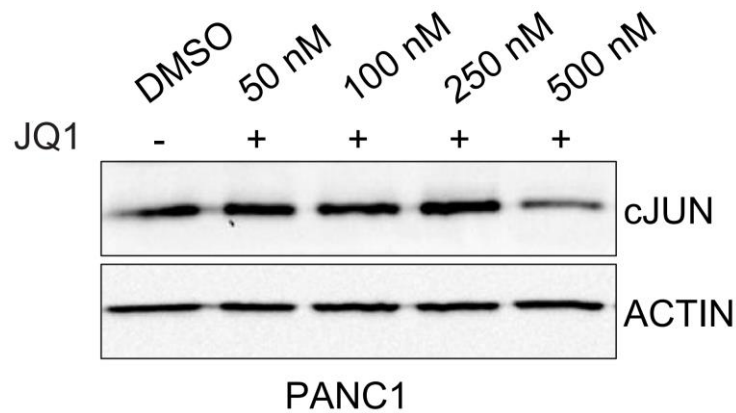
Figure 33. JQ1 treatment leads to reduction of cJUN. PANC1 cells were treated with JQ1 at indicated concentrations. After 24 h, cells were harvest and subjected for Western blot analysis for cJUN. Actin was used as loading control. Representative of three independent experiments.

To investigate the therapeutic effect of JQ1 inhibition on the cJUN-CCL2 signaling axis *in vivo*, we established a syngeneic orthotopic KPC mouse model using tumor cells derived from KPC mice implanted in 10-week old male C57BL/6J mice (**Figure 34A**). Tumor growth was detected by sonography on day 10 post-transplantation. After tumor development, mice were treated with DMSO or JQ1 (50 mg/kg bodyweight) daily over three weeks. Survival data was recorded when mice reached end point criteria, as mentioned previously. Under DMSO control treatment, mice only survived for 18 days (median survival). However, JQ1 treatment significantly prolonged median survival to 29 days, thereby supporting a favorable prognosis in the syngeneic KPC mice (**Figure 34B**).
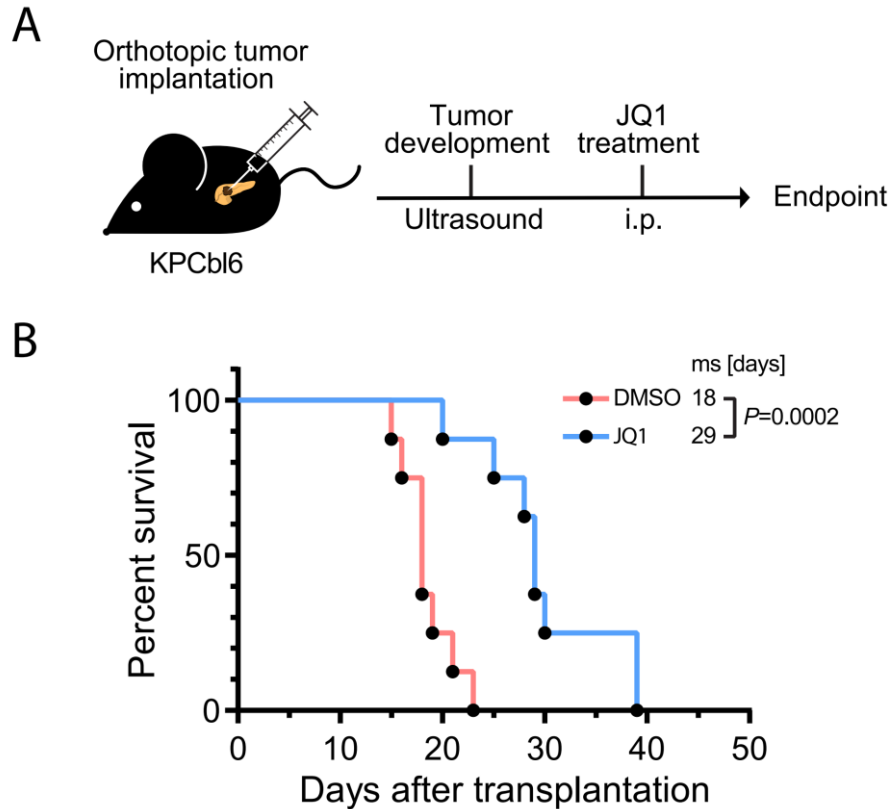
Figure 34. JQ1 resulted in a significant improvement of survival. (A) Diagram of experimental settings to investigate the therapeutic effect of JQ1 *in vivo*. 10-weeks old male C57BL/6J mice were orthotopically implanted with 3.5 x 10^4 KPC tumor cells derived from KPC mice. After 10 days of transplantation, (B) Ultrasound was performed to detect tumor growth. Mice were administrated with JQ1 (50 mg/kg bodyweight) and DMSO control daily. (B) Kaplan-Meier plot indicating survival of DMSO (red) and JQ1-treated (blue) syngeneic KPC mice. Median survival (ms) as well as significance (as per log-rank test) are indicated.

In order to evaluate the potential changes of tumor histology following JQ1 treatment, H&E staining was performed in the DMSO- and JQ1-treated syngeneic KPC tumors followed by whole tissue tile image scans (**Figure 35A**). Of note, PDAC tumors derived from syngeneic KPC mice exhibit BL/poorly differentiated histology. Notably, JQ1-treated tumors were observed to gain a more differentiated phenotype, which significantly recapitulates a CLA phenotypic state. The proportion of well differentiated tumor area was considerably induced in the JQ1-treated tumors over DMSO control (**Figure 35B**).
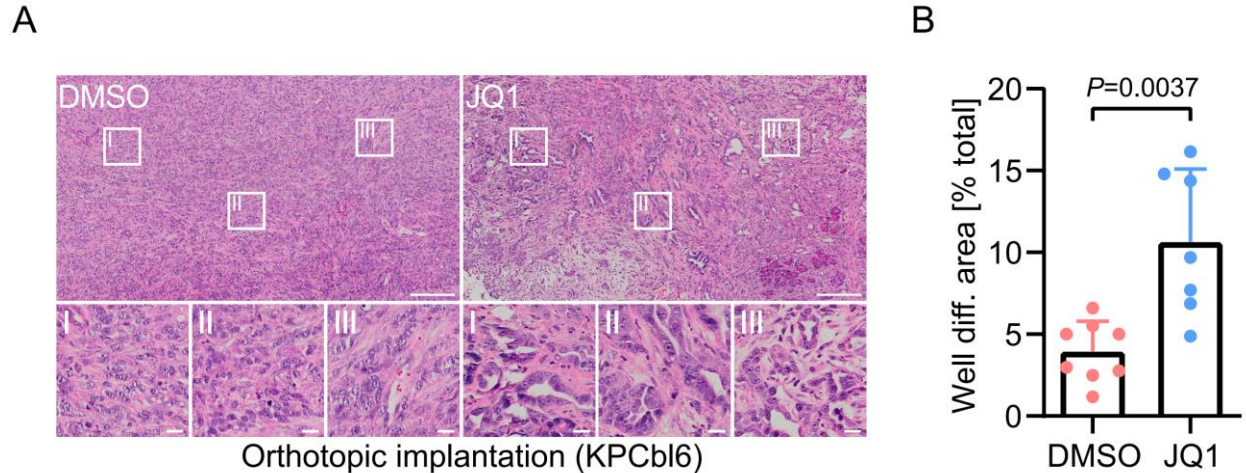
Figure 35. JQ1 treatment restrains tumor dedifferentiation. (A) Representative images of H&E staining in pancreatic tumor tissues derived from DMSO control and JQ1-treated syngeneic KPC model. I-III depict higher magnification images. Scale bar: representative images (top): 200 μm; higher magnification images (bottom): 10 μm. (B) Scatter plot showing quantification of well differentiated tumor area as percentage of the total tumor area in DMSO- and JQ1-treated mice, as well as means ± s.d. as bar graphs. n=8, DMSO; n=7, JQ1. Mann-Whitney test was used for statistical analysis.

Since a phenotypic switch could be seen in the JQ1 treated tumor tissues, we investigated how tumor cells changed their cellular plasticity. Firstly, VIM expression was investigated by performing IF staining in the DMSO- and JQ1-treated tumors. A significant reduction of VIM with the application of JQ1 was observed (**Figure 36A and 36B**), which could partially explain the reduced poorly differentiated phenotype in the JQ1-treated tumors. To further validate whether the JQ1-triggered phenotypic switch was mediated through cJUN, the expression of TNFα and cJUN as well as CCL2 were probed in the syngeneic KPC tumors. It showed that cJUN was dramatically reduced in the treatment of JQ1 (**Figure 36A and 36C**), concomitant with a reduction in the expression TNFα and CCL2 (**Figure 36A, 36D and 36E**), resulting a reduction of the infiltration of CD45⁺ cells (**Figure 36A and 36F**). Taken together, these data suggest that inhibition of BRD4 by JQ1 abrogates the cJUN-CCL2-TNFα regulatory axis in neoplastic cells, which further inhibits

the infiltration of TNFα+ immune cells in the TME, and thus, supports a favorable prognosis in PDAC.
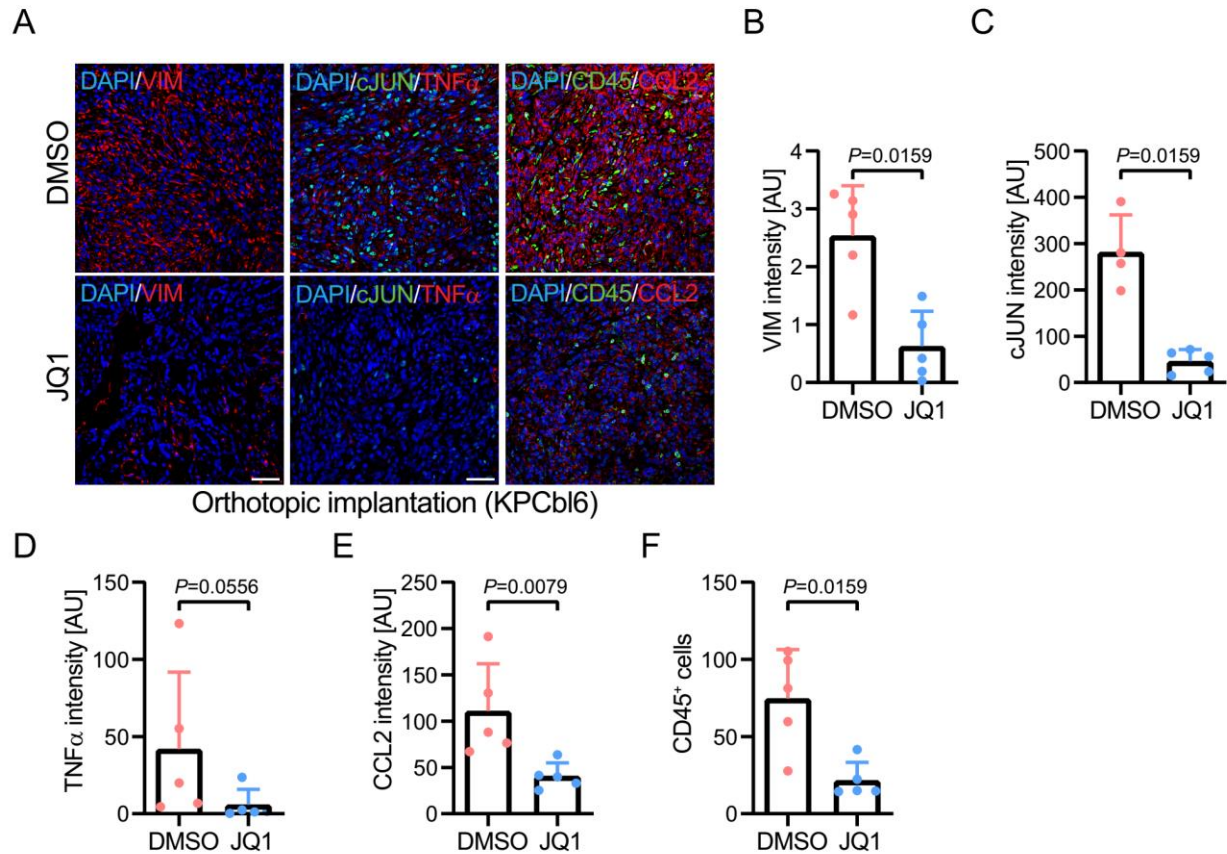
Figure 36. JQ1 alone reduces inflammatory immune microenvironment and EMT factors. (A) Representative images of IF staining for vimentin (VIM), cJUN, TNFα, CCL2, and CD45 in syngeneic KPC tumors with DMSO and JQ1 treatment. (B-E) Intensity quantification of VIM (B), cJUN (C), TNFα (D), and CCL2 (E). Scatter plots show values in arbitrary units (AU) as an average per animal, as well as means ± s.d. as bar graphs. n=5 in DMSO; n=5 in JQ1. Mann-Whitney test was used for statistical analysis. (F) CD45+ cells of (A). Scatter plots show average count values per animal per F.o.V. as well as means ± s.d. as bar graphs. Mann-Whitney test was used for statistical analysis. n=5 in DMSO; n=5 in JQ1.

4 Discussion

4.1 The role of TNFα in PDAC plasticity

Tumor subtype-specific environmental factors play a major role in disease prognosis. In PDAC, the subtype-specific inflammatory immune signals determine distinct prognosis in patients. Recent transcriptional profiling studies in PDAC tumors identified a complex heterogeneity within stromal immune components (activated stroma vs. immune components) and tumor epithelium (CLA vs. BL) (Moffitt et al., 2015; Puleo et al., 2018). CLA subtype is correlated with better prognosis compared to BL subtype (Moffitt et al., 2015). Nevertheless, how subtype-specific molecular events shape the inflammatory immune microenvironment, and hence determines PDAC prognosis remains unclear.

As a key inflammatory cytokine, TNFα was originally identified to induce the necrosis of transplanted methylcholanthrene-induced sarcomas in mice (Carswell et al., 1975). However, subsequent evidence unveiled a paradoxical role of TNFα in tumor promotion (Calcinotto et al., 2012). In ovarian cancer, TNFα was able to promote tumor cell spreading to other organs by upregulating a range of cytokines (Kulbe et al., 2007). Besides, TNFα concentrations was higher in non-small-cell lung cancer patient serum sample; increased TNFα level was associated with high lymphoid and distant metastasis (Shang et al., 2017). Similar findings were reported in PDAC, where TNFα levels were negatively correlated with PDAC patient survival, as revealed by TMA analysis. TNFα neutralization in combination with chemotherapeutics significantly improved mice survival (Zhao et al., 2016).

Based on the notion that TNFα may play a role in promoting PDAC progression, we demonstrated the correlation between high-level TNFα and high-grade/poorly differentiated tumors of KPC mice and PDAC patient biopsies. Mouse orthotopic transplantation model using the CLA and BL cells also confirmed the profound enrichment of TNFα in the BL tumors. Thus, we show a phenotype-dependent expression of TNFα. Addtionally, studies in PDAC suggest a marked correlation of TNFα-related signatures to inflammatory stromal and BL subtypes (Miyabayashi et al., 2020; Puleo et al., 2018;

Chan-Seng-Yue et al., 2020). For instance, transcriptomic analysis of PDAC patient tumors revealed a significant enrichment of TNFα signaling pathway in the inflammatory stromal component corresponding to BL subtype (Puleo et al., 2018). Additionally, studies from Chan-Seng-Yue et al. and Miyabayashi et al. noted that TNFα-signaling pathway was significantly enriched in the BL tumors and invasive PDAC phenotypes (Miyabayashi et al., 2020; Chan-Seng-Yue et al., 2020). However, whether PDAC subtype-specific TNFα expression restrain or promote disease aggressiveness remains to be established.

We show that exogenous TNFα administration switched W/M differentiated tumors into poorly differentiated BL phenotypic state of a CLA-derived orthotopic mouse model. This phenotypic change was further validated with IF staining for the BL-specific marker KRT81 (Noll et al., 2016; Muckenhuber et al., 2018), which is highly expressed in the TNFα-treated CLA orthotopic tumors, highlighting the significant role of TNFα in tumor-promoting and subtype-switching in PDAC. Besides tumor subtype switch, we also observed that TNFα-induced BL phenotypic state was associated with an increased infiltration of CD45^{+} immune cells.

TNFα was found to induce the invasive capacity of the CLA cells, concomitant with reduction of a low-grade specific TF KLF5 and induction of EMT inducer ZEB1. ZEB1 is a vital TF known to enhance the invasive and metastatic capacity of PDAC (Krebs et al., 2017). Tumor cells lacking ZEB1 switched from mesenchymal to an epithelial phenotype in PDAC (Wellner et al., 2009). On the other hand, KLF5 was shown to be specifically expressed in the CLA cells as well as low-grade tumors in PDAC (Diaferia et al., 2016). KLF5 plays an essential role in the maintenance of the CLA phenotype via regulating a subset of epithelial gene signatures (Diaferia et al., 2016). There are lineage genes and TFs, which are important for the maintenance of subtype identity (Neph et al., 2012). Studies have uncovered an association of ELF3, HNF1B, and GATA6 with low-grade tumors, and they are characterized as CLA lineage markers (Collisson et al., 2011; Diaferia et al., 2016; Martinelli et al., 2017; Somerville et al., 2018). However, TP63, GLI2 are required for the BL subtype identity (Adams et al., 2019; Somerville et al., 2018). Together, for the first time, we show that TNFα can switch the phenotypic identity by changing the expression of the lineage-specific gene regulatory program.

Hallmarks of EMT and inflammatory response were significantly enriched in the TNFα-treated CLA cells revealed by RNA-seq analysis, in line with our previous observations of TNFα induced BL phenotype *in vivo* and *in vitro*. 'KRAS signaling down' and 'myogenesis' pathways induced by TNFα also appeared in the aggressive PDAC phenotypes evidenced by Miyabayashi et al. (Miyabayashi et al., 2020). Additionally, we show that TNFα caused downregulation of majority of the CLA gene signatures including ELF3, FOXQ1, CEACAM6, CEACAM5, as well as AGR2, and upregulation of BL markers such as KRT5, KRT14, and EGFR. Taken together, TNFα was firstly evidenced to induce CLA to inflammatory BL phenotypic switch and favors tumor progression via regulation of epithelial plasticity in PDAC (**Figure 37**).

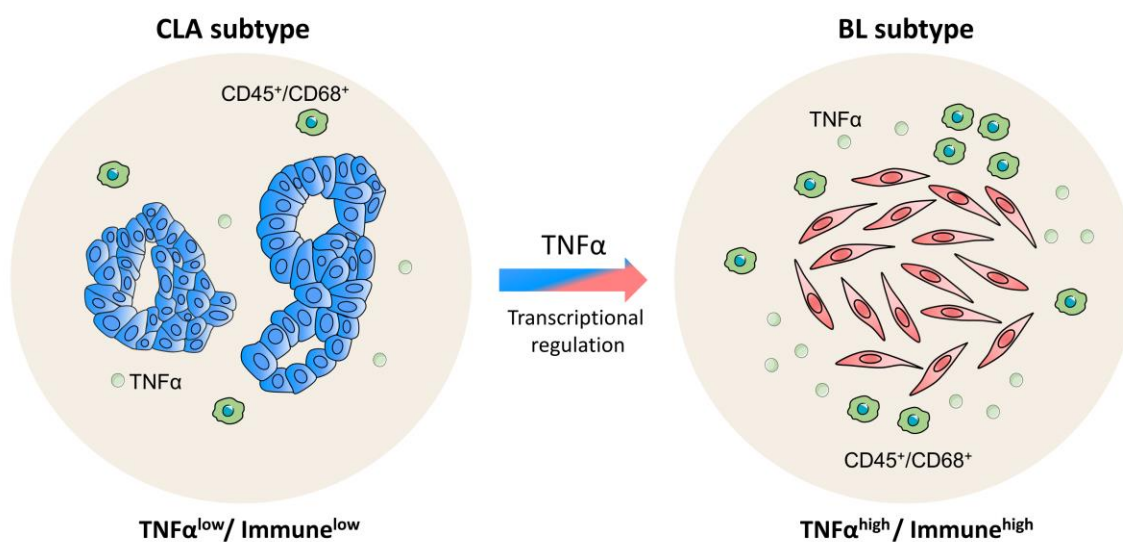**Figure 37. Illustration of TNFα induced CLA to BL subtype switch.** CLA PDAC subtype displays well-differentiated tumor phenotype with limited expression of TNFα and CD45^{+} cells. Conversely, BL subtype has abundant TNFα in tumor tissues. Exogenous TNFα leads to subtype switch from CLA to BL phenotypic state via downregulation of CLA-associated transcriptional network, accompanied by increased infiltration of CD45^{+} cells.

4.2 PDAC subtype-dependent stromal microenvironment

Based on the observations of subtype-dependent expression of TNFα in tumor tissues, the initial hypothesis was that TNFα was produced by BL tumor cells. However surprisingly, contrary to Zho et al. who reported the source of TNFα expression from the PDAC cell lines (i.e. PANC1 and MiaPaCa2 cell lines) (Zhao et al., 2016), we found that none of the PDAC cells including CAPAN1, CAPAN2, PANC1, and MiaPaC2 express TNFα. Though different antibodies were used for flow cytometry analysis, cell lines might differ in the aspects of source and passages. We further validated that these cells do not produce soluble TNFα via ELISA, suggesting that PDAC cells are not the source of TNFα in the BL tumors.

Except for the epithelial cells in the TME, stromal immune counterpart is equally important for modulating subtype identity (Ho et al., 2020). We speculated that TNFα might come from the inflammatory microenvironment of the BL subtype. Examination of human- and murine-specific TNFα revealed that only murine TNFα was detected in the BL orthotopic transplanted mice with no trace of human TNFα, indicating the source of TNFα being host inflammatory microenvironment. In the BL tumors, CD45+ and CD68+ cells were highly infiltrated relative to the CLA tumors. Recently, single-cell analysis in PDAC mouse models unveiled that macrophage was the most predominant cell population in the late stage of the disease (Hosein et al., 2019). Thus, it is highly likely that TNFα-producing CD68+ macrophages present in PDAC in a subtype-dependent manner.

In the TME, CCL2 is a chemotactic cytokine known to recruits macrophages through CCL2-CCR2 signaling (Nagarsheth et al., 2017). Mounting evidence have reported that CCL2 signaling-mediated macrophages contribute to tumor progression and metastasis in multiple cancers (Chen et al., 2018; Fader et al., 2010; Qian et al., 2011; Zhang et al., 2010). To take an example of breast cancer, CCL2 was reported to recruit macrophages to facilitate tumor cell metastasize to the lung (Qian et al., 2011). However, after blockage of CCL2 by anti-CCL2 antibody, infiltrated macrophages were dramatically reduced, as well as lung metastases. Consequently, mice survival was significantly prolonged (Qian et al., 2011). Moreover, a high level of CCL2 was associated with poor prognosis in lung

cancer, ovarian cancer, as well as breast cancer (Li et al., 2018; Ueno et al., 2000). In our study, levels of several cytokines including CCL2 were extremely high in the BL cells analyzed by RNA-seq data obtained from publicly available dataset (Bailey et al., 2016). High-level CCL2 in the BL cells was further validated by human cytokine profiler kit. Furthermore, a strong association of CCL2 with the squamous (i.e. BL) PDAC subtype (Puleo et al., 2018) could be seen. Thus, we show that different PDAC subtype links to distinct TME. Compared to CLA, BL subtype has an inflammatory TME with high expression of CCL2 and infiltration of TNFα-producing CD68^{+} macrophages.

Similarly, the work from Li et al. highlighted that tumor intrinsic cytokine determines the immune heterogeneity of PDAC (Li et al., 2018). They identified CXCL1 as a pivotal intrinsic factor that changes the subtype identity from T cell-low to T cell-high tumors. Besides, inhibition of colony stimulating factor 1 receptor (CSF1R) was able to alter the composition of TME (Candido et al., 2018). Ligand CSF1 mediated signaling is important for the differentiation and maintenance of macrophage (Sehgal et al., 2018). Targeting of CSF1R led to significantly reduction of macrophages in tumor tissues. Therefore, tumor switched from BL to CLA phenotype and mice survived longer (Candido et al., 2018), suggesting the significant role of macrophage in subtype identity.

4.3 The role of JUN/AP1 family in tumor plasticity

AP1 transcription factor has been extensively studied of its function regarding the regulation of inflammatory response (Lopez-Bergami et al., 2010). However, the implication of AP1 family TF complexes in PDAC aggressiveness remains elusive. AP1 TF complexes consist of JUN (cJUN, JUNB, JUND), Fos (c-FOs, FOSB, FRA1, FRA2), activating transcription factor (ATF) (ATF2, ATF3, B-ATF, JDP1, JDP2), as well as musculoaponeurotic fibrosarcoma (MAF) (c-Maf, MafB, MafA, MafG/F/K and Nrl) (Shaulian and Karin, 2002). They form either homo- or heterodimeric protein complexes (e.g. cJUN-cJUN, cJUN-FOS) for enhancing DNA binding to regulate their gene targets (Eckert et al., 2013). In recent years, emerging studies unveiled the potential role of AP1 in regulating tumor phenotypic identity (Diaferia et al., 2016; Milan et al., 2019; Roe et al., 2017).

We identified that JUN/AP1 pathway was significantly associated with the PDAC subtype identity. cJUN/AP1 and JUNB/AP1 were mutually exclusively expressed in the PDAC subtype specific manner. Our *in vitro* and *in vivo* findings suggest that cJUN is mainly involved in the maintenance of BL-inflammatory program, whereas JUNB is exclusively expressed in the CLA tumors. In line with our findings, Diaferia et al. have identified high expression of JUNB in low-grade tumors based on immunochemistry staining (Diaferia et al., 2016), confirming the correlation of JUNB with the CLA subtype. Although, a recent study has shown that cJUN/AP1 induces inflammatory program in chronic pancreatitis (Cobo et al., 2018), the transcriptional activation of cJUN in PDAC subtype specificity remains unresolved.

By intersecting JUNB or cJUN targets with CLA-related or BL-related ATAC-peaks respectively, we find that 'cell-cell adhesion regulation' and 'epithelial cell differentiation' gene sets were enriched in JUNB/CLA-related regions, which support our findings that JUNB restricted to well-differentiated tumors. On the other hand, pathways of 'response to growth factor', 'leukocyte migration', as well as 'regulation of cytokine production' were enriched in cJUN/BL-related regions, suggesting the role of cJUN in immune regulation. Consistently, we detected strong occupancy of JUNB on *CDH1* at promoter and enhancer sites, associated with H3K27ac occupancy. *CDH1* encodes for ECAD, which is a transmembrane protein, involved in the formation of adherens junctions to mediate cell to cell connections (van Roy and Berx, 2008). ECAD is typically expressed in the epithelial cells, playing an essential role in the maintenance of epithelial structure (Natalwala et al., 2008). In the BL cells, we show that cJUN occupies both promoter and enhancer loci of *VIM*. VIM is a family member of intermediate filaments, maintaining mesenchymal features (Ivaska et al., 2007). These findings support the idea that JUNB might involve in maintenance of epithelial differentiation in the CLA subtype, while cJUN is, in fact, required for the tumor dedifferentiation in the BL subtype.

Together, we show that cJUN and JUNB exert distinct functions in PDAC subtype maintenance. We proposed a model to elaborate cJUN- and JUNB- mediated PDAC subtype identity (**Figure 38**).
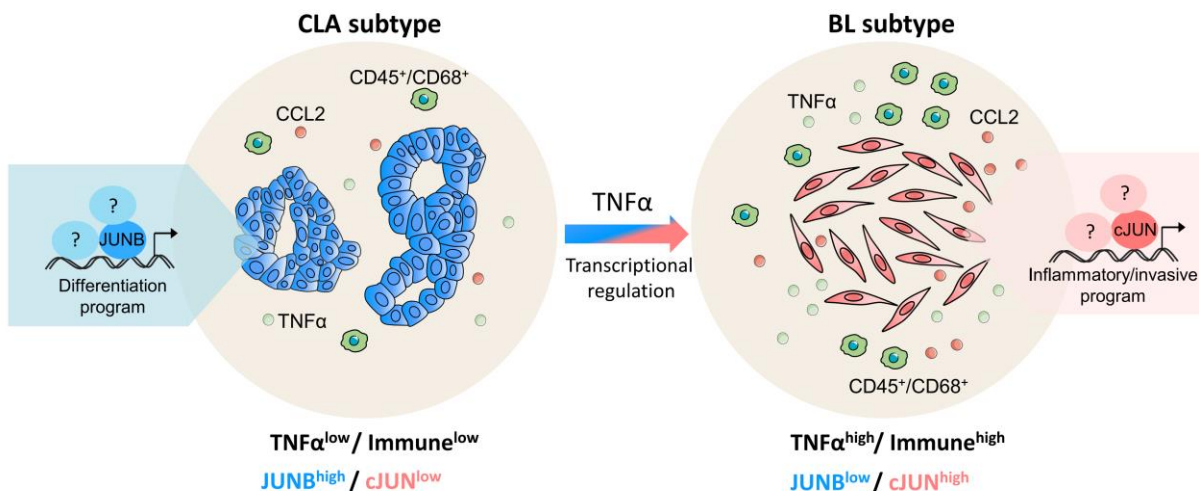
Figure 38. JUNB and cJUN in controlling PDAC subtype identity. JUNB is selectively expressed in the CLA PDAC subtype and maintain the epithelial differentiation. cJUN is restricted to the BL PDAC subtype which is highly infiltrated with CD68^{+} cells. The possibility of other lineage transcription factors cooperative with JUNB or cJUN still needs to be tested.

4.4 cJUN-regulatory network in macrophages recruitment and therapy resistance

We show that cJUN-OE cells displayed an invasive phenotype in CLA PDAC cells. Our findings align with the previous report where cJUN overexpression showed similar phenotype in MCF-7 breast cancer cells (Smith et al., 1999). Notably, MCF7 cell line identified as luminal A subtype (Adelaide et al., 2007), which displays identical phenotype to the PDAC low-grade/CLA subtype (Adelaide et al., 2007). Consistently, another finding in breast cancer model showed that loss of cJUN activity associated with reduced tumor cell migration and invasive behavior (Jiao et al., 2010). Thus, cJUN promotes the shift of CLA tumors into more invasive BL phenotypic state. Moreover, BL tumor aggressiveness is often associated with increased chemoresistance profile in PDAC (Aung et al., 2018). Since cJUN-OE switched cells towards a more BL phenotype, we proposed that cJUN-OE cells might exhibit chemoresistant properties. Of note, PDAC patients with CLA

tumors respond efficiently to chemotherapy, in particular with m-FOLFIRINOX and nap-paclitaxel/gemcitabine (Aung et al., 2018). We compared IC_{50} of oxaliplatin, SN38 (an activate metabolite of irinotecan) that are the active components of FLOFIRINOX, as well as gemcitabine in cJUN-OE cells. Oxaliplatin was designed based on platinum, forming DNA-platinum adducts to inhibit DNA replication and induce cell apoptosis (Zoetemelk et al., 2020). While irinotecan is a topoisomerase inhibitor and it slightly inhibits DNA synthesis (Zoetemelk et al., 2020). However, the effect was much more augmented when it is transformed into an activated metabolite SN38. SN38 accelerates DNA damage via generating chromosome aberrations and ultimately leads to apoptosis (Zoetemelk et al., 2020). cJUN-OE cells showed more resistance to these drugs compared to EV cells. Similarly, Lipner et al. reported that cJUN is essential for conferring resistance to FOLFOX (combination of 5-FU and oxaliplatin) treatment in PDAC mouse models (Lipner et al., 2020). Furthermore, lentiviral-mediated cJUN depletion significantly increased the sensitivity of PDAC cells to FOLFOX (Lipner et al., 2020), confirming the crucial role of cJUN in chemoresistance, thereby maintaining BL phenotypic state.

Besides cJUN functions in the neoplastic-epithelial plasticity, we also identified its crucial role in the recruitment of inflammatory immune cells. We hypothesized that cJUN might transcriptionally regulate CCL2 for the recruitment of TNFα-producing macrophages in the BL tumors. Our novel findings show that cJUN directly controls CCL2 expression via enhancer-promoter regulation in BL PDAC cells. Importantly, cJUN-mediated CCL2 expressions is found in the established PDAC cells as well as cJUN-high cell lines isolated from patient-derived xenograft (PDX). Together, these findings suggest that cJUN positively regulates CCL2 for the maintenance of TNFα-mediated inflammatory program in the BL PDAC subtype. Of note, we showed that high expressions of TNFα is linked to inflammatory and poorly differentiated/BL phenotypic state.

Interestingly, our results show that TNFα induces cJUN-CCL2 feed-forward loop in CLA PDAC subtype. Constitutive expression of TNFα in the CLA cells led to a highly invasive/BL phenotypic identity, which is functionally similar to the cJUN-OE CLA PDAC cell lines. Importantly, loss of cJUN significantly suppressed the TNFα induced CCL2, indicating that cJUN is essential for the TNFα mediated upregulation of CCL2.Together,

we identified a cJUN-driven inflammatory BL program, which is essential for maintenance of TNFα-mediated PDAC aggressiveness (**Figure 39**).
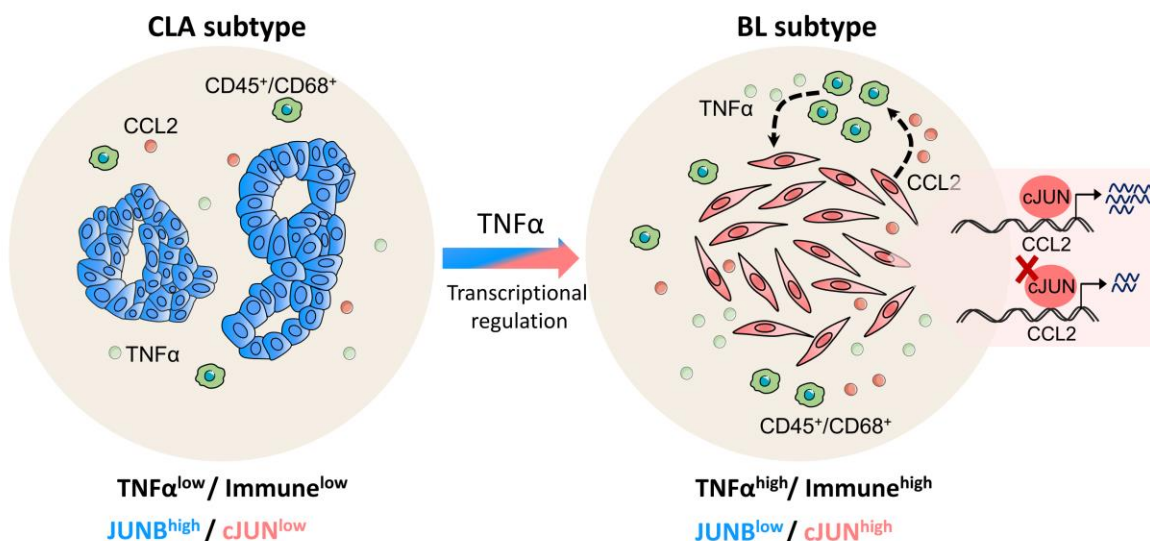

Figure 39. Illustration model of cJUN-CCL2-TNFα positive feedforward loop. cJUN activates CCL2 to recruit CD68^{+} macrophages which secrete TNFα, and in turn, fostering tumor cells and activating cJUN-CCL2 signaling axis to promote a worse phenotype.

4.5 Monotherapy of anti-TNFα is not ideal for PDAC

Anti-TNFα monotherapy has been approved in clinical use for many types of chronic inflammatory disease including rheumatoid arthritis, Crohn's disease, psoriatic arthritis, ankylosing spondylitis, ulcerative colitis, as well as severe psoriasis (Feldmann, 2002; Jackson, 2007; Thalayasingam and Isaacs, 2011). To date, there are five distinct monoclonal antibodies available for targeting TNFα: etanercept, infliximab, adalimumab, golimumab, and certolizumab (Thalayasingam and Isaacs, 2011). Despite the promising effect of anti-TNFα conferred in the inflammatory disease, whether it is effective for cancer treatment is still debatable.

In our study, anti-TNFα treatment did not improve the overall survival of syngeneic KPC mice, which is a highly aggressive immunocompetent mouse model. We anticipated that TNFα monotherapy might switch the BL tumors into more favorable CLA-like phenotype. However, neither tumor differentiation nor recruitment of inflammatory immune cells (CD45^{+} and CD68^{+}) were altered following TNFα monotherapy. There could be two major reasons for the failure of anti-TNFα monotherapy: (i) tumors developed from syngeneic KPC mice are highly heterogeneous and surrounded by dense stroma tissues including fibroblasts, extracellular matrix, and vasculature (Neesse et al., 2011; Ying et al., 2016). Desmoplastic reaction makes it difficult for TNFα neutralizing antibodies to penetrate and reach PDAC tumors. Similarly, CCL2 neutralizing antibody alone did not improve the survival of PDAC mouse model (Kalbasi et al., 2017); (ii) KPC-derived tumors display extremely aggressive phenotype, which constitutively expresses cJUN-mediated CCL2-TNFα axis. Therefore, targeting TNFα alone is not sufficient to prevent the overall tumor progression. Therefore, targeting cJUN alone or in combination with TNFα monotherapy may improve the outcome of BL tumors.

4.6 Preclinical inhibition of BRD4 confers favorable prognosis of BL tumors

Considering that anti-TNFα therapy failed to improve the prognosis in PDAC, and there was no pharmacological inhibitor available to specifically target cJUN, we assumed that a potential chromatin regulator could be serve as a candidate for the blocking cJUN-mediated signaling axis. Interestingly, our data showed that chromatin regulator BRD4 was highly enriched in the BL subtype (Diaferia et al., 2016). BRD4 belongs to bromodomain and extraterminal domain (BET) family, it is a chromatin remodeler that functions as a chromatin 'reader' to recognizes the acetylated histones and regulate gene expression (Belkina and Denis, 2012; Wu et al., 2013). Study has shown that BRD4 was highly expressed in the late stage of PDAC mouse tumors (Hosein et al., 2019). Most recently, the work from Shu et al. revealed that in breast cancer patients, BRD4 was significantly higher expressed in the basal (likely to BL PDAC) tumors compared to luminal (likely to CLA PDAC) tumors (Shu et al., 2020).

This enrichment analysis gave us an indication that there might be a regulation between BRD4 and cJUN. And if so, BRD4 could be exploit as a therapeutic target for inhibiting cJUN. JQ1 is a small molecular inhibitor, which competitively binds to the pocket of the bromodomain and replaces the BRD4 protein from acetylated histones (Filippakopoulos et al., 2010). By reanalyzing public ChIP-seq data in acute myeloid leukemia (AML) cells (Bhagwat et al., 2016), we showed that JQ1 led to decreased BRD4 occupancy at enhancer regions of *cJUN*. Consistently, JQ1 resulted in reduced occupancy of BRD4 at *cJUN* enhancer sites in PDAC, as validated by ChIP-qPCR. The positive regulation of BRD4 on cJUN was confirmed by reduced expression of cJUN upon abrogation of BRD4 by siRNA. As expected, BET inhibitor JQ1 led to reduction of cJUN in the BL cells.

Mazur et al. showed that JQ1 resulted in reduced expression of CD45$^+$ cells as well as F4/80$^+$ macrophages. The JQ1 therapy alone, or in combination with histone deacetylase (HDAC) inhibitor, significantly improved the survival of PDAC mouse model (Mazur et al., 2015, Andricovich et al., 2018). Thus, pharmacological inhibition of BRD4 via JQ1 significantly improve the pre-clinical outcome of PDAC. Importantly, we show that JQ1 monotherapy switched the highly aggressive/BL tumors into more CLA-like phenotypic state, which was not feasible with anti-TNFα monotherapy. We provide a very strong evidence that pharmacological inhibition of BRD4 via JQ1 significantly disrupted cJUN-mediated BL inflammatory program. Together, our findings suggest that JQ1 therapy could specifically be applied for cJUN^{high}/TNFα^{high} BL PDAC tumors (**Figure 40**).
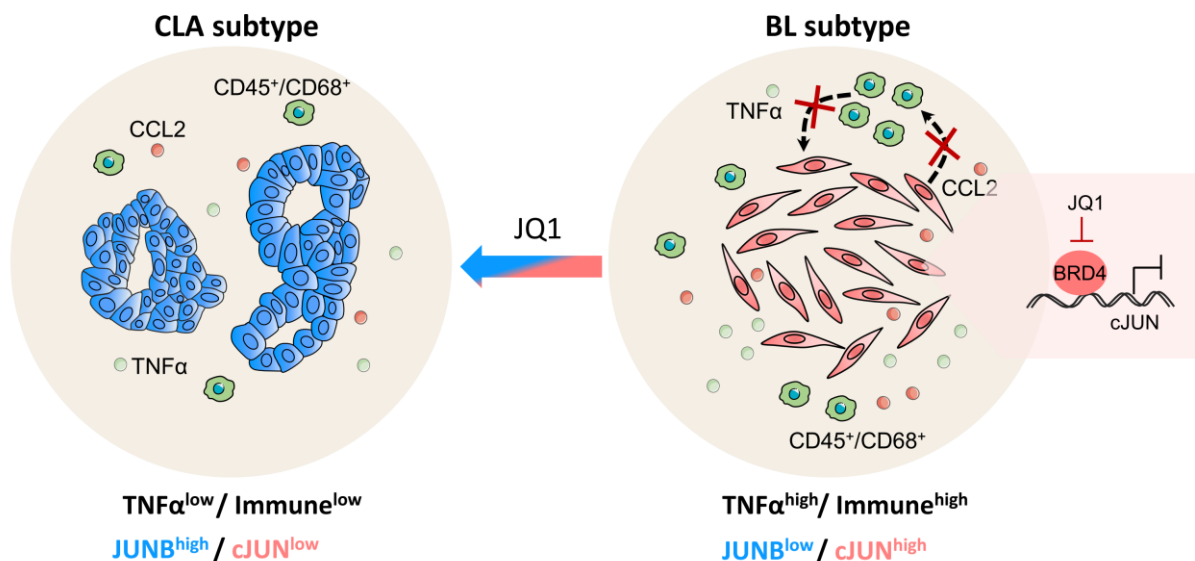
Figure 40. Schematic illustration of JQ1 mediated favorable prognosis in PDAC. cJUN could be targeted by inhibiting of BRD4 with BET inhibitor JQ1, thus, leading to well differentiated phenotype and less infiltrates for favoring a better prognosis.

4.7 Concluding remarks

Complex tumor stroma heterogeneity and cancer cell plasticity are the major challenges in PDAC poor prognosis and therapy resistance. Recent molecular subtyping of PDAC has significantly improved the molecular understanding of this lethal disease. Studies have shown that lineage-specific TFs and their associated gene signatures tightly control PDAC subtype identity and disease aggressiveness. In addition, the tumor subtype identity can be shaped by external stimuli from the existing tumor immune microenvironment. However, the precise mechanism of how this regulatory program operates is still largely unknown.

We provide a set of compelling evidence that explains how neoplastic-specific transcriptional reprograming modulates intra-tumor immune heterogeneity, which profoundly influences prognostic and therapeutic outcomes. Pharmacological inhibition

can indeed modulate these epigenetic-driven transcriptional networking and allow us to induce a favorable subtype switch.

Collectively, we report that:

➢ High expression of TNFα is restricted to the high-grade/poorly differentiated BL subtype, whereas CLA subtype is low-grade/well-to-moderately differentiated with low-proinflammatory immune infiltrations;

➢ Two antithetical and mutually exclusive AP1-driven transcriptional programs determine subtype identity and, thus, prognosis. JUNB/AP1 controls CLA tumor identity, whereas cJUN/AP1 controls the BL phenotype;

➢ BL-restricted cJUN maintains a pro-inflammatory gene expression program by controlling chromatin accessibility and enhancer potentiation; it thus recruits TNFα$^+$ macrophages in the microenvironment via CCL2 to sustain an inflammatory niche;

➢ CLA-restricted JUNB cannot support this pro-inflammatory identity and precludes macrophages recruitment; however, TNFα treatment suffices for switching CLA-tumors towards the aggressive BL identity;

➢ BRD4-bound enhancers support the cJUN-CCL2-TNFα axis, and hence, macrophages recruitment. Treatment with a known BET inhibitor disrupts this axis and allows reprogramming of poorly differentiated/BL-tumors into more differentiated/CLA ones that are amenable to chemotherapy.

5 References

Adams, C.R., Htwe, H.H., Marsh, T., Wang, A.L., Montoya, M.L., Subbaraj, L., Tward, A.D., Bardeesy, N., and Perera, R.M. (2019). Transcriptional control of subtype switching ensures adaptation and growth of pancreatic cancer. eLife *8*.

Adamska, A., Domenichini, A., and Falasca, M. (2017). Pancreatic Ductal Adenocarcinoma: Current and Evolving Therapies. International journal of molecular sciences *18*.

Adelaide, J., Finetti, P., Bekhouche, I., Repellini, L., Geneix, J., Sircoulomb, F., Charafe-Jauffret, E., Cervera, N., Desplans, J., Parzy, D.*, et al.* (2007). Integrated profiling of basal and luminal breast cancers. Cancer research *67*, 11565-11575.

Aggarwal, B.B., Moffat, B., and Harkins, R.N. (1984). Human lymphotoxin. Production by a lymphoblastoid cell line, purification, and initial characterization. The Journal of biological chemistry *259*, 686-691.

Andre, F., and Pusztai, L. (2006). Molecular classification of breast cancer: implications for selection of adjuvant chemotherapy. Nature clinical practice. Oncology *3*, 621-632.

Anders, S., Pyl, P.T., and Huber, W. (2015). HTSeq--a Python framework to work with high-throughput sequencing data. Bioinformatics *31*, 166-169.

Andricovich, J., Perkail, S., Kai, Y., Casasanta, N., Peng, W., and Tzatsos, A. (2018). Loss of KDM6A Activates Super-Enhancers to Induce Gender-Specific Squamous-like Pancreatic Cancer and Confers Sensitivity to BET Inhibitors. Cancer cell *33*, 512-526 e518.

Aung, K.L., Fischer, S.E., Denroche, R.E., Jang, G.H., Dodd, A., Creighton, S., Southwood, B., Liang, S.B., Chadwick, D., Zhang, A.*, et al.* (2018). Genomics-Driven Precision Medicine for Advanced Pancreatic Cancer: Early Results from the COMPASS Trial. Clinical cancer research : an official journal of the American Association for Cancer Research *24*, 1344-1354.

Bailey, P., Chang, D.K., Nones, K., Johns, A.L., Patch, A.M., Gingras, M.C., Miller, D.K., Christ, A.N., Bruxner, T.J., Quinn, M.C.*, et al.* (2016). Genomic analyses identify molecular subtypes of pancreatic cancer. Nature *531*, 47-52.

Balkwill, F. (2006). TNF-alpha in promotion and progression of cancer. Cancer metastasis reviews *25*, 409-416.

Balkwill, F. (2009). Tumour necrosis factor and cancer. Nature reviews. Cancer *9*, 361-371.

Bartsch, D. K., Sina-Frey, M., Lang, S., Wild, A., Gerdes, B., Barth, P., Kress, R., Grutzmann, R., Colombo-Benkmann, M., Ziegler, A*., et al.* (2002). CDKN2A germline mutations in familial pancreatic cancer. Annals of surgery *236*, 730-737.

Belkina, A.C., and Denis, G.V. (2012). BET domain co-regulators in obesity, inflammation and cancer. Nature reviews. Cancer *12*, 465-477.

Bhagwat, A.S., Roe, J.S., Mok, B.Y.L., Hohmann, A.F., Shi, J., and Vakoc, C.R. (2016). BET Bromodomain Inhibition Releases the Mediator Complex from Select cis-Regulatory Elements. Cell reports *15*, 519-530.

Biffi, G., Oni, T.E., Spielman, B., Hao, Y., Elyada, E., Park, Y., Preall, J., and Tuveson, D.A. (2019). IL1-Induced JAK/STAT Signaling Is Antagonized by TGFbeta to Shape CAF Heterogeneity in Pancreatic Ductal Adenocarcinoma. Cancer discovery *9*, 282-301.

Brahmer, J., Reckamp, K.L., Baas, P., Crino, L., Eberhardt, W.E., Poddubskaya, E., Antonia, S., Pluzanski, A., Vokes, E.E., Holgado, E*., et al.* (2015). Nivolumab versus Docetaxel in Advanced Squamous-Cell Non-Small-Cell Lung Cancer. The New England journal of medicine *373*, 123-135.

Brunton, H., Caligiuri, G., Cunningham, R., Upstill-Goddard, R., Bailey, U.M., Garner, I.M., Nourse, C., Dreyer, S., Jones, M., Moran-Jones, K*., et al.* (2020). HNF4A and GATA6 Loss Reveals Therapeutically Actionable Subtypes in Pancreatic Cancer. Cell reports *31*, 107625.

Burris, H. A., 3rd, Moore, M. J., Andersen, J., Green, M. R., Rothenberg, M. L., Modiano, M. R., Cripps, M. C., Portenoy, R. K., Storniolo, A. M., Tarassoff, P*., et al.* (1997). Improvements in survival and clinical benefit with gemcitabine as first-line therapy for patients with advanced pancreas cancer: a randomized trial. Journal of clinical oncology : official journal of the American Society of Clinical Oncology *15*, 2403-2413.

Cancer Genome Atlas Research Network. Electronic address, a.a.d.h.e., and Cancer Genome Atlas Research, N. (2017). Integrated Genomic Characterization of Pancreatic Ductal Adenocarcinoma. Cancer cell *32*, 185-203 e113.

Calcinotto, A., Grioni, M., Jachetti, E., Curnis, F., Mondino, A., Parmiani, G., Corti, A., and Bellone, M. (2012). Targeting TNF-alpha to neoangiogenic vessels enhances lymphocyte infiltration in tumors and increases the therapeutic potential of immunotherapy. Journal of immunology *188*, 2687-2694.

Candido, J.B., Morton, J.P., Bailey, P., Campbell, A.D., Karim, S.A., Jamieson, T., Lapienyte, L., Gopinathan, A., Clark, W., McGhee, E.J*., et al.* (2018). CSF1R(+) Macrophages Sustain Pancreatic Tumor Growth through T Cell Suppression and Maintenance of Key Gene Programs that Define the Squamous Subtype. Cell reports *23*, 1448-1460.

Carswell, E.A., Old, L.J., Kassel, R.L., Green, S., Fiore, N., and Williamson, B. (1975). An endotoxin-induced serum factor that causes necrosis of tumors. Proceedings of the National Academy of Sciences of the United States of America *72*, 3666-3670.

Chan-Seng-Yue, M., Kim, J.C., Wilson, G.W., Ng, K., Figueroa, E.F., O'Kane, G.M., Connor, A.A., Denroche, R.E., Grant, R.C., McLeod, J.*, et al.* (2020). Transcription phenotypes of pancreatic cancer are driven by genomic events during tumor evolution. Nature genetics *52*, 231-240.

Chen, C., He, W., Huang, J., Wang, B., Li, H., Cai, Q., Su, F., Bi, J., Liu, H., Zhang, B.*, et al.* (2018). LNMAT1 promotes lymphatic metastasis of bladder cancer via CCL2 dependent macrophage recruitment. Nature communications *9*, 3826.

Chen, E.Y., Tan, C.M., Kou, Y., Duan, Q., Wang, Z., Meirelles, G.V., Clark, N.R., and Ma'ayan, A. (2013). Enrichr: interactive and collaborative HTML5 gene list enrichment analysis tool. BMC bioinformatics *14*, 128.

Cobo, I., Martinelli, P., Flandez, M., Bakiri, L., Zhang, M., Carrillo-de-Santa-Pau, E., Jia, J., Sanchez-Arevalo Lobo, V.J., Megias, D., Felipe, I.*, et al.* (2018). Transcriptional regulation by NR5A2 links differentiation and inflammation in the pancreas. Nature *554*, 533-537.

Colleoni, M., Rotmensz, N., Maisonneuve, P., Mastropasqua, M.G., Luini, A., Veronesi, P., Intra, M., Montagna, E., Cancello, G., Cardillo, A.*, et al.* (2012). Outcome of special types of luminal breast cancer. Annals of oncology : official journal of the European Society for Medical Oncology *23*, 1428-1436.

Collisson, E.A., Sadanandam, A., Olson, P., Gibb, W.J., Truitt, M., Gu, S., Cooc, J., Weinkle, J., Kim, G.E., Jakkula, L.*, et al.* (2011). Subtypes of pancreatic ductal adenocarcinoma and their differing responses to therapy. Nature medicine *17*, 500-503.

Conroy, T., Desseigne, F., Ychou, M., Bouche, O., Guimbaud, R., Becouarn, Y., Adenis, A., Raoul, J. L., Gourgou-Bourgade, S., de la Fouchardiere, C.*, et al.* (2011). FOLFIRINOX versus gemcitabine for metastatic pancreatic cancer. The New England journal of medicine *364*, 1817-1825.

Diaferia, G.R., Balestrieri, C., Prosperini, E., Nicoli, P., Spaggiari, P., Zerbi, A., and Natoli, G. (2016). Dissection of transcriptional and cis-regulatory control of differentiation in human pancreatic cancer. The EMBO journal *35*, 595-617.

Dobin, A., Davis, C.A., Schlesinger, F., Drenkow, J., Zaleski, C., Jha, S., Batut, P., Chaisson, M., and Gingeras, T.R. (2013). STAR: ultrafast universal RNA-seq aligner. Bioinformatics *29*, 15-21.

Eckert, R.L., Adhikary, G., Young, C.A., Jans, R., Crish, J.F., Xu, W., and Rorke, E.A. (2013). AP1 transcription factors in epidermal differentiation and skin cancer. Journal of skin cancer *2013*, 537028.

Egberts, J.H., Cloosters, V., Noack, A., Schniewind, B., Thon, L., Klose, S., Kettler, B., von Forstner, C., Kneitz, C., Tepel, J.*, et al.* (2008). Anti-tumor necrosis factor therapy inhibits pancreatic tumor growth and metastasis. Cancer research *68*, 1443-1450.

Ellenrieder, V., Konig, A., and Seufferlein, T. (2016). Current Standard and Future Perspectives in First- and Second-Line Treatment of Metastatic Pancreatic Adenocarcinoma. Digestion *94*, 44-49.

Ellis, C.A., and Clark, G. (2000). The importance of being K-Ras. Cellular signalling *12*, 425-434.

Fader, A.N., Rasool, N., Vaziri, S.A., Kozuki, T., Faber, P.W., Elson, P., Biscotti, C.V., Michener, C.M., Rose, P.G., Rojas-Espaillat, L.*, et al.* (2010). CCL2 expression in primary ovarian carcinoma is correlated with chemotherapy response and survival outcomes. Anticancer research *30*, 4791-4798.

Feldmann, M. (2002). Development of anti-TNF therapy for rheumatoid arthritis. Nature reviews. Immunology *2*, 364-371.

Filippakopoulos, P., Qi, J., Picaud, S., Shen, Y., Smith, W.B., Fedorov, O., Morse, E.M., Keates, T., Hickman, T.T., Felletar, I.*, et al.* (2010). Selective inhibition of BET bromodomains. Nature *468*, 1067-1073.

Finer, M.H., Dull, T.J., Qin, L., Farson, D., and Roberts, M.R. (1994). kat: a high-efficiency retroviral transduction system for primary human T lymphocytes. Blood *83*, 43-50.

Ford, E., Nikopoulou, C., Kokkalis, A., and Thanos, D. (2014). A method for generating highly multiplexed ChIP-seq libraries. BMC research notes *7*, 312.

Garon, E.B., Rizvi, N.A., Hui, R., Leighl, N., Balmanoukian, A.S., Eder, J.P., Patnaik, A., Aggarwal, C., Gubens, M., Horn, L.*, et al.* (2015). Pembrolizumab for the treatment of non-small-cell lung cancer. The New England journal of medicine *372*, 2018-2028.

Ghaneh, P., Costello, E., and Neoptolemos, J.P. (2008). Biology and management of pancreatic cancer. Postgraduate medical journal *84*, 478-497.

Golan, T., Hammel, P., Reni, M., Van Cutsem, E., Macarulla, T., Hall, M.J., Park, J.O., Hochhauser, D., Arnold, D., Oh, D.Y.*, et al.* (2019). Maintenance Olaparib for Germline BRCA-Mutated Metastatic Pancreatic Cancer. The New England journal of medicine *381*, 317-327.

Goldstein, D., El-Maraghi, R.H., Hammel, P., Heinemann, V., Kunzmann, V., Sastre, J., Scheithauer, W., Siena, S., Tabernero, J., Teixeira, L.*, et al.* (2015). nab-Paclitaxel plus gemcitabine for metastatic pancreatic cancer: long-term survival from a phase III trial. Journal of the National Cancer Institute *107*.

Grivennikov, S.I., Greten, F.R., and Karin, M. (2010). Immunity, inflammation, and cancer. Cell *140*, 883-899.

Guerra, C., Schuhmacher, A.J., Canamero, M., Grippo, P.J., Verdaguer, L., Perez-Gallego, L., Dubus, P., Sandgren, E.P., and Barbacid, M. (2007). Chronic pancreatitis is essential for induction of pancreatic ductal adenocarcinoma by K-Ras oncogenes in adult mice. Cancer cell *11*, 291-302.

Halbrook, C.J., Pontious, C., Kovalenko, I., Lapienyte, L., Dreyer, S., Lee, H.J., Thurston, G., Zhang, Y., Lazarus, J., Sajjakulnukit, P.*, et al.* (2019). Macrophage-Released Pyrimidines Inhibit Gemcitabine Therapy in Pancreatic Cancer. Cell metabolism *29*, 1390-1399 e1396.

Hale, M.A., Swift, G.H., Hoang, C.Q., Deering, T.G., Masui, T., Lee, Y.K., Xue, J., and MacDonald, R.J. (2014). The nuclear hormone receptor family member NR5A2 controls aspects of multipotent progenitor cell formation and acinar differentiation during pancreatic organogenesis. Development *141*, 3123-3133.

Hartwig, W., Werner, J., Jager, D., Debus, J., and Buchler, M.W. (2013). Improvement of surgical results for pancreatic cancer. The Lancet. Oncology *14*, e476-e485.

Hessmann, E., Buchholz, S.M., Demir, I.E., Singh, S.K., Gress, T.M., Ellenrieder, V., and Neesse, A. (2020). Microenvironmental Determinants of Pancreatic Cancer. Physiological reviews *100*, 1707-1751.

Hezel, A. F., Kimmelman, A. C., Stanger, B. Z., Bardeesy, N., & DePinho, R. A. (2006). Genetics and biology of pancreatic ductal adenocarcinoma. Genes and Development, 20(10), 1218–1249.

Hingorani, S. R., Petricoin, E. F., Maitra, A., Rajapakse, V., King, C., Jacobetz, M. A., Ross, S., Conrads, T. P., Veenstra, T. D., Hitt, B. A.*, et al.* (2003). Preinvasive and invasive ductal pancreatic cancer and its early detection in the mouse. Cancer cell *4*, 437-450.

Hingorani, S.R., Wang, L., Multani, A.S., Combs, C., Deramaudt, T.B., Hruban, R.H., Rustgi, A.K., Chang, S., and Tuveson, D.A. (2005). Trp53R172H and KrasG12D cooperate to promote chromosomal instability and widely metastatic pancreatic ductal adenocarcinoma in mice. Cancer cell *7*, 469-483.

Ho, W.J., Jaffee, E.M., and Zheng, L. (2020). The tumour microenvironment in pancreatic cancer - clinical challenges and opportunities. Nature reviews. Clinical oncology *17*, 527-540.

Hodi, F.S., O'Day, S.J., McDermott, D.F., Weber, R.W., Sosman, J.A., Haanen, J.B., Gonzalez, R., Robert, C., Schadendorf, D., Hassel, J.C.*, et al.* (2010). Improved survival with ipilimumab in patients with metastatic melanoma. The New England journal of medicine *363*, 711-723.

Hosein, A.N., Huang, H., Wang, Z., Parmar, K., Du, W., Huang, J., Maitra, A., Olson, E., Verma, U., and Brekken, R.A. (2019). Cellular heterogeneity during mouse pancreatic ductal adenocarcinoma progression at single-cell resolution. JCI insight *5*.

Hruban, R.H., Adsay, N.V., Albores-Saavedra, J., Compton, C., Garrett, E.S., Goodman, S.N., Kern, S.E., Klimstra, D.S., Kloppel, G., Longnecker, D.S.*, et al.* (2001). Pancreatic intraepithelial neoplasia: a new nomenclature and classification system for pancreatic duct lesions. The American journal of surgical pathology *25*, 579-586.

Huang, H., Zhang, Y., Gallegos, V., Sorrelle, N., Zaid, M.M., Toombs, J., Du, W., Wright, S., Hagopian, M., Wang, Z.*, et al.* (2019). Targeting TGFbetaR2-mutant tumors exposes vulnerabilities to stromal TGFbeta blockade in pancreatic cancer. EMBO molecular medicine *11*, e10515.

Huang, S., Ernberg, I., and Kauffman, S. (2009). Cancer attractors: a systems view of tumors from a gene network dynamics and developmental perspective. Seminars in cell & developmental biology *20*, 869-876.

Iacobuzio-Donahue, C.A. (2012). Genetic evolution of pancreatic cancer: lessons learnt from the pancreatic cancer genome sequencing project. Gut *61*, 1085-1094.

Iguchi, E., Safgren, S. L., Marks, D. L., Olson, R. L., and Fernandez-Zapico, M. E. (2016). Pancreatic Cancer, A Mis-interpreter of the Epigenetic Language. The Yale journal of biology and medicine *89*, 575-590.

Ikemoto, S., Sugimura, K., Yoshida, N., Wada, S., Yamamoto, K., and Kishimoto, T. (2000). TNF alpha, IL-1 beta and IL-6 production by peripheral blood monocytes in patients with renal cell carcinoma. Anticancer research *20*, 317-321.

Ivaska, J., Pallari, H.M., Nevo, J., and Eriksson, J.E. (2007). Novel functions of vimentin in cell adhesion, migration, and signaling. Experimental cell research *313*, 2050-2062.

Jackson, J.M. (2007). TNF- alpha inhibitors. Dermatologic therapy *20*, 251-264.

Jiao, X., Katiyar, S., Willmarth, N.E., Liu, M., Ma, X., Flomenberg, N., Lisanti, M.P., and Pestell, R.G. (2010). c-Jun induces mammary epithelial cellular invasion and breast cancer stem cell expansion. The Journal of biological chemistry *285*, 8218-8226.

Kalbasi, A., Komar, C., Tooker, G.M., Liu, M., Lee, J.W., Gladney, W.L., Ben-Josef, E., and Beatty, G.L. (2017). Tumor-Derived CCL2 Mediates Resistance to Radiotherapy in Pancreatic Ductal Adenocarcinoma. Clinical cancer research : an official journal of the American Association for Cancer Research *23*, 137-148.

Kanda, M., Matthaei, H., Wu, J., Hong, S.M., Yu, J., Borges, M., Hruban, R.H., Maitra, A., Kinzler, K., Vogelstein, B.*, et al.* (2012). Presence of somatic mutations in most early-stage pancreatic intraepithelial neoplasia. Gastroenterology *142*, 730-733 e739.

Karakhanova, S., Link, J., Heinrich, M., Shevchenko, I., Yang, Y., Hassenpflug, M., Bunge, H., von Ahn, K., Brecht, R., Mathes, A.*, et al.* (2015). Characterization of myeloid leukocytes and soluble mediators in pancreatic cancer: importance of myeloid-derived suppressor cells. Oncoimmunology *4*, e998519.

Khorana, A.A., Mangu, P.B., Berlin, J., Engebretson, A., Hong, T.S., Maitra, A., Mohile, S.G., Mumber, M., Schulick, R., Shapiro, M.*, et al.* (2017). Potentially Curable Pancreatic Cancer: American Society of Clinical Oncology Clinical Practice Guideline Update. Journal of clinical oncology : official journal of the American Society of Clinical Oncology *35*, 2324-2328.

Kleeff, J., Korc, M., Apte, M., La Vecchia, C., Johnson, C. D., Biankin, A. V., Neale, R. E., Tempero, M., Tuveson, D. A., Hruban, R. H., and Neoptolemos, J. P. (2016). Pancreatic cancer. Nature reviews Disease primers *2*, 16022.

Komohara, Y., Jinushi, M., and Takeya, M. (2014). Clinical significance of macrophage heterogeneity in human malignant tumors. Cancer science *105*, 1-8.

Koorstra, J.B., Hong, S.M., Shi, C., Meeker, A.K., Ryu, J.K., Offerhaus, G.J., Goggins, M.G., Hruban, R.H., and Maitra, A. (2009). Widespread activation of the DNA damage response in human pancreatic intraepithelial neoplasia. Modern pathology : an official journal of the United States and Canadian Academy of Pathology, Inc *22*, 1439-1445.

Krebs, A.M., Mitschke, J., Lasierra Losada, M., Schmalhofer, O., Boerries, M., Busch, H., Boettcher, M., Mougiakakos, D., Reichardt, W., Bronsert, P.*, et al.* (2017). The EMT-activator Zeb1 is a key factor for cell plasticity and promotes metastasis in pancreatic cancer. Nature cell biology *19*, 518-529.

Kulbe, H., Thompson, R., Wilson, J.L., Robinson, S., Hagemann, T., Fatah, R., Gould, D., Ayhan, A., and Balkwill, F. (2007). The inflammatory cytokine tumor necrosis factor-alpha generates an autocrine tumor-promoting network in epithelial ovarian cancer cells. Cancer research *67*, 585-592.

Kuleshov, M.V., Jones, M.R., Rouillard, A.D., Fernandez, N.F., Duan, Q., Wang, Z., Koplev, S., Jenkins, S.L., Jagodnik, K.M., Lachmann, A.*, et al.* (2016). Enrichr: a comprehensive gene set enrichment analysis web server 2016 update. Nucleic acids research *44*, W90-97.

Larkin, J., Chiarion-Sileni, V., Gonzalez, R., Grob, J.J., Cowey, C.L., Lao, C.D., Schadendorf, D., Dummer, R., Smylie, M., Rutkowski, P.*, et al.* (2015). Combined Nivolumab and Ipilimumab or Monotherapy in Untreated Melanoma. The New England journal of medicine *373*, 23-34.

Li, H., and Durbin, R. (2010). Fast and accurate long-read alignment with Burrows-Wheeler transform. Bioinformatics *26*, 589-595.

Li, J., Byrne, K.T., Yan, F., Yamazoe, T., Chen, Z., Baslan, T., Richman, L.P., Lin, J.H., Sun, Y.H., Rech, A.J.*, et al.* (2018). Tumor Cell-Intrinsic Factors Underlie Heterogeneity of Immune Cell Infiltration and Response to Immunotherapy. Immunity *49*, 178-193 e177.

Li, L., Liu, Y.D., Zhan, Y.T., Zhu, Y.H., Li, Y., Xie, D., and Guan, X.Y. (2018). High levels of CCL2 or CCL4 in the tumor microenvironment predict unfavorable survival in lung adenocarcinoma. Thoracic cancer *9*, 775-784.

Lind, M.H., Rozell, B., Wallin, R.P., van Hogerlinden, M., Ljunggren, H.G., Toftgard, R., and Sur, I. (2004). Tumor necrosis factor receptor 1-mediated signaling is required for skin cancer development induced by NF-kappaB inhibition. Proceedings of the National Academy of Sciences of the United States of America *101*, 4972-4977.

Lipner, M.B., Peng, X.L., Jin, C., Xu, Y., Gao, Y., East, M.P., Rashid, N.U., Moffitt, R.A., Herrera Loeza, S.G., Morrison, A.B.*, et al.* (2020). Irreversible JNK1-JUN inhibition by JNK-IN-8 sensitizes pancreatic cancer to 5-FU/FOLFOX chemotherapy. JCI insight *5*.

Liou, G.Y., Doppler, H., Necela, B., Krishna, M., Crawford, H.C., Raimondo, M., and Storz, P. (2013). Macrophage-secreted cytokines drive pancreatic acinar-to-ductal metaplasia through NF-kappaB and MMPs. The Journal of cell biology *202*, 563-577.

Liu, F., Ai, F., Tian, L., Liu, S., Zhao, L., and Wang, X. (2016). Infliximab enhances the therapeutic effects of 5-fluorouracil resulting in tumor regression in colon cancer. OncoTargets and therapy *9*, 5999-6008.

Logsdon, C.D., and Ji, B. (2009). Ras activity in acinar cells links chronic pancreatitis and pancreatic cancer. Clinical gastroenterology and hepatology : the official clinical practice journal of the American Gastroenterological Association *7*, S40-43.

Lopez-Bergami, P., Lau, E., and Ronai, Z. (2010). Emerging roles of ATF2 and the dynamic AP1 network in cancer. Nature reviews. Cancer *10*, 65-76.

Love, M.I., Huber, W., and Anders, S. (2014). Moderated estimation of fold change and dispersion for RNA-seq data with DESeq2. Genome biology *15*, 550.

Mantovani, A., Allavena, P., Sica, A., and Balkwill, F. (2008). Cancer-related inflammation. Nature *454*, 436-444.

Maurer, C., Holmstrom, S.R., He, J., Laise, P., Su, T., Ahmed, A., Hibshoosh, H., Chabot, J.A., Oberstein, P.E., Sepulveda, A.R*., et al.* (2019). Experimental microdissection enables functional harmonisation of pancreatic cancer subtypes. Gut *68*, 1034-1043.

Mariani, O., Brennetot, C., Coindre, J.M., Gruel, N., Ganem, C., Delattre, O., Stern, M.H., and Aurias, A. (2007). JUN oncogene amplification and overexpression block adipocytic differentiation in highly aggressive sarcomas. Cancer cell *11*, 361-374.

Martinelli, P., Carrillo-de Santa Pau, E., Cox, T., Sainz, B., Jr., Dusetti, N., Greenhalf, W., Rinaldi, L., Costello, E., Ghaneh, P., Malats, N*., et al.* (2017). GATA6 regulates EMT and tumour dissemination, and is a marker of response to adjuvant chemotherapy in pancreatic cancer. Gut *66*, 1665-1676.

Mazur, P.K., Herner, A., Mello, S.S., Wirth, M., Hausmann, S., Sanchez-Rivera, F.J., Lofgren, S.M., Kuschma, T., Hahn, S.A., Vangala, D*., et al.* (2015). Combined inhibition of BET family proteins and histone deacetylases as a potential epigenetics-based therapy for pancreatic ductal adenocarcinoma. Nature medicine *21*, 1163-1171.

McWilliams, R. R., Wieben, E. D., Rabe, K. G., Pedersen, K. S., Wu, Y., Sicotte, H., and Petersen, G. M. (2011). Prevalence of CDKN2A mutations in pancreatic cancer patients: implications for genetic counseling. European journal of human genetics : EJHG *19*, 472-478.

Milan, M., Balestrieri, C., Alfarano, G., Polletti, S., Prosperini, E., Spaggiari, P., Zerbi, A., Diaferia, G.R., and Natoli, G. (2019). FOXA2 controls the cis-regulatory networks of pancreatic cancer cells in a differentiation grade-specific manner. The EMBO journal *38*, e102161.

Mini, E., Nobili, S., Caciagli, B., Landini, I., and Mazzei, T. (2006). Cellular pharmacology of gemcitabine. Annals of oncology : official journal of the European Society for Medical Oncology *17 Suppl 5*, v7-12.

Mishra, V.K., Wegwitz, F., Kosinsky, R.L., Sen, M., Baumgartner, R., Wulff, T., Siveke, J.T., Schildhaus, H.U., Najafova, Z., Kari, V*., et al.* (2017). Histone deacetylase class-I inhibition promotes epithelial gene expression in pancreatic cancer cells in a BRD4- and MYC-dependent manner. Nucleic acids research *45*, 6334-6349.

Miyabayashi, K., Baker, L.A., Deschenes, A., Traub, B., Caligiuri, G., Plenker, D., Alagesan, B., Belleau, P., Li, S., Kendall, J*., et al.* (2020). Intraductal Transplantation

Models of Human Pancreatic Ductal Adenocarcinoma Reveal Progressive Transition of Molecular Subtypes. Cancer discovery *10*, 1566-1589.

Moffitt, R.A., Marayati, R., Flate, E.L., Volmar, K.E., Loeza, S.G., Hoadley, K.A., Rashid, N.U., Williams, L.A., Eaton, S.C., Chung, A.H*., et al.* (2015). Virtual microdissection identifies distinct tumor- and stroma-specific subtypes of pancreatic ductal adenocarcinoma. Nature genetics *47*, 1168-1178.

Motzer, R.J., Escudier, B., McDermott, D.F., George, S., Hammers, H.J., Srinivas, S., Tykodi, S.S., Sosman, J.A., Procopio, G., Plimack, E.R*., et al.* (2015). Nivolumab versus Everolimus in Advanced Renal-Cell Carcinoma. The New England journal of medicine *373*, 1803-1813.

Muckenhuber, A., Berger, A. K., Schlitter, A. M., Steiger, K., Konukiewitz, B., Trumpp, A., Eils, R., Werner, J., Friess, H., Esposito, I*., et al.* (2018). Pancreatic Ductal Adenocarcinoma Subtyping Using the Biomarkers Hepatocyte Nuclear Factor-1A and Cytokeratin-81 Correlates with Outcome and Treatment Response. Clinical cancer research : an official journal of the American Association for Cancer Research *24*, 351-359.

Nagarsheth, N., Wicha, M.S., and Zou, W. (2017). Chemokines in the cancer microenvironment and their relevance in cancer immunotherapy. Nature reviews. Immunology *17*, 559-572.

Nagrial, A.M., Chin, V.T., Sjoquist, K.M., Pajic, M., Horvath, L.G., Biankin, A.V., and Yip, D. (2015). Second-line treatment in inoperable pancreatic adenocarcinoma: A systematic review and synthesis of all clinical trials. Critical reviews in oncology/hematology *96*, 483-497.

Natalwala, A., Spychal, R., and Tselepis, C. (2008). Epithelial-mesenchymal transition mediated tumourigenesis in the gastrointestinal tract. World journal of gastroenterology *14*, 3792-3797.

Neoptolemos, J.P., Kleeff, J., Michl, P., Costello, E., Greenhalf, W., and Palmer, D.H. (2018). Therapeutic developments in pancreatic cancer: current and future perspectives. Nature reviews. Gastroenterology & hepatology *15*, 333-348.

Neoptolemos, J.P., Palmer, D.H., Ghaneh, P., Psarelli, E.E., Valle, J.W., Halloran, C.M., Faluyi, O., O'Reilly, D.A., Cunningham, D., Wadsley, J*., et al.* (2017). Comparison of adjuvant gemcitabine and capecitabine with gemcitabine monotherapy in patients with resected pancreatic cancer (ESPAC-4): a multicentre, open-label, randomised, phase 3 trial. Lancet *389*, 1011-1024.

Neph, S., Vierstra, J., Stergachis, A. B., Reynolds, A. P., Haugen, E., Vernot, B., Thurman, R. E., John, S., Sandstrom, R., Johnson, A. K.*, et al.* (2012). An expansive human regulatory lexicon encoded in transcription factor footprints. Nature *489*, 83-90.

Neesse, A., Michl, P., Frese, K.K., Feig, C., Cook, N., Jacobetz, M.A., Lolkema, M.P., Buchholz, M., Olive, K.P., Gress, T.M.*, et al.* (2011). Stromal biology and therapy in pancreatic cancer. Gut *60*, 861-868.

Nitsche, U., Wenzel, P., Siveke, J.T., Braren, R., Holzapfel, K., Schlitter, A.M., Stoss, C., Kong, B., Esposito, I., Erkan, M.*, et al.* (2015). Resectability After First-Line FOLFIRINOX in Initially Unresectable Locally Advanced Pancreatic Cancer: A Single-Center Experience. Annals of surgical oncology *22 Suppl 3*, S1212-1220.

Noll, E.M., Eisen, C., Stenzinger, A., Espinet, E., Muckenhuber, A., Klein, C., Vogel, V., Klaus, B., Nadler, W., Rosli, C.*, et al.* (2016). CYP3A5 mediates basal and acquired therapy resistance in different subtypes of pancreatic ductal adenocarcinoma. Nature medicine *22*, 278-287.

Notta, F., Chan-Seng-Yue, M., Lemire, M., Li, Y., Wilson, G.W., Connor, A.A., Denroche, R.E., Liang, S.B., Brown, A.M., Kim, J.C.*, et al.* (2016). A renewed model of pancreatic cancer evolution based on genomic rearrangement patterns. Nature *538*, 378-382.

Olive, K. P., and Tuveson, D. A. (2006). The use of targeted mouse models for preclinical testing of novel cancer therapeutics. Clinical cancer research : an official journal of the American Association for Cancer Research *12*, 5277-5287.

Onoue, M., Terada, T., Okuda, M., Fujimoto, K., Doi, R., Imamura, M., and Inui, K. (2004). Surgical resection deteriorates gemcitabine-induced leukopenia in pancreatic cancer. International journal of clinical oncology *9*, 174-178.

Patzak, M.S., Kari, V., Patil, S., Hamdan, F.H., Goetze, R.G., Brunner, M., Gaedcke, J., Kitz, J., Jodrell, D.I., Richards, F.M.*, et al.* (2019). Cytosolic 5'-nucleotidase 1A is overexpressed in pancreatic cancer and mediates gemcitabine resistance by reducing intracellular gemcitabine metabolites. EBioMedicine *40*, 394-405.

Petrelli, F., Coinu, A., Borgonovo, K., Cabiddu, M., Ghilardi, M., Lonati, V., Aitini, E., Barni, S., and Gruppo Italiano per lo Studio dei Carcinomi dell'Apparato, D. (2015). FOLFIRINOX-based neoadjuvant therapy in borderline resectable or unresectable pancreatic cancer: a meta-analytical review of published studies. Pancreas *44*, 515-521.

Puleo, F., Nicolle, R., Blum, Y., Cros, J., Marisa, L., Demetter, P., Quertinmont, E., Svrcek, M., Elarouci, N., Iovanna, J.*, et al.* (2018). Stratification of Pancreatic Ductal Adenocarcinomas Based on Tumor and Microenvironment Features. Gastroenterology *155*, 1999-2013 e1993.

Prinz, C. (2012). Pankreas. In Basiswissen Innere Medizin. Springer-Lehrbuch. Heidelberg: Springer Medizin Verlag. pp. 232– 246.

Raghavan, S., Winter, P.S., Navia, A.W., Williams,H.L., DenAdel, A., Kalekar, R.L., Galvez-Reyes, J. *et al.* (2021) "The tumor microenvironment drives transcriptional phenotypes and their plasticity in metastatic pancreatic cancer." BioRxiv, 2020-08.

Qian, B.Z., Li, J., Zhang, H., Kitamura, T., Zhang, J., Campion, L.R., Kaiser, E.A., Snyder, L.A., and Pollard, J.W. (2011). CCL2 recruits inflammatory monocytes to facilitate breast-tumour metastasis. Nature *475*, 222-225.

Qiao, Y., He, H., Jonsson, P., Sinha, I., Zhao, C., and Dahlman-Wright, K. (2016). AP-1 is a key regulator of proinflammatory cytokine TNFalpha-mediated triple-negative breast cancer progression. The Journal of biological chemistry *291*, 18309.

Rahib, L., Smith, B.D., Aizenberg, R., Rosenzweig, A.B., Fleshman, J.M., and Matrisian, L.M. (2014). Projecting cancer incidence and deaths to 2030: the unexpected burden of thyroid, liver, and pancreas cancers in the United States. Cancer research *74*, 2913-2921.

Rhim, A.D., Mirek, E.T., Aiello, N.M., Maitra, A., Bailey, J.M., McAllister, F., Reichert, M., Beatty, G.L., Rustgi, A.K., Vonderheide, R.H.*, et al.* (2012). EMT and dissemination precede pancreatic tumor formation. Cell *148*, 349-361.

Roe, J.S., Hwang, C.I., Somerville, T.D.D., Milazzo, J.P., Lee, E.J., Da Silva, B., Maiorino, L., Tiriac, H., Young, C.M., Miyabayashi, K.*, et al.* (2017). Enhancer Reprogramming Promotes Pancreatic Cancer Metastasis. Cell *170*, 875-888 e820.

Rooman, I., and Real, F.X. (2012). Pancreatic ductal adenocarcinoma and acinar cells: a matter of differentiation and development? Gut *61*, 449-458.

Rudin, C.M., Poirier, J.T., Byers, L.A., Dive, C., Dowlati, A., George, J., Heymach, J.V., Johnson, J.E., Lehman, J.M., MacPherson, D.*, et al.* (2019). Molecular subtypes of small cell lung cancer: a synthesis of human and mouse model data. Nature reviews. Cancer *19*, 289-297.

Schindelin, J., Arganda-Carreras, I., Frise, E., Kaynig, V., Longair, M., Pietzsch, T., Preibisch, S., Rueden, C., Saalfeld, S., Schmid, B.*, et al.* (2012). Fiji: an open-source platform for biological-image analysis. Nature methods *9*, 676-682.

Sehgal, A., Donaldson, D.S., Pridans, C., Sauter, K.A., Hume, D.A., and Mabbott, N.A. (2018). The role of CSF1R-dependent macrophages in control of the intestinal stem-cell niche. Nature communications *9*, 1272.

Sethi, G., Sung, B., and Aggarwal, B.B. (2008). TNF: a master switch for inflammation to cancer. Frontiers in bioscience : a journal and virtual library *13*, 5094-5107.

Shadhu, K., and Xi, C. (2019). Inflammation and pancreatic cancer: An updated review. Saudi journal of gastroenterology : official journal of the Saudi Gastroenterology Association *25*, 3-13.

Shang, G.S., Liu, L., and Qin, Y.W. (2017). IL-6 and TNF-alpha promote metastasis of lung cancer by inducing epithelial-mesenchymal transition. Oncology letters *13*, 4657-4660.

Shaulian, E., and Karin, M. (2002). AP-1 as a regulator of cell life and death. Nature cell biology *4*, E131-136.

Shen, W., Tao, G.Q., Zhang, Y., Cai, B., Sun, J., and Tian, Z.Q. (2017). TGF-beta in pancreatic cancer initiation and progression: two sides of the same coin. Cell & bioscience *7*, 39.

Shu, S., Wu, H.J., Ge, J.Y., Zeid, R., Harris, I.S., Jovanovic, B., Murphy, K., Wang, B., Qiu, X., Endress, J.E.*, et al.* (2020). Synthetic Lethal and Resistance Interactions with BET Bromodomain Inhibitors in Triple-Negative Breast Cancer. Molecular cell *78*, 1096-1113 e1098.

Siegel, R.L., Miller, K.D., and Jemal, A. (2020). Cancer statistics, 2020. CA: a cancer journal for clinicians *70*, 7-30.

Singh, S. K., Chen, N. M., Hessmann, E., Siveke, J., Lahmann, M., Singh, G., Voelker, N., Vogt, S., Esposito, I., Schmidt, A.*, et al.* (2015). Antithetical NFATc1-Sox2 and p53-miR200 signaling networks govern pancreatic cancer cell plasticity. The EMBO journal *34*, 517-530.

Singh, S., Hasselluhn, M.C. & Neesse, A. (2019). A tangled tale of molecular subtypes in pancreatic cancer. Gut 68, 953-954.

Smith, L.M., Wise, S.C., Hendricks, D.T., Sabichi, A.L., Bos, T., Reddy, P., Brown, P.H., and Birrer, M.J. (1999). cJun overexpression in MCF-7 breast cancer cells produces a tumorigenic, invasive and hormone resistant phenotype. Oncogene *18*, 6063-6070.

Somerville, T.D.D., Xu, Y., Miyabayashi, K., Tiriac, H., Cleary, C.R., Maia-Silva, D., Milazzo, J.P., Tuveson, D.A., and Vakoc, C.R. (2018). TP63-Mediated Enhancer Reprogramming Drives the Squamous Subtype of Pancreatic Ductal Adenocarcinoma. Cell reports *25*, 1741-1755 e1747.

Spaderna, S., Schmalhofer, O., Hlubek, F., Berx, G., Eger, A., Merkel, S., Jung, A., Kirchner, T., and Brabletz, T. (2006). A transient, EMT-linked loss of basement membranes indicates metastasis and poor survival in colorectal cancer. Gastroenterology *131*, 830-840.

Stanger, B.Z., and Hebrok, M. (2013). Control of cell identity in pancreas development and regeneration. Gastroenterology *144*, 1170-1179.

Strobel, O., Neoptolemos, J., Jager, D., and Buchler, M.W. (2019). Optimizing the outcomes of pancreatic cancer surgery. Nature reviews. Clinical oncology *16*, 11-26.

Suganuma, M., Okabe, S., Marino, M.W., Sakai, A., Sueoka, E., and Fujiki, H. (1999). Essential role of tumor necrosis factor alpha (TNF-alpha) in tumor promotion as revealed by TNF-alpha-deficient mice. Cancer research *59*, 4516-4518.

Thalayasingam, N., and Isaacs, J.D. (2011). Anti-TNF therapy. Best practice & research. Clinical rheumatology *25*, 549-567.

Topalian, S.L., Sznol, M., McDermott, D.F., Kluger, H.M., Carvajal, R.D., Sharfman, W.H., Brahmer, J.R., Lawrence, D.P., Atkins, M.B., Powderly, J.D*., et al.* (2014). Survival, durable tumor remission, and long-term safety in patients with advanced melanoma receiving nivolumab. Journal of clinical oncology : official journal of the American Society of Clinical Oncology *32*, 1020-1030.

Tsao, M.S., Marguet, S., Le Teuff, G., Lantuejoul, S., Shepherd, F.A., Seymour, L., Kratzke, R., Graziano, S.L., Popper, H.H., Rosell, R*., et al.* (2015). Subtype Classification of Lung Adenocarcinoma Predicts Benefit From Adjuvant Chemotherapy in Patients Undergoing Complete Resection. Journal of clinical oncology : official journal of the American Society of Clinical Oncology *33*, 3439-3446.

Ueno, T., Toi, M., Saji, H., Muta, M., Bando, H., Kuroi, K., Koike, M., Inadera, H., and Matsushima, K. (2000). Significance of macrophage chemoattractant protein-1 in macrophage recruitment, angiogenesis, and survival in human breast cancer. Clinical cancer research : an official journal of the American Association for Cancer Research *6*, 3282-3289.

Vaccaro, V., Sperduti, I., and Milella, M. (2011). FOLFIRINOX versus gemcitabine for metastatic pancreatic cancer. The New England journal of medicine *365*, 768-769; author reply 769.

van Roy, F., and Berx, G. (2008). The cell-cell adhesion molecule E-cadherin. Cellular and molecular life sciences : CMLS *65*, 3756-3788.

Vigil, D., Cherfils, J., Rossman, K. L., and Der, C. J. (2010). Ras superfamily GEFs and GAPs: validated and tractable targets for cancer therapy? Nature reviews Cancer *10*, 842-857.

Voulgari, A., and Pintzas, A. (2009). Epithelial-mesenchymal transition in cancer metastasis: mechanisms, markers and strategies to overcome drug resistance in the clinic. Biochimica et biophysica acta *1796*, 75-90.

Wang-Gillam, A., Li, C.P., Bodoky, G., Dean, A., Shan, Y.S., Jameson, G., Macarulla, T., Lee, K.H., Cunningham, D., Blanc, J.F.*, et al.* (2016). Nanoliposomal irinotecan with fluorouracil and folinic acid in metastatic pancreatic cancer after previous gemcitabine-based therapy (NAPOLI-1): a global, randomised, open-label, phase 3 trial. Lancet *387*, 545-557.

Wajant, H. (2009). The role of TNF in cancer. Results and problems in cell differentiation *49*, 1-15.

Waters, A. M., and Der, C. J. (2018). KRAS: The Critical Driver and Therapeutic Target for Pancreatic Cancer. Cold Spring Harbor perspectives in medicine *8*.

Wellner, U., Schubert, J., Burk, U.C., Schmalhofer, O., Zhu, F., Sonntag, A., Waldvogel, B., Vannier, C., Darling, D., zur Hausen, A.*, et al.* (2009). The EMT-activator ZEB1 promotes tumorigenicity by repressing stemness-inhibiting microRNAs. Nature cell biology *11*, 1487-1495.

Wilentz, R.E., Geradts, J., Maynard, R., Offerhaus, G.J., Kang, M., Goggins, M., Yeo, C.J., Kern, S.E., and Hruban, R.H. (1998). Inactivation of the p16 (INK4A) tumor-suppressor gene in pancreatic duct lesions: loss of intranuclear expression. Cancer research *58*, 4740-4744.

Wu, S.Y., Lee, A.Y., Lai, H.T., Zhang, H., and Chiang, C.M. (2013). Phospho switch triggers Brd4 chromatin binding and activator recruitment for gene-specific targeting. Molecular cell *49*, 843-857.

Xia, X., Wu, W., Huang, C., Cen, G., Jiang, T., Cao, J., Huang, K., and Qiu, Z. (2015). SMAD4 and its role in pancreatic cancer. Tumour biology : the journal of the International Society for Oncodevelopmental Biology and Medicine *36*, 111-119.

Yadav, D., and Lowenfels, A.B. (2013). The epidemiology of pancreatitis and pancreatic cancer. Gastroenterology *144*, 1252-1261.

Ying, H., Dey, P., Yao, W., Kimmelman, A.C., Draetta, G.F., Maitra, A., and DePinho, R.A. (2016). Genetics and biology of pancreatic ductal adenocarcinoma. Genes & development *30*, 355-385.

Zhang, J., Lu, Y., and Pienta, K.J. (2010). Multiple roles of chemokine (C-C motif) ligand 2 in promoting prostate cancer growth. Journal of the National Cancer Institute *102*, 522-528.

Zhang, Q.W., Liu, L., Gong, C.Y., Shi, H.S., Zeng, Y.H., Wang, X.Z., Zhao, Y.W., and Wei, Y.Q. (2012). Prognostic significance of tumor-associated macrophages in solid tumor: a meta-analysis of the literature. PloS one *7*, e50946.

Zhang, Z., Lin, G., Yan, Y., Li, X., Hu, Y., Wang, J., Yin, B., Wu, Y., Li, Z., and Yang, X.P. (2018). Transmembrane TNF-alpha promotes chemoresistance in breast cancer cells. Oncogene *37*, 3456-3470.

Zhao, X., Fan, W., Xu, Z., Chen, H., He, Y., Yang, G., Yang, G., Hu, H., Tang, S., Wang, P.*, et al.* (2016). Inhibiting tumor necrosis factor-alpha diminishes desmoplasia and inflammation to overcome chemoresistance in pancreatic ductal adenocarcinoma. Oncotarget *7*, 81110-81122.

Zhao, R., Choi, B. Y., Lee, M. H., Bode, A. M., and Dong, Z. (2016). Implications of Genetic and Epigenetic Alterations of CDKN2A (p16(INK4a)) in Cancer. EBioMedicine *8*, 30-39.

Zhou, Q., and Melton, D.A. (2018). Pancreas regeneration. Nature *557*, 351-358.

Zidi, I., Mestiri, S., Bartegi, A., and Amor, N.B. (2010). TNF-alpha and its inhibitors in cancer. Medical oncology *27*, 185-198.

Zoetemelk, M., Ramzy, G.M., Rausch, M., and Nowak-Sliwinska, P. (2020). Drug-Drug Interactions of Irinotecan, 5-Fluorouracil, Folinic Acid and Oxaliplatin and Its Activity in Colorectal Carcinoma Treatment. Molecules *25*.

Acknowledgements

"Everything happens for the best". In retrospect, I am very glad that I have made the decision to take the doctoral adventure which is particularly worthy and memorable. The last four years have been integrated with both highlighted moments of achievement and adverse circumstances. When looking back, it is like an evolution – I have been equipped with higher learning capacity and passion, as well as more strength to handle failure and dark time in life. I owe all those to the people who accompanied me throughout the whole Ph.D. journey. What I achieved today will never ever be possible without you.

First of all, I sincerely thank my supervisor Dr. Shiv K. Singh for guiding me with this super interesting research project. It has sure been a wonderful time working with him. He has given me continuous guidance and encouragement with his great patience throughout my doctoral study. I really admire his delicate perception of the front edge research and newly developed methods which always inspires the whole working group. He is a great mentor of leading me how to think logically and scientifically. It was really a great honor to be a member of this active and excellent lab.

On a special note, I am very grateful to Prof. Dr. med. Volker Ellenrieder for providing me the opportunity to work in this collaborative department. I really appreciate Prof. Dr. Sabine Mihm for helping me settle in Göttingen. I thank PD. Dr. med. Elisabeth Hessmann for all the support and help during my Ph.D.

I would like to express sincere gratitude to my thesis advisory committee members Prof. Dr. Holger Reichardt and Prof. Dr. Dieter Kube for their constructive advice and feedback of my project during the TAC meetings throughout my Ph.D. years. Moreover, I would like to thank Dr. Ufuk Günesdogan and Prof. Dr. Argyris Papantonis for the highly efficient cooperations and the immense help in the NGS data processing. Besides, I am very thankful to my external examination members Prof. Dr. Argyris Papantonis, Dr. Ufuk Günesdogan, and Dr. Nico Posnien for their great support of my thesis defense arrangement.

Last but not least, I whole-heartedly thank my parents, who are the biggest supporters of my life. My strength and power in pursuing my dreams was attributed to their limitless trust and faith in me.